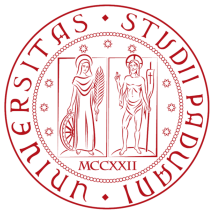

UNIVERSITÀ DEGLI STUDI DI PADOVA

Department of Information Engineering

Master's Degree in Electronic Engineering

DESIGN AND IMPLEMENTATION OF LIMIT CHARGE FUNCTION CIRCUIT FOR 48V 100Ah TLC LI-ION BATTERY

Advisor:

Prof. Nicola Trivellin

Candidate:

Federico Griso

Student nr. 2096418

Academic Year 2024/25

Abstract

The objective of this project is to analyse the behaviour of two different Li-ion TLC prototype batteries, with a specific focus on limit charge function.
The limit charge function is designed to regulate the charging current when it exceeds a threshold that the battery is not able to safely handle. This regulation ensures the continuation of the charging process without causing damage or triggering the Battery Management System (BMS) to disconnect the charging MOSFETs. While one of the batteries is equipped with this protective feature, the other does not present such functionality.
This research aims to evaluate the performance disparities between the two prototypes and subsequently design and develop a solution to integrate the limit charge feature into the second battery.
This is made by simulating system behaviour with Simulink and LTSpice and, afterwards, limit charge function is implemented on a prototype board to evaluate its real behaviour. In conclusion, a PCB prototype board is designed and implemented to be introduced to the battery pack.

Contents

List of Figures

List of Tables

Chapter 1

Introduction

1.1 FIAMM Energy Technology S.p.A

FIAMM Energy Technology is a multinational company, which works on battery production and distribution for car vehicles and industrial applications.
It has numerous sales and technical offices (Italy, Germany, UK, France, Spain, Singapore, China and Slovakia to name but a few) and a widespread network of importers and distributors all over the world.
It counts more than 1000 employees, 10 sales offices and 2 production plants.

Figure 1.1: FIAMM logo.
www.fiamm.com

The company was founded by Giulio Dolcetta in 1942 with the name of Fabbrica Italiana Accumulatori Motocarri Montecchio (FIAMM). After the end of the war the company grew a lot thanks to car industry development. In 1950, a FIAMM battery was mounted on the Ferrari car that won the Mille Miglia.
In 1970, in addition to car battery production, the company started to design also motorcycle batteries and it became the original equipment supplier for the most important car manufacturers. While in stationary battery sector it could boast customers such as SIP and Enel.
In the '80s, FIAMM started to export stationary batteries in the USA and entered the two main European markets with FIAMM Germany and FIAMM France. It marked a beginning of a period of acquisitions for the company in Austria, Spain, Germany and France. The new international dimension of the company involved strong investments in

technology. Therefore, the company reinforce its presence in motorsport such as Rally, Formula 1, Formula Indy, Paris Dakar and more.
In 2017, Hitachi Chemical acquired 51% of FIAMM Energy Technology S.p.A shares. While three years later (2020), all of the shares possessed by Hitachi Chemical has been acquired by Showa Denko, which commercial name has been changed to Resonac Corporation since 2023.
In 2022, the company celebrated its 80^{th} anniversary.
Nowadays, the headquarter is located at Montecchio Maggiore (VI).

Figure 1.2: FIAMM headquarter.
www.fiamm.com

The company started with the production of Lead acid batteries and it is a leader in the field. Recently, it began to develop some lithium-ion battery solutions which would be launched on the market.
The group has two subdivisions: Mobility Power Solutions and Reserve Power Solutions. The former has the aim of satisfying the current and future requirements of energy storage in the mobility sector. Whereas, the latter offers a broad range of stationary batteries, designed to guarantee uninterrupted power supply. Main applications refer to Telecom, Data Center, Industry & Utilities, Security & Emergency, Motion, Renewables and much more.
The main technologies for battery construction are:

- Absorbed Glass Mat (AGM): improved performance with faster charging, longer life and safer operation. An absorbent glass-mat separator is used between positive and negative plates.
- GEL: uses a jellified electrolyte between positive and negative plates. Excellent long life and good performance in a wide range of temperature conditions.
- Flooded: extremely robust and longest life between lead acid accumulators.

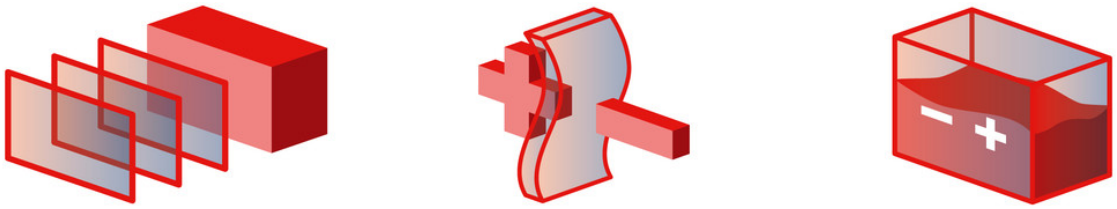

Figure 1.3: Main battery technologies.
www.fiamm.com

1.2 Project outline

Lithium-ion (Li-ion) batteries have become an essential part of modern electronic systems, powering a wide selection of devices ranging from portable devices to electric vehicles.
Their increasing usage is related to their high energy density, low self-discharge rate and long cycle life compared to other battery technologies.
However, maintaining the safety and the performance of Li-ion batteries requires good management of charging and discharging processes.
The Battery Management System (BMS) plays a key role in monitoring and controlling such processes. The BMS ensures that the battery operates in safe conditions optimising the performance by monitoring voltage, current, and temperature.
Since the charging process is a crucial point for extending the battery life, managing such phase is fundamental because charging the battery with too high current can deteriorate the battery status causing over-charging, over-heating and inefficiency.
The objective of this project is to analyse the behaviour of two different Li-ion TLC prototype batteries, with a specific focus on limit charge function.
The limit charge function is designed to regulate the charging current when it exceeds a threshold that the battery is not able to safely handle. This regulation ensures the continuation of the charging process without causing damage, excessive heating of battery cells, or triggering the Battery Management System (BMS) to disconnect the charging MOSFETs. While one of the batteries is equipped with this protective feature, the other lacks this functionality.
This research aims to evaluate the performance disparities between the two prototypes and subsequently design and develop a solution to integrate the limit charge feature into the second battery.
The objective is reached by designing and testing the system through simulation tools such as Simulink and LTSpice. After having verified the system design correction, some limit charge function circuit board are developed and tested to verify the previous results.
The design steps are better explained in the following chapters of this paper.
This research not only addresses the critical differences in performance due to the presence or absence of the limit charge function but also proposes a practical solution to enhance the safety and efficiency of Li-ion batteries.

1.3 48V lithium-ion TLC application

Telecom networks has changed a lot during the last decade. This lead to a huge increase of telecom sites around the world. Those sites are placed in locations where the conditions could be very different one from the other. For example, there might be places in which temperature is very low or very high, or sites in which the grid is more stable than the others. Independently from those cases, the main goal for telecom providers is to significantly reduce costs, space and energy consumption. Those characteristics result in a particular attention to equip them with energy storing systems (ESS), which are responsible for the continuity of service provided by the operators in case of grid interruptions or malfunctions.
For a very long time lead acid batteries were the main characters for this scope. However, with the development of lithium-ion batteries, most of the operators have started to replace previous batteries with them. This is because some of the main drawbacks of lead acid battery are related to short life expectancy at higher temperature, shorter cycle life and the necessity to engage more space compared to the lithium-ion alternative.
Li-ion batteries are a good alternative because they are suitable for both indoor and outdoor sites, they have a long cycle life even at high temperature, they are easy to install, they are safe, reliable and they can be considered as a *smart battery* allowing communication with the network in order to monitor the good functioning of the system.
In the following figure it is reported a comparison of DOD between lead acid battery and Li-ion battery. It is evident that the latter permits a better usage affecting the increasing of battery cycle life.

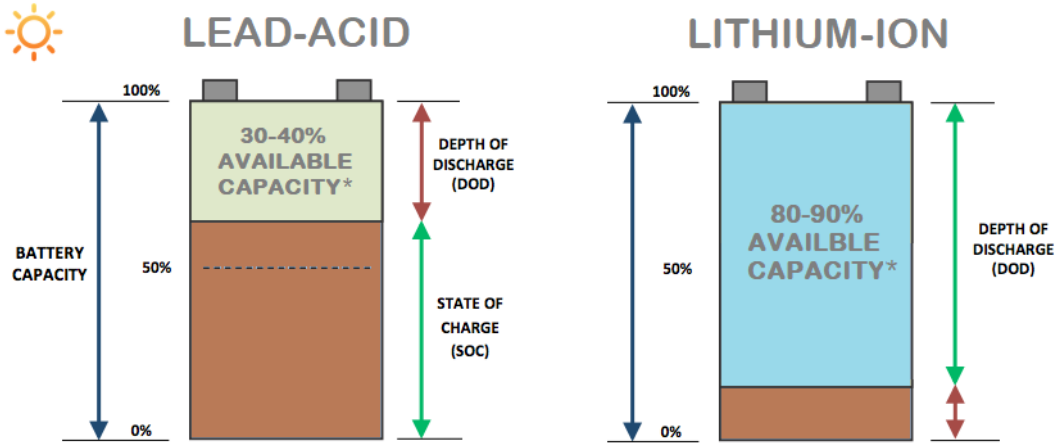

Figure 1.4: Lead acid and Li-ion batteries depth discharge.
www.redwaypower.com

Due to safety reasons, a typical battery configuration for TLC purposes is 48V 100Ah.
Different types of Li-ion batteries are available on the market and they will be briefly examined in Section 2.2.3.
The cells are typically connected in series in order to obtain the desired voltage, then modules are connected in parallel to obtain the desired capacity for the system.
For this reason it is necessary to constantly monitor all the batteries involved in the system. Measurement of cells' voltage, temperature and current are performed and sent

to the microprocessor for the monitoring and controlling of the system.

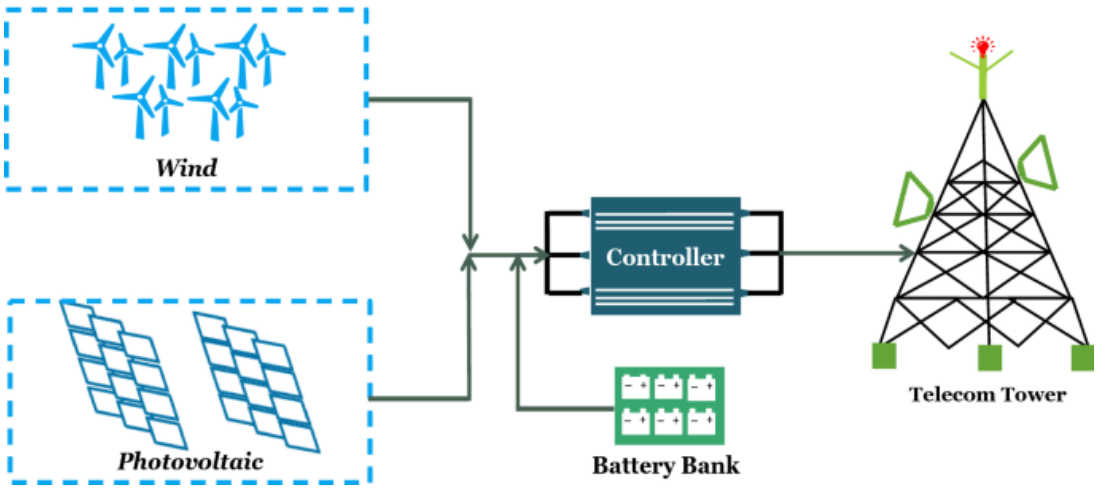

Figure 1.5: Example of ESS for TLC application.
www.link.springer.com

Chapter 2

Lithium-ion battery

2.1 Battery description

A battery is an electrochemical device that stores and converts chemical energy into electrical energy. A battery is normally composed of more than two elementary cells.

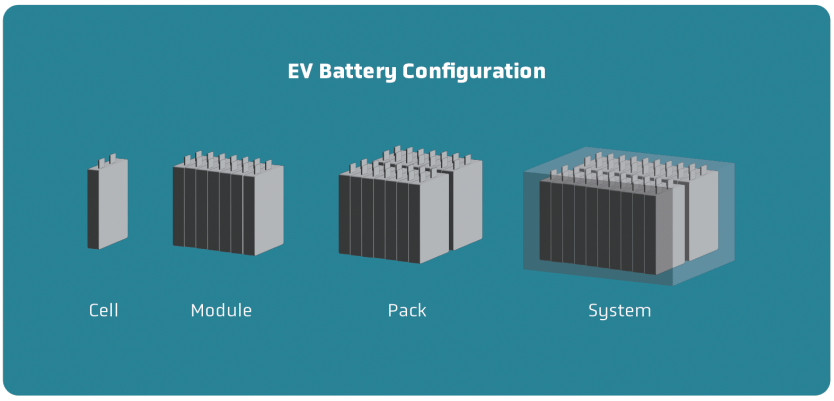

Figure 2.1: Battery configuration.
www.quantumscape.com

2.2 Lithium-ion technology

A lithium-ion battery is a type of rechargeable battery that uses a reversible property of Li^+ ions to store energy. The invention and the commercialization of this type of cells may have had one of the greatest impacts of technology in human history.
The basic structure of a Li-ion cell is the same as described in the previous section and highlighted in Figure 2.2.

- **Anode:** traditionally made of graphite and other carbon materials. These materials are used because of their abundance in nature. The oxidation takes place in the electrode and produces positively charged Li-ions and electrons. At this stage, lithium ions move through the electrolyte and electrons flow through the external circuit towards the cathode. This process produces energy on the external circuit.

- **Cathode:** it is the electrode which accepts the electrons arriving from the external circuit in order to be recombined with the cathode materials providing a reduction reaction.
- **Separator:** it is a membrane whose purpose is to avoid conduction between positive and negative electrodes.
- **Electrolyte:** provides a conductive medium for lithium ions in order to move from one electrode to the other, but it does not participate to the battery chemical reaction and it is composed of lithium salts in an organic solvent.

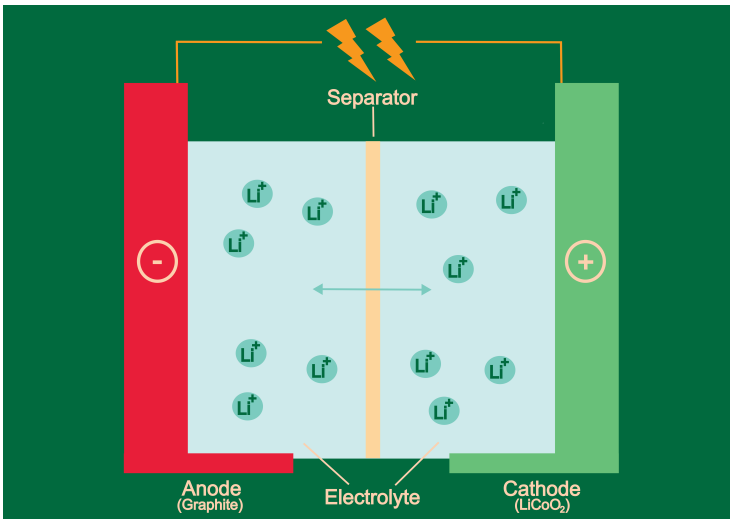

Figure 2.2: Cell internal structure.
www.ista.ac.at

2.2.1 Working principle

The basic function of the anode and the cathode is to hold the lithium ions as they pass back and forth during charge and discharge of a battery.
On charging, Li-ions are released from the cathode and they migrate into the carbon of the anode passing through the electrolyte. The reverse reaction occurs during discharging. This process of attracting the ions to the surface of the active material is known as adsorption or intercalation.
As a rule, designers prefer to project electrodes with large surface areas with the aim of reducing losses of energy. This is obtained by using porous materials that permit the electrolyte to penetrate inside the porouses. This lead to a better travelling of lithium-ions through the active material.
It is very important to choose a separator which is able to ensure high efficiency and long life on the lithium-ion battery, because this is the interface that permits ions to migrate from one electrode to the other without letting them touch. In case of separator corruption, this results to short-circuit between the electrodes, leading to the subsequent break of the battery itself.

The main chemical process that takes place inside the battery is the reduction/oxidation process (red-ox). This process is related to the movement of lithium-ions from anode to cathode and viceversa. In practice, when an atom gains an electron it is said to have been reduced, while if the atom loses an electron it is said to have been oxidized.
During charging, oxidation takes place at the cathode and it releases electrons, whereas at the anode happens a reduction process in which atoms gain electrons.
In a different manner, during discharging the oxidation takes place at the anode allowing electrons to flow out of it. While reduction occurs at the cathode, where atoms are able to gain electrons flowing in from the external circuit.
The current is considered positive if the electrons flow out of the anode and oxidation occurs (discharging). On the other hand, it is considered negative if the electrons are accepted by the anode and reduction occurs (charging).
If this process can't take place, cells are not able to be recharged. This leads to a loss of the electrons once they have been spent and the cell can be considered dead.

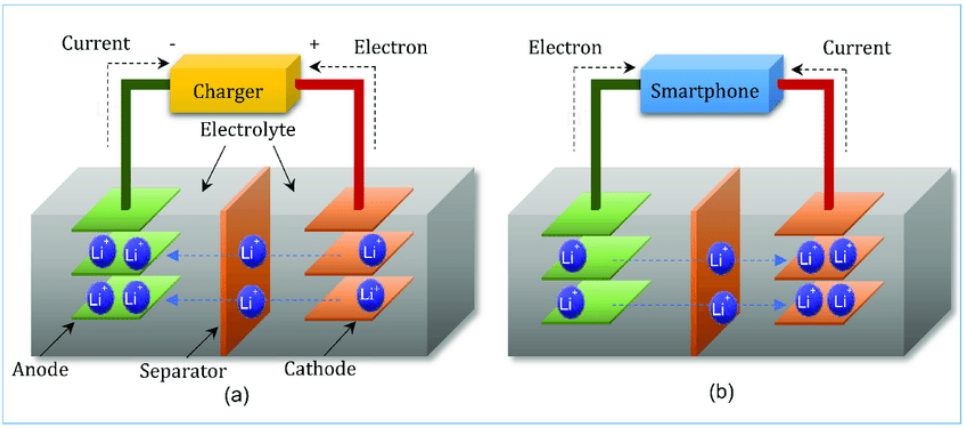

Figure 2.3: Charging (a) and discharging (b) of a lithium-ion cell.
www.researchgate.net

The standard charging process for a lithium-ion battery consists in CC-CV (constant current-constant voltage). Firstly, the battery is charged with a constant current until a specific voltage is reached. After that, it is charged imposing a constant voltage until a certain current value is reached. Overcharging batteries can lead to serious hazards. In the worst-case scenario the battery may be irreversibly damaged and potentially catching fire. Nevertheless, overcharging leads to a deterioration of the battery.

2.2.2 Applications

Lithium-ion batteries are becoming widespread in a lot of possible applications.
Sony introduced the first lithium-ion battery in a portable telephone in 1991. Since then, many improvements were done to system's energy density and rate capability.
Lithium-ion batteries made of multiple cylindrical cells are finding more and more applications in electronic portable devices because of their high energy density, low weight and longer cycle life compared to previous solutions.
In recent years, lithium-ion batteries are being involved in Electric Vehicles (EV) and military applications. For this purpose large prismatic cells have been considered.

Traditionally, prismatic cells have been preferred for applications with moderate energy requirements as their form factor results in 15% to 30% capacity advantage respect to cylindrical solution.
This technology will increasingly gain importance in the future. This will include energy supply for computer and mobile phones, but it is also true for power systems and electric vehicles.
Actually, the use of these systems have considerably increased in hybrid vehicles in recent years. Meanwhile, prototypes are being developed for their employment in stationary storage systems, such as UPS, in order to stabilise grid voltage or to store energy to be used in case of grid power interruption. Nowadays, lithium-ion batteries are used as small storage devices with around 2 kWh up to 40 MWh in larger plants.
In electric mobility, lithium-ion batteries play an increasingly key role. They are used in electric bicycles and scooters and hybrid or electric buses, for example.
Depending on the application, single battery cell or multiple cells connected in series, as module, could be used. In some applications, such as automotive battery systems or energy storage systems, it is necessary to introduce a Battery Management System (BMS) which is able to monitor and regulate the correct functioning of the battery in order to avoid any hazards or breaking of the system. In Chapter 3, additional information about this system will be outlined.

Figure 2.4: Applications overview.
www.researchgate.net

2.2.3 Types of lithium-ion batteries

The main commercial typologies are the followings:

- Cobalt oxide: LCO
- Manganese oxide: LMO
- Nickel Manganese Cobalt oxide: NMC
- Iron Phosphate: LFP
- Titanate oxide: LTO

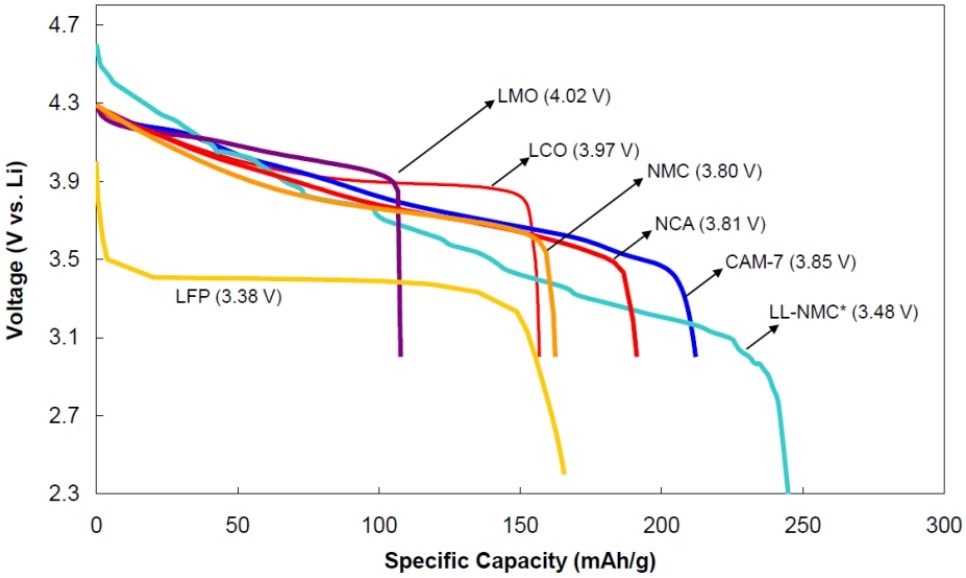

Figure 2.5: Specific capacity vs Voltage of different cell types.
www.emove360.com

Material	LCO	LMO	NMC	LFP	LTO
Cell voltage [V]	3.6	3.7	3.6	3.2	2.2
Specific energy [Wh/kg]	160	150	170	120	80
Temperature range [°C]	$-20 \div 60$	$-20 \div 60$	$-20 \div 60$	$-20 \div 60$	$-40 \div 55$
Cycle life	$500 \div 1000$	500	3000	$2700 \div 10000$	5500

Table 2.1: Characteristics of Li-ion cells.

Table 2.1 shows that there are different solutions for battery applications. The selection of a suitable type depends not only on the main characteristics, but also on costs, service life and safety.
NMC actually grants high energy density but it is less safe than other types of cells. On the other hand, LFP can be identified as the safest cell and its production costs are significantly lower. These features make the LFP one of the best alternative to NMC because it has not a remarked difference in energy density but it shows no thermal effects up to high temperatures.

2.3 Formats

Cell batteries can have different formats and building methods. Main topologies are the following ones:

- Cylindrical
- Prismatic
- Pouch

All of them have different characteristics. The main difference lies in the design of the cell casing and the setup of cathode, anode and separator.

2.3.1 Cylindrical cells

In recent years, cylindrical cells have gained strong relevance and popularity among automotive manufacturers. They are packaged in a hard case and they contains electrode webs wound with separators to form a jelly roll. This type of cell is generally identified with a code, e.g. 4680, in which 46 represents the diameter of the cell in mm and 80 refers to the height of it.
Current and thermal transport between the jelly road and the cell is conducted by contacting elements called tabs.
One of the drawbacks of this topology regards the inhomogeneity of temperature, this could lead to a decrease of cycle lifetime of the cell, a risk of thermal runaway and efficiency losses.
On the other hand, the advantages are related to great power and energy density, higher safety standards, better rate capability, and low production costs.

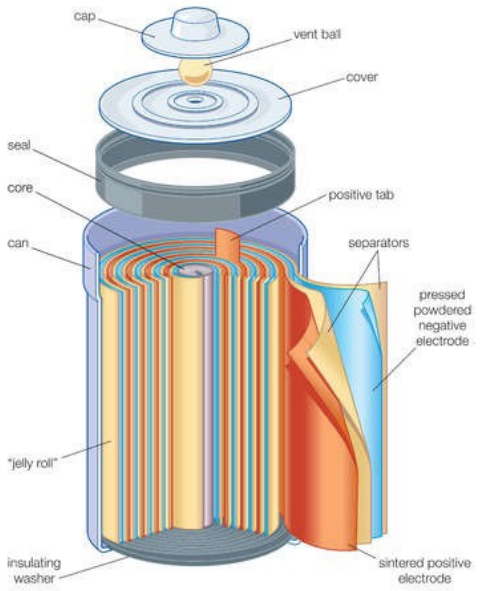

Figure 2.6: Cylindrical cell.
www.alamy.it

2.3.2 Prismatic cells

They are packaged in a hard case, such as the cylindrical cell, and are composed of electrolytes arranged in foils covered with aluminium or steel.
They are characterized by higher energy density but less charge and discharge power compared to cylindrical batteries. Typically, they are bigger. This means that in comparison, it is necessary to use fewer cells in order to achieve the same energy content.

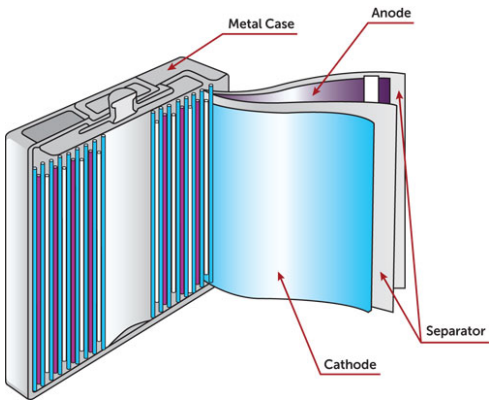

Figure 2.7: Prismatic cell.
www.ecolithiumbattery.com

2.3.3 Pouch cells

Pouch cells are packaged in multilayer aluminium composite foils and they exclusively employ stacked arrangement. Its advantages refer to high energy and packaging density and low manufacturing costs.
They are composed of flexible electrolyte pockets wrapped in films. This configuration allows to obtain much lighter batteries. Therefore, unfortunately, they don't have high mechanical strength. On the other hand, charging and discharging power are less sensitive to temperature changes.

Figure 2.8: Pouch cell.
www.servovision.com

2.4 Battery parameters

In order to identify and characterize a battery, a list of terminology and parameters are needed.

- **Nominal voltage [V]:** is the battery voltage reference which helps the identification.
- **Nominal capacity [Ah]:** indicates the total current a battery can provide in one hour time.
- **Maximum charging voltage [V]:** is the maximum voltage a battery can reach before destroying itself. It depends on the type of battery used. For most of the cells it is in a range between 3.2V and 3.7V, with the only exclusion of LTO.
- **Minimum discharging voltage [V]:** is a similar concept to the maximum charging voltage, but it indicates the voltage where the battery is considered empty.
- **Charge and discharge rate (C-rate):** is a parameter related to the battery capacity, where 1C-rate indicates that a battery is being charged/discharged at the nominal capacity of the battery. In this way, the battery will be charged/discharged, more or less, in one hour.

$$\text{C-rate} = \frac{\text{CH/DCH current [A]}}{\text{Nominal capacity [Ah]}}$$

- **State-of-Charge (SOC) [%]:** represents the percentage of available energy in the battery.

$$SOC = \frac{\text{Capacity remaining [Ah]}}{\text{Nominal capacity [Ah]}}$$

- **State-of-Health (SOH):** indicates the battery condition with respect to the one provided by the manufacturing. It degrades with ageing and it is not easy to derive.
- **Cycle life:** total number of charging and discharging cycles that a battery can perform.
- **End-of-Life (EOL):** it is the condition when the maximum battery capacity reaches 80% of the nominal one because of degradation with time.
- **Shelf life:** length of time in which a battery can maintain the stored energy before being used.
- **Self discharge [%]:** rate at which the battery discharges when it is not connected neither the grid nor the load. This rate is dependent to the temperature. A typical monthly self discharge rate is about 1-2%.
- **Weight energy density [Wh/kg]:** indication of energy density per weight unit.

$$\text{Weight energy density} = \frac{Voltage \cdot Capacity}{Weight} \left[\frac{Wh}{kg}\right]$$

- **Volume energy density [Wh/l]:** indication of energy density per volume unit.

$$\text{Volume energy density} = \frac{Voltage \cdot Capacity}{Volume} \left[\frac{Wh}{l}\right]$$

- **Internal Resistance (IR)** $[m\Omega]$**:** it is the sum of electric and ionic resistances of cell components. It is responsible for energy losses and temperature increase. It is the cause of the behaviour deviation respect to the theoretical one. It is expressed in the order of $m\Omega$. The objective is to maintain this parameter as little as possible. There are two measurement techniques. The first one is a DC method done by measuring the voltage drop at a specified current. The other one is the most used method which consists on a AC measurement to evaluate the reactance by using a specific tool. It provides a sinusoidal input and it measures the frequency response of the current in order to derive the impedance.

- **Relaxation:** phase after a charge or discharge where the battery voltage tends to reach a steady state due to its chemical properties.

- **Open circuit voltage (OCV):** voltage measured after the relaxation phase in no load condition.

Chapter 3

Battery Management System (BMS)

3.1 Introduction

The growing use of Li-ion batteries increases the complexity of the systems involved. The increasing demand for electrical distribution created the necessity of developing big energy storage systems (ESS). As a result, the implementation of Battery Management Systems (BMS) has become essential in order to monitor and control such plants, increasing battery life and consequently reducing costs.
The main features of a BMS can be identified in monitoring, balancing and protection.
Lithium-ion batteries started to substitute Lead acid batteries because of their low self discharge rate, high energy density and longer life cycles. However, those type of batteries have some side effects. In fact, they need a much more controlled environment in order to reduce ageing and loss of performance.
Nowadays, there is not a specific standard for the development of a BMS, but in the last years a lot of improvements have been done and many manufacturers are providing a personal version of this device.
The BMS software offers multi-tasking capabilities. This means that it is introduced a real time operating system (RTOS) that is able to perform simultaneously different tasks, such as voltage/current measurement, over-voltage/current protection and temperature measurement. This is very important in order to ensure safety and good performance.

3.2 Features

The main purpose of BMS is to supervise the battery pack safety. To do so, the BMS is able to monitor and regulate some battery parameters in order to avoid damages on the accumulators. It is also able to calculate some informative parameters, regarding the state of a battery, by elaborating data measured from the plant.
Some of this parameters are SOC, SOH and DOD and other key parameters.

3.2.1 Monitoring

In general, BMS is used to manage multiple strings composed of multiple batteries. However, the BMS is not only able to monitor a string of batteries, but it is also able to check the good functioning of a single cell inside the string.

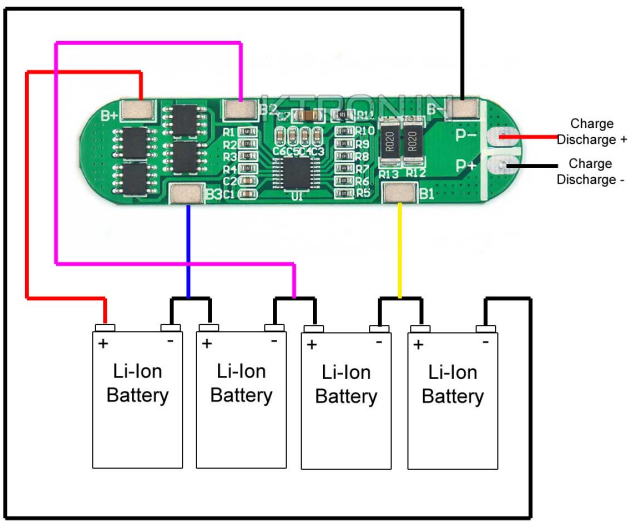

Figure 3.1: Example of a BMS connection.
www.ktron.in

The monitoring feature is very important for the analysis and regulation of batteries functioning in order to improve both performance and efficiency of the whole system safely.
A very useful function derived from the monitoring activity is the estimation of the state of charge of a battery, in order to obtain an accurate value it is important to design the system properly.
It uses sensors and functions in order to monitor cell voltages and temperatures. It also monitors the current and switches on or off the battery system in case of errors.
Main monitoring activities regard the monitoring of voltage, current, temperature, isolation and interlock.
Isolation is very important because whether a human body comes into contact with a high voltage exposed part, it can causes death or several injuries.

3.2.2 Protection

A BMS must ensure protection against any type of hazard.
In addition, BMS is able to control the charge and discharge cycles so as to avoid over-charging or over-discharging that can cause over-heating on the battery and damages to the system.
To do so, it constantly monitors the state of the batteries and it reacts to any unusual situation it detects.

3.2.3 Balancing

This feature is fundamental for energy service performance optimization.
To clarify, this function has to balance the battery cells to the same voltage in order to avoid unbalance and unequal charge. Since a battery of 48V is composed of 15 cells, it is necessary to equalise the charge of each cell.
Two methods could be adopted to do so.

- Passive balance
- Active balance

Passive method: voltage of each cell is monitored by the microcontroller inside the BMS. If the voltage of any cell exceeds a maximum delta compared to the others, the microcontroller begins to discharge the more charged cells via a small resistor placed in parallel to the cell.
The loss of energy produced by the discharge of higher cells represents the biggest disadvantage. Indeed, if only a single cell has lower voltage compared to the others, all of the other cells has to be discharged in order to reach the level of voltage of that cell and all the energy is lost.
However, this balancing is necessary because if a single cell has a lower voltage during the discharging phase, the BMS stops the discharge when that cell is completely empty, leaving the other cells only partially discharged. This causes lower DoD (Depth of Discharge) and subsequently less capacity of the battery.
The same result could be related to the charging phase, in fact, if a cell is more charged than the others, the BMS stops the charge when it is fully charged even though the others are not completely full. This causes, as in the previous case, loss of capacity.

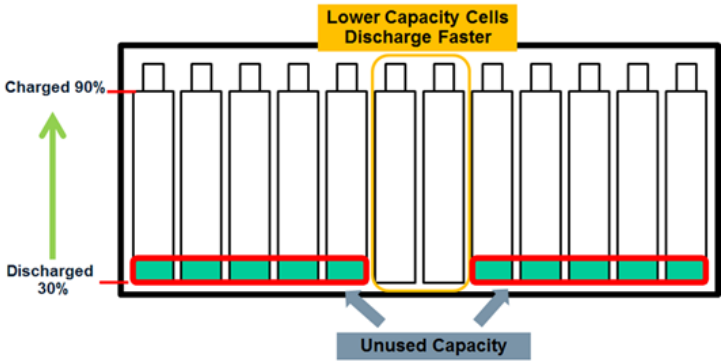

Figure 3.2: Lower capacity due to unbalance.
www.analog.com

This is the most used method because of its cheaper costs due to the simplicity of the design. Another reason is that most of the time, cell unbalances are minimal and energy loss is limited to just a few mW.

Active method: this solution consists in discharging the higher voltage cell to the lower one. This technique ideally prevents energy losses. In reality, a loss of energy occurs during the charging and the discharging of the capacitor, but it is limited compared to

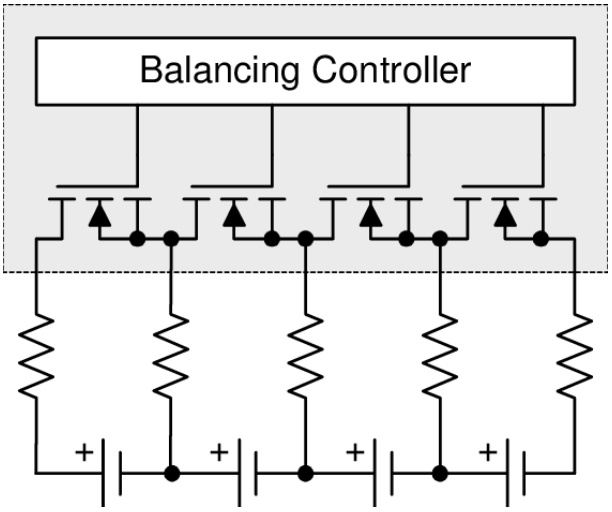

Figure 3.3: Passive balance.
www.researchgate.net

passive balancing. The higher voltage cell indeed charges a capacitor which is subsequently discharged to the lower voltage cell in order to balance the average cells voltage. Other techniques could be used in order to obtain the same effect but this is the most popular one.
Although this method can ideally prevent energy losses, it is rarely used because of its complexity, costs and the space occupied on the board.

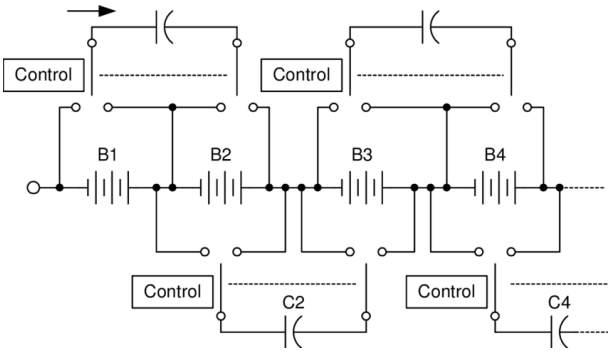

Figure 3.4: Active balance.
www.researchgate.net

Various algorithms could be employed to determine when to activate the system.
The followings are three of the most popular examples:

- Balancing during charge only
- Balancing at high states of charge only
- Simultaneous multi-cell balancing

3.2.4 Diagnosis

BMS is able to estimate and predict some parameters indicating the current state of a battery. All these information are derived from the measurement performed on the battery and are reported on a specific tool provided by the manufacturer.
The main parameters regard SOC, SOH, DOD, battery capacity, cell temperature and more. These parameters are essential for understanding the good state of the battery.
In fact, BMS is also responsible for detecting faults occurred in the system.

3.3 Topologies

Three types of implementation for the system design are going to be analysed.

- Centralized
- Distributed
- Modular

For what concerns the centralized topology, a single control unit (BMS) is used to monitor a series of multiple battery cells and the monitoring is done through multiple wires. This solution is the cheapest one.

Figure 3.5: Centralized topology.
www.linkedin.com

In a distributed topology, each control unit is dedicated to a single battery cell and a single communication cable is necessary for each cell. This solution is the easiest among the others and it is simple to install.

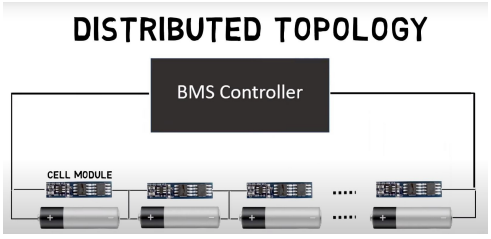

Figure 3.6: Distributed topology.
www.linkedin.com

Lastly, for what concerns a modular topology, each battery has a specific control unit, but the control units are interconnected to each other. This solution is the most challenging one because it requires more hardware and more software effort. It is a mitigation of the other two solutions.

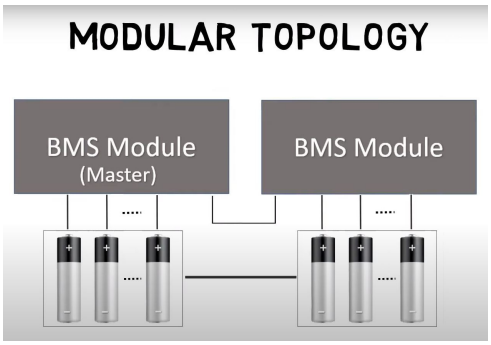

Figure 3.7: Modular topology.
www.linkedin.com

Chapter 4

Laboratory features

4.1 Instrumentation

The following part of this paper moves on to describe in greater detail the characteristics of the instruments used to test and verify the behaviour of batteries.

4.1.1 Digatron

This device is a battery cycler capable of charging and discharging batteries. Thanks to a proprietary software it is possible to set some parameters, such as current, voltage and time, in order to define the phases of charge and discharge.
The software also allows data to be saved and exported on an Excel file. This facilitates subsequent analysis and plotting in order to verify if test has performed well. The log saves information such as voltage, current, time and charged or discharged capacity.
The following list will briefly introduce the specifications of Digatron.

- Voltage range: $10V \div 60V$ (Charge), $5V \div 50V$ (Discharge)
- Current range: $0.1A \div 100A$
- Charge current peak: 125A (max 10 sec)
- Discharge current peak: 160A (max 10 sec)

4.1.2 Hioki BT3554

This device is able to measure the internal resistance and voltage of both cells and battery. It uses the AC method which will be thoroughly described in Section 4.2.3.
The specifications of this tester are the following.

- Resistance measurement range: $3m\Omega(\pm 1\mu\Omega)$ to $3\Omega(\pm 1m\Omega)$
- Testing frequency: $1kHz \pm 80Hz$
- Voltage measurement range: $\pm 6V(\pm 1mV)$ to $\pm 60V(\pm 10mV)$

	A	B	C	D	E	F	G	I	J	L	M	N	O
30	Time Stamp	Step	Status	Prog Time	Step Time	Cycle	Cycle Level	Voltage	Current	AhAccu	AhStep	Energy	WhStep
82	05/11/2024 11:32	5	DCH	00:00:28.363	00:00:10.007	0	0	53,40224	-299,992	-0,83341	0,83341	-44,9146	44,91455
83	05/11/2024 11:32	5	DCH	00:00:29.361	00:00:11.005	0	0	53,34991	-299,992	-0,91658	0,91658	-49,3538	49,35375
84	05/11/2024 11:32	5	DCH	00:00:30.362	00:00:12.006	0	0	53,29959	-299,987	-1,00008	1,00008	-53,8064	53,80641
85	05/11/2024 11:32	5	DCH	00:00:31.363	00:00:13.007	0	0	53,25531	-299,992	-1,08349	1,08349	-58,2507	58,2507
86	05/11/2024 11:32	5	DCH	00:00:32.363	00:00:14.007	0	0	53,21304	-299,992	-1,16674	1,16674	-62,6825	62,68247
87	05/11/2024 11:32	5	DCH	00:00:33.361	00:00:15.005	0	0	53,17078	-299,992	-1,24999	1,24999	-67,1106	67,11064
88	05/11/2024 11:32	5	DCH	00:00:34.361	00:00:16.005	0	0	53,13455	-299,987	-1,33333	1,33333	-71,5401	71,54013
89	05/11/2024 11:32	5	DCH	00:00:35.361	00:00:17.005	0	0	53,09832	-299,992	-1,41666	1,41666	-75,9665	75,96654
90	05/11/2024 11:32	5	DCH	00:00:36.361	00:00:18.005	0	0	53,05806	-299,992	-1,49999	1,49999	-80,39	80,38997
91	05/11/2024 11:32	5	DCH	00:00:37.359	00:00:19.003	0	0	53,0319	-299,997	-1,58332	1,58332	-84,8104	84,81035
92	05/11/2024 11:32	5	DCH	00:00:38.361	00:00:20.005	0	0	52,99969	-300,003	-1,66666	1,66666	-89,2283	89,22833
93	05/11/2024 11:32	5	DCH	00:00:39.360	00:00:21.004	0	0	52,97151	-299,997	-1,7499	1,7499	-93,6394	93,63941
94	05/11/2024 11:32	5	DCH	00:00:40.360	00:00:22.004	0	0	52,93126	-299,997	-1,83324	1,83324	-98,0522	98,05218
95	05/11/2024 11:32	5	DCH	00:00:41.361	00:00:23.005	0	0	52,91314	-299,992	-1,91665	1,91665	-102,467	102,4665
96	05/11/2024 11:32	5	DCH	00:00:42.362	00:00:24.006	0	0	52,88698	-299,992	-1,99998	1,99998	-106,875	106,8748
97	05/11/2024 11:32	5	DCH	00:00:43.363	00:00:25.007	0	0	52,86081	-299,997	-2,08348	2,08348	-111,29	111,2897
98	05/11/2024 11:32	5	DCH	00:00:44.360	00:00:26.004	0	0	52,83666	-299,997	-2,16656	2,16656	-115,681	115,6805
99	05/11/2024 11:32	5	DCH	00:00:45.361	00:00:27.005	0	0	52,81049	-299,997	-2,24998	2,24998	-120,087	120,0868
100	05/11/2024 11:32	5	DCH	00:00:46.360	00:00:28.004	0	0	52,78634	-299,997	-2,33322	2,33322	-124,482	124,4821
101	05/11/2024 11:32	5	DCH	00:00:47.361	00:00:29.005	0	0	52,7642	-299,992	-2,41664	2,41664	-128,884	128,8844
102	05/11/2024 11:32	5	DCH	00:00:48.360	00:00:30.004	0	0	52,74005	-299,992	-2,50022	2,50022	-133,293	133,2935
103	05/11/2024 11:33	5	DCH	00:00:49.361	00:00:31.005	0	0	52,71992	-299,987	-2,58338	2,58338	-137,679	137,6788
104	05/11/2024 11:33	5	DCH	00:00:50.362	00:00:32.006	0	0	52,69778	-299,987	-2,6668	2,6668	-142,075	142,0754
105	05/11/2024 11:33	5	DCH	00:00:51.362	00:00:33.006	0	0	52,67564	-299,992	-2,74996	2,74996	-146,457	146,4572
106	05/11/2024 11:33	5	DCH	00:00:52.360	00:00:34.004	0	0	52,65551	-299,997	-2,83321	2,83321	-150,841	150,8414
107	05/11/2024 11:33	5	DCH	00:00:53.362	00:00:35.006	0	0	52,63539	-299,992	-2,91671	2,91671	-155,237	155,2373

Figure 4.1: Example of data log from Digatron.

Figure 4.2: Hioki BT3554.
www.hioki.com

4.2 Testing procedures

4.2.1 Charging method

The presence of BMS on lithium batteries makes it crucial to adopt charging algorithms in order to optimise their cycle life and performance.
Many algorithms have been developed, for instance the multistage charging algorithm and the constant current/constant voltage (CC/CV). The latter is the most used and its functioning is relatively simple. A constant current is applied to charge the battery until its voltage reaches a predefined value. Subsequently, a constant voltage is applied and the charging current is exponentially reduced. Finally, the charging process is stopped when the current reaches another predefined value.
These predefined values must be defined after having evaluated all the characteristics of the battery or cell to be charged.

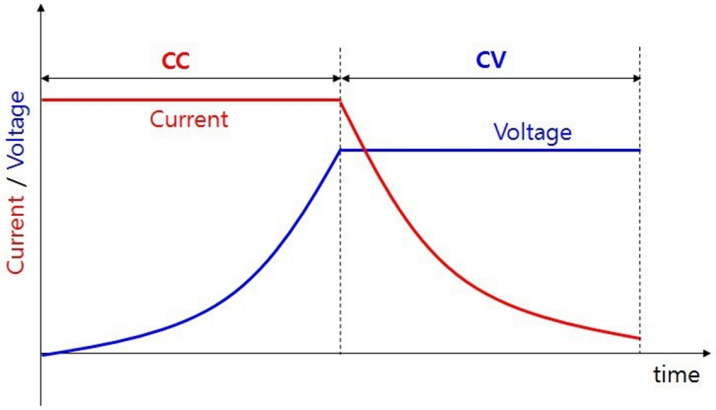

Figure 4.3: CC/CV curve.
www.researchgate.net

During tests performed on 48V 100Ah batteries, the following values are fixed:

- **Constant voltage:** 57.6V
- **EoC current:** 1.5A

Additional parameters must be set in order to minimize risks, such as the maximum charging time, after which the charger independently stops, and the maximum voltage, at which the charger stops due to a probable battery failure.
In general, the lower the charging current, the higher the charging efficiency and battery life.

4.2.2 Discharging method

In contrast to the method previously outlined, using a constant current is preferable to efficiently discharge a lithium battery. This permits to prevent over-current and over-temperature. When the voltage goes below a certain threshold the discharge phase is considered ended and it prevents damages both for the battery and its cells. In fact, if different cells try to provide different current, this can cause unbalance and consequently different levels of charge on them, creating different temperatures within the battery.

4.2.3 Measurement of internal resistance (IR)

Internal resistance of a battery is one of the main parameters to take into account in order to evaluate the health of it.
This resistance is majorly dependant on chemical aspects of production and it influences the performance of a battery. In fact, during discharge, the external voltage measured by tester is dependant on current flowing and internal resistance as showed by the following equation.

$$V_{measured} = OCV - R \cdot I \tag{4.1}$$

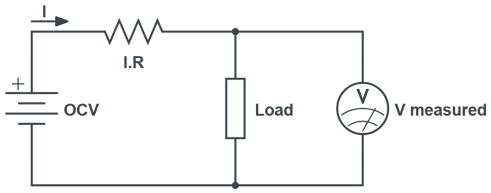

Figure 4.4: General schematic of a battery.

This equation helps to understand the importance of maintaining the value of resistance as low as possible.
A significant problem is related to the numeric evaluation of the resistance because it is not possible to measure it like a simple resistor using a multimeter. Another important aspect is that the resistance varies with the battery's state of charge. This variation occurs because the internal resistance is related to battery chemistry, as explained before. This is the reason why there are two methods to evaluate the resistance. Those methodologies are explained by *Normative IEC 62620*. Those methods are expressed as D.C. resistance and A.C. resistance.

D.C. method: after having discharged the battery to 50% SoC, the following steps have to be performed.

1. Battery is discharged at a constant current I_1 for 30 seconds and value of voltage V_1 is measured.

2. Discharge current is immediately increased to I_2 for 5 seconds and value of voltage V_2 is measured.

Final value of internal resistance is calculated adopting the following equation.

$$IR = \frac{V_1 - V_2}{I_2 - I_1} \tag{4.2}$$

A.C. method: this is the methodology used by Hioki BT3554. The battery is discharged to 50% SoC as in the previous case. After that, an alternating RMS voltage V has to be measured while applying an alternating RMS current I at a frequency of 1kHz to the battery for a period of $1 \div 5$ seconds.
Final value of resistance is derived by a straightforward calculation.

$$IR = \frac{V_{RMS}}{I_{RMS}} \tag{4.3}$$

Note that the alternating current is selected in order to have a peak voltage of maximum 20mV.

Chapter 5

Limit Charge

5.1 Introduction

The following part of this paper moves on to describe in greater detail the limit charge function, which is implemented on the BMS. It is a very important function that is necessary in order to avoid damages and over-current on batteries, especially when they are connected in parallel and they do not have the same voltage. This causes the higher voltage battery to charge the lower voltage battery. The problem is related to the low value of resistance due to cables and internal resistance of batteries. This is a meaningful event even if there is a difference of voltage of some mV, in fact, cable resistances and IR are in the order of few $m\Omega$. This means that even with some mV, lots of Ampere could flow from one battery to the other with risks of damaging the device. This aspect will be analysed in much more details in a following test.
In addition, having a limit charge function is important when a high charging current is applied to a system of few batteries put in parallel. This can cause some unbalances during the final part of charging phase due to batteries' chemical aspects. It may happen that a battery, when fully charged, opens the charging MOSFETs before another one. The problem is that now the total charging current is used to charge the other batteries. If this current is much higher than the construction limit, limit charge takes action and allows the battery to complete the charging phase. By doing this, the BMS does not enter into protection mode and does not stop charging even though maximum charging current is exceeded.
There is also another case in which the limit charge takes action, that is represented by the case in which a battery with low voltage is charged with high current. In this case limit charge reacts and limits the current in order to avoid battery damages due to the fact that at low voltage is more probable that cells are unbalanced and this can cause severe problems to the battery and particular attention has to be paid.
In general, limit charge is a fundamental feature for battery in order to efficiently manage over-currents and unbalances that could affect performance and safety for people and battery itself.

5.2 Testing

In order to have an idea of why such feature is fundamental for the good working of batteries, some tests have been performed on batteries with limit charge implementation and others without it. In order to better understand the following tests, *Supplier A* indicates batteries with limit charge, *Supplier B* indicates batteries that do not integrate such function on its BMS.

5.2.1 Battery without Limit Charge (Supplier B)

In order to clarify the usefulness of implementing a limit charge function on the BMS, some test are performed on batteries that do not include limit charge on their BMS.
Maximum charging current for the battery provided by Supplier B is set to 59A by the manufacturer. When this threshold is exceeded, the charging MOSFETs are opened and the battery does not permit to be charged any more until the alarm is reset.
Initially, a single battery has been tested with a charging current that starts from 25A and reaches 75A.

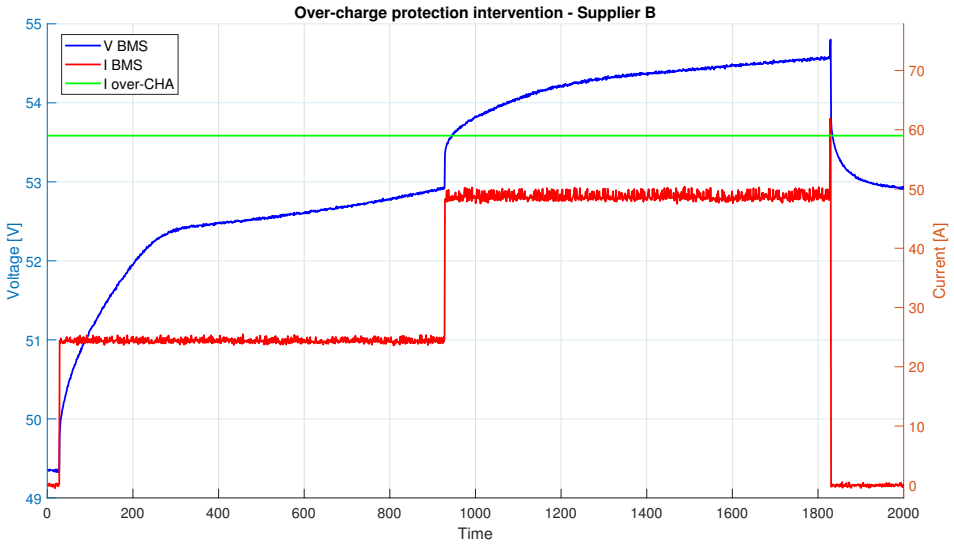

Figure 5.1: Over-charge protection when the threshold is exceeded - Supplier B.

In Figure 5.1 is verified that the battery opens the MOSFETs when the threshold is exceeded and the charging process is stopped, leaving the battery not completely charged causing loss of power.
Another test is performed by using two batteries provided by Supplier B. This test reports the behaviour of the batteries when they are charging at 80A and one battery opens the charging MOSFETs due to over-temperature.
As expected, Figure 5.2 puts in evidence when the over-heated battery opens the MOSFETs, the remaining battery receives all the current provided by the charger (80A) which is much higher than the design threshold. The consequence is that even that battery opens the charging MOSFETs and the process is terminated without having fully charged both batteries.

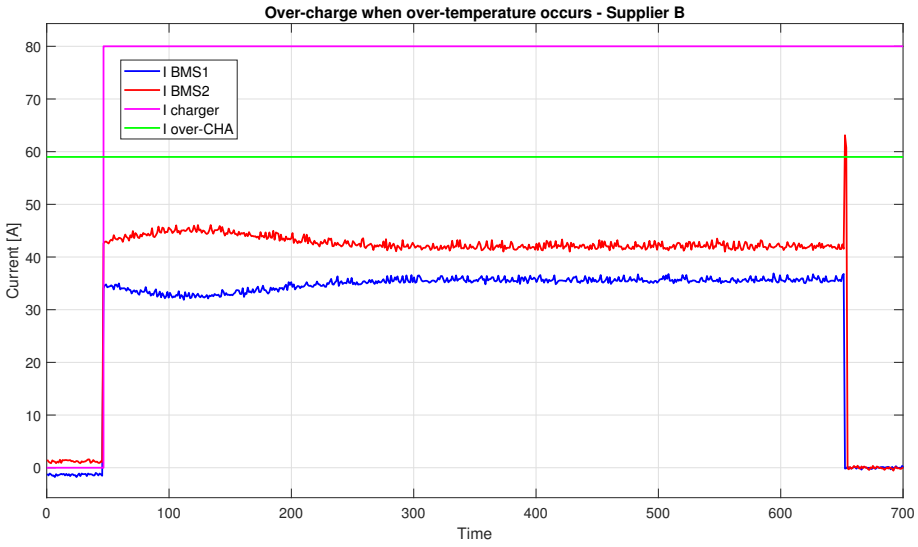

Figure 5.2: Over-charge when over-temperature on one battery occurs - Supplier B.

The difference on charging current that can be noticed in Figure 5.2 is due to the batteries non perfectly balanced.
The effect of over-charge protection in the case of one battery opening the MOSFETs for over-temperature is clarified in Figure 5.3 that reports the zoom of the previous plot.

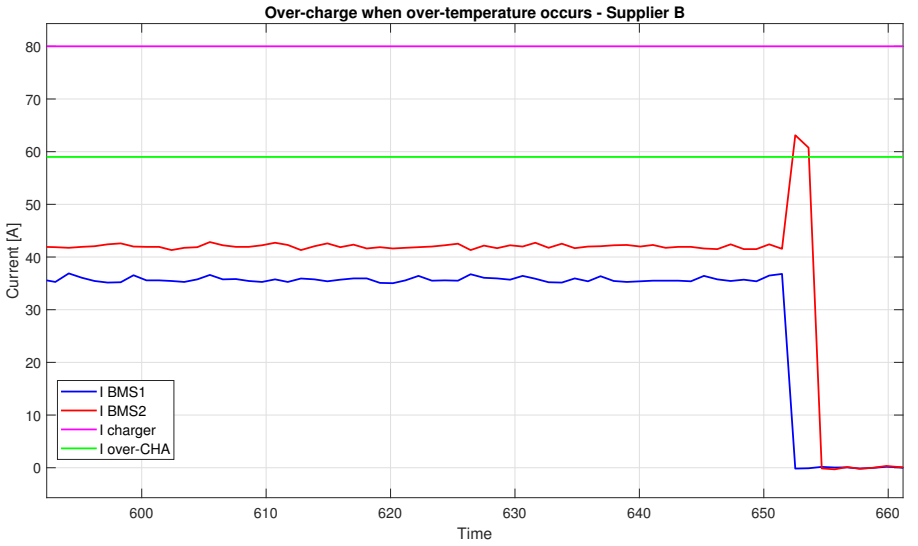

Figure 5.3: Zoom of over-charge protection when over-temperature occurs - Supplier B.

The last test performed has the objective of verifying the behaviour when two batteries at different SoC are charged. The battery with higher SoC maintains the charging MOSFETs open and it is not charged until both batteries reach the same voltage.
The problem of this approach can be identified when the charging current exceeds the threshold imposed by the manufacturer because even the battery with lower voltage opens the MOSFETs and the charging process is stopped causing loss of available energy.

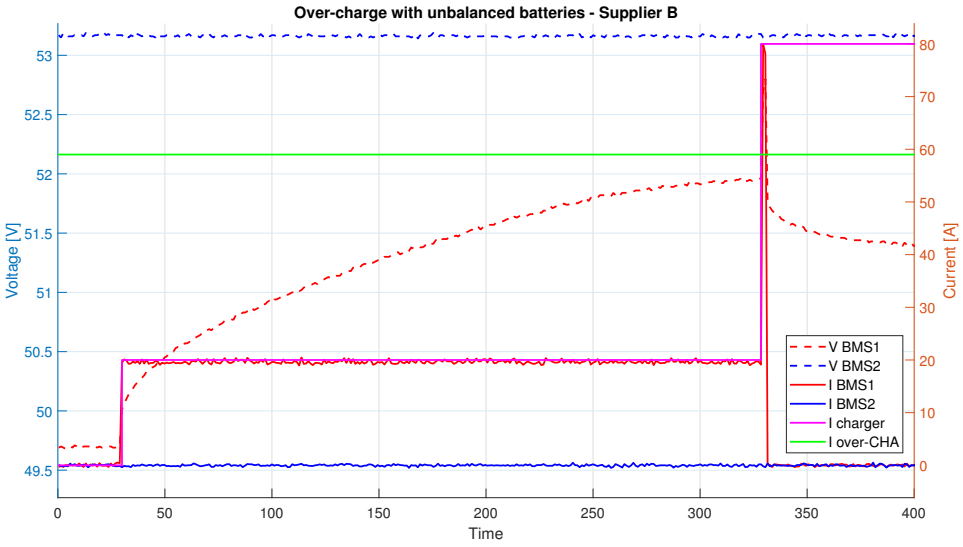

Figure 5.4: Over-charge protection with unbalanced parallel batteries - Supplier B.

The different voltage levels of the batteries can verify the imbalance of them. During the entire charging test performed, the voltages do not reach the same level and the consequence is that all the current flows through the lower voltage battery.
Initially, charging current is set to 20A which is lower than the over-charge threshold current (59A). The lower voltage battery can be charged and the higher voltage battery maintains the MOSFETs open. However, when current is set to 80A the lower voltage battery opens the MOSFETs because of over-charge protection and the charging process is terminated without having fully charged the complete system.
Unfortunately, this is the worst case the system can face because this leads to power loss.
In order to clarify the plot in Figure 5.4 a zoom of the over-charge activation moment is reported.

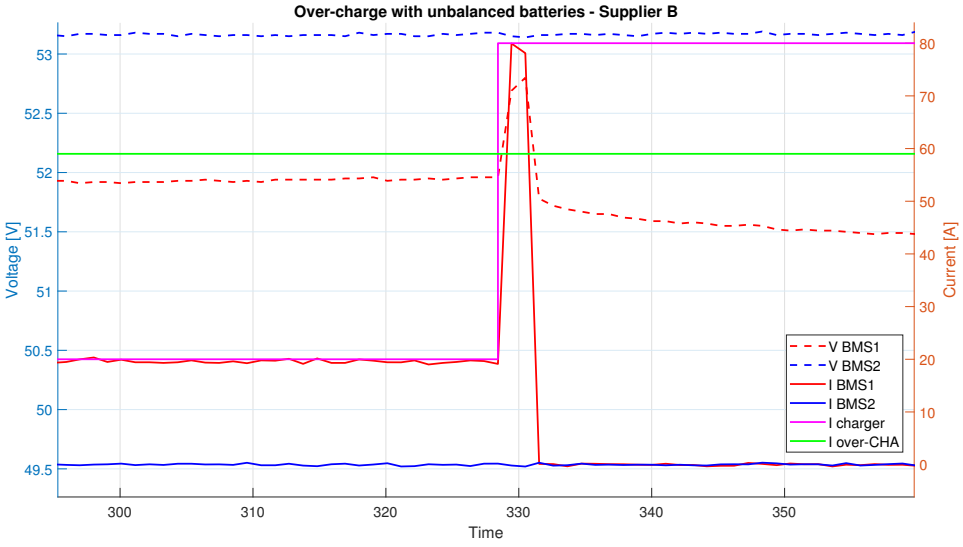

Figure 5.5: Zoom of over-charge protection with unbalanced batteries - Supplier B.

5.2.2 Battery with Limit Charge (Supplier A)

Secondly, some test is performed on batteries that implement limit charge on its BMS. As in the previous case, two batteries with different State of Charge are put in parallel and the behaviour has been observed.

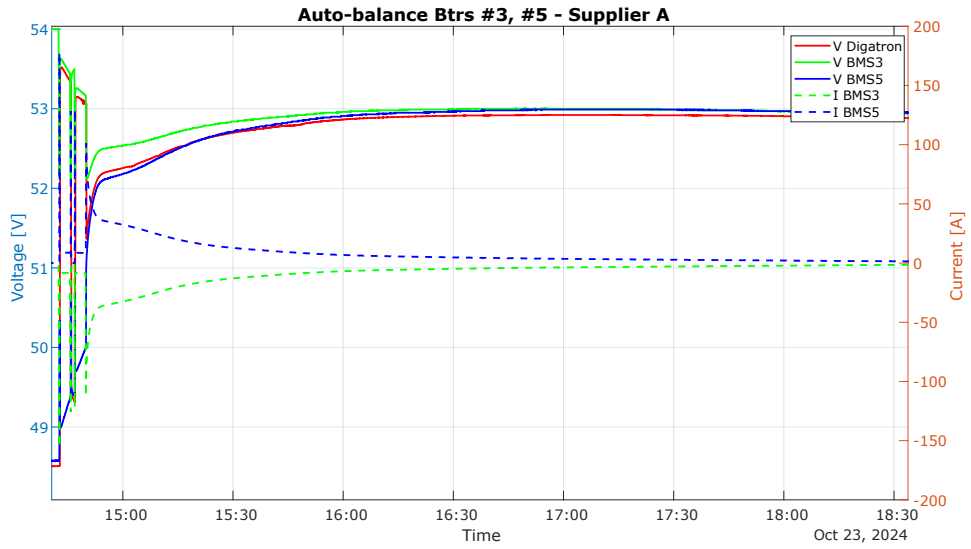

Figure 5.6: Auto-balance of 2 batteries - Supplier A.

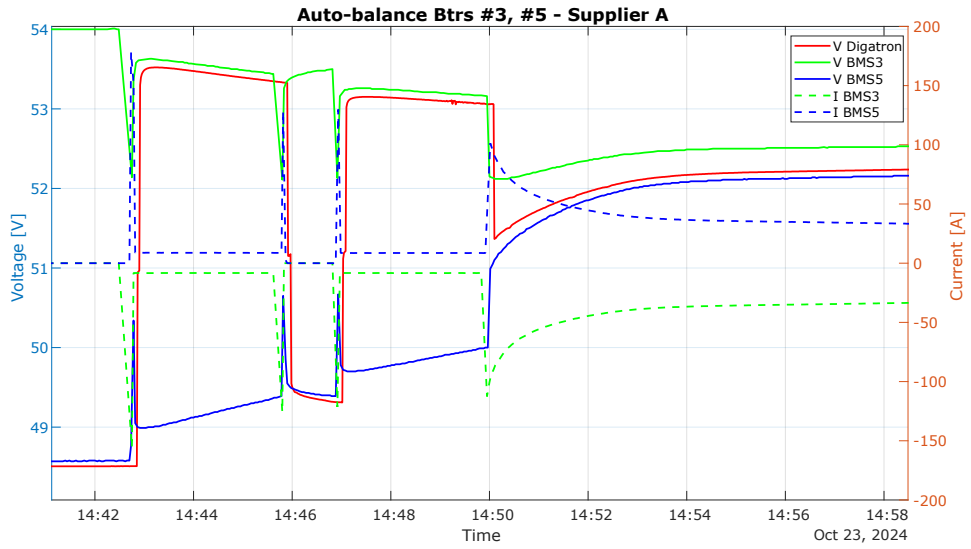

Figure 5.7: Zoom of auto-balance of 2 batteries - Supplier A.

It is important to specify that positive current indicates charging current, while negative current indicates the discharging one.
Figure 5.9 shows that when current exceeds approximately 120A, limit charge function reacts and limits instantly the current to almost 8A. Then, what can be seen in Figure 5.7, is that the limit charge function remains active for 3 minutes. Thereafter, the BMS tries to charge the battery with higher current. However, even though ΔV is reduced, the

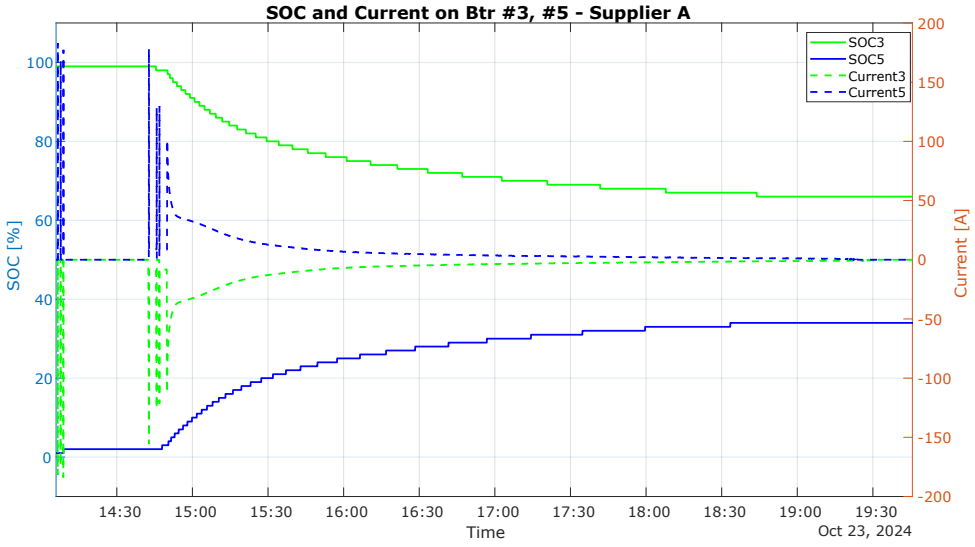

Figure 5.8: SoC during auto-balance of 2 batteries - Supplier A.

1	Recordid	Address	Date_Time	Status	Current_I	M
1004	1003	COM3_5	23/10/2024 14:46	Stand by	0	
1005	1004	COM3_5	23/10/2024 14:46	Stand by	0	
1006	1005	COM3_5	23/10/2024 14:46	Stand by	0	
1007	1006	COM3_5	23/10/2024 14:46	Stand by	0	
1008	1007	COM3_5	23/10/2024 14:46	Charging	129,8	
1009	1008	COM3_5	23/10/2024 14:46	Charging Lmt	8,62	
1010	1009	COM3_5	23/10/2024 14:47	Charging Lmt	8,62	
1011	1010	COM3_5	23/10/2024 14:47	Charging Lmt	8,55	

Figure 5.9: Data of limit charge intervention.

charging current still exceeds previous threshold and must be limited again. The issue is that the manufacturer has imposed a reaction time of 3 seconds for both the limit charge and the over-discharge protection. Consequently, the batteries are in conflict. The higher voltage battery wins the contention and it opens the charging MOSFET, preventing any current to flow through the circuit.
In this case, over-discharge protection remains active for 60 seconds and then MOSFETs are closed again in order to permit the discharging on the other battery.
As in the previous case, current exceeds the threshold of 120A, and limit charge is able to react in time. This limits the current to 8A for 3 minutes.
Finally, when limit charge is deactivated, charging current stays lower compared to the threshold and the batteries are free to exchange the maximum current they can provide and accept in order to balance each other and reach the same voltage.
A similar test has been performed by putting 3 batteries in parallel respectively with 100%, 30% and 0% SoC.

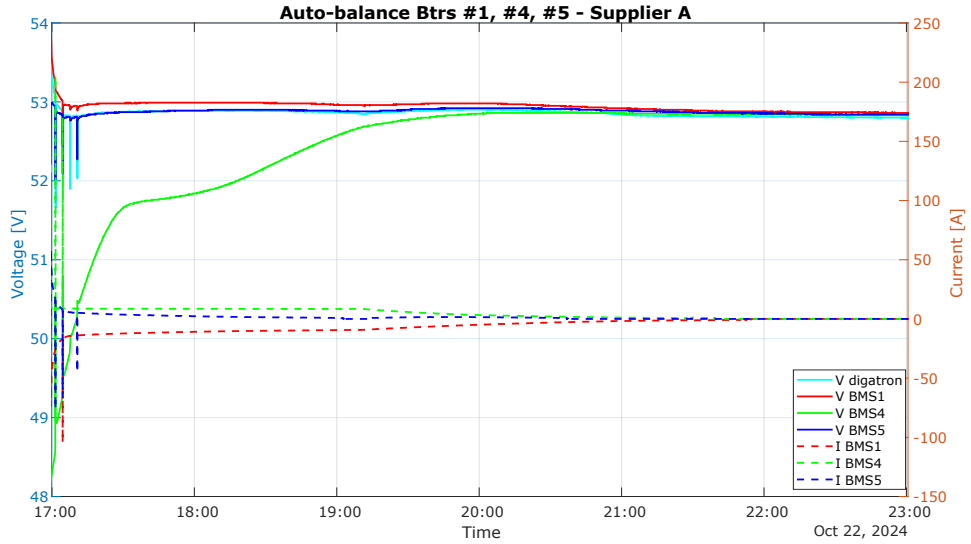

Figure 5.10: Auto-balance of 3 batteries - Supplier A.

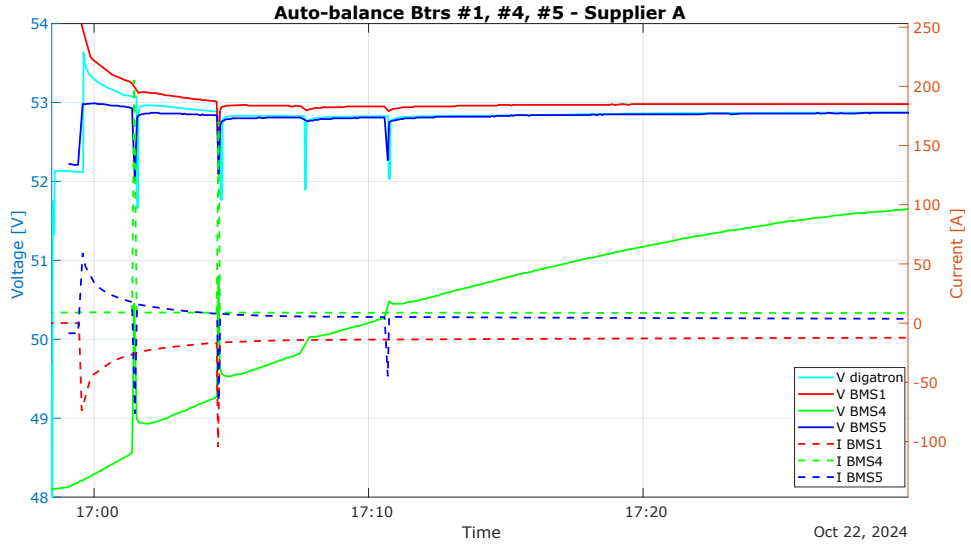

Figure 5.11: Zoom of auto-balance of 3 btrs - Supplier A.

In this case, from Figure 5.11, it is possible to notice that batteries with 100% and 30% can exchange a current that does not exceed the intervention limit of the limit charge. Whereas, the lower voltage battery experiences a charging current that is too high, activating the limit charge. After 5 attempts to charge the battery with total current, the BMS is programmed to maintain limit charge active until the end of the charging process. In addition, from Figure 5.8 is clear that the aim of the limit charge is not to equalise the SoC of all the parallel-connected batteries, as this would overly complicate the system. Instead, the primary objective of this feature is to equalise the voltage of the parallel batteries so as to prevent over-current from flowing through the entire system.

Chapter 6

System design

After having outlined the benefits of introducing limit charge function inside BMS in order to avoid over-current and over-temperature that can damage irreparably the batteries, a possible solution to implement such function is described in the following paragraphs.
Initially, a choice of possible circuits capable of limiting current flowing has been performed.
In fact, the simplest solution could be the introduction of a series resistor between charger and battery that needs to be charged. However, it is not the most appropriate solution because it leads to loss of power and high increase in the temperature of the system. This means that one of the main problems outlined previously is not solved and other efficiency problems are highlighted.
As a result, the best choice for reducing current flowing into the system is to adopt a buck DC-DC converter with current mode controller.
Buck converter is the best choice because it has high efficiency and low power losses. In fact, compared to series resistor, with this solution it is possible to modulate the current absorbed by the battery even with voltage variation of the battery. This is crucial because as the battery is charged, its voltage increases. By adopting a series resistor, the modulation of current is not achieved.
This is the reason why buck converter is adopted and in order to regulate the current, an average current control loop is introduced, which is composed by a comparator with a reference current and a PI controller that is able to modulate the duty cycle of the switching MOSFET.
In the following paragraphs the schematic and the steps performed in order to design the system are reported.

6.1 Simulink

In order to simulate the behavior of the system, a comprehensive model has been implemented using Simulink.
The following sections will provide a detailed explanation and design for each component of the model.

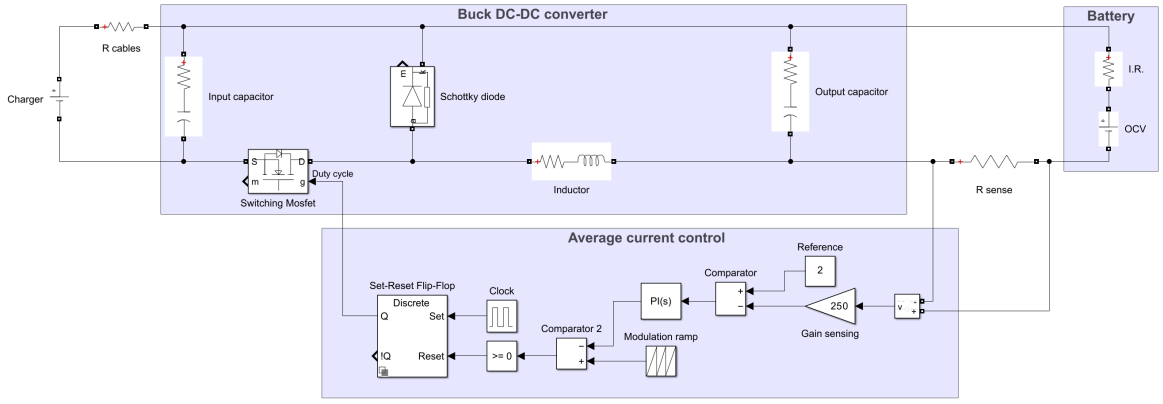

Figure 6.1: Simulink model.

6.1.1 Buck DC-DC converter

A buck converter, also known as step-down converter, is one of the most commonly used circuits.
It is designed to produce a lower, constant output voltage compared to the input voltage, even if the input voltage varies over time if properly controlled.

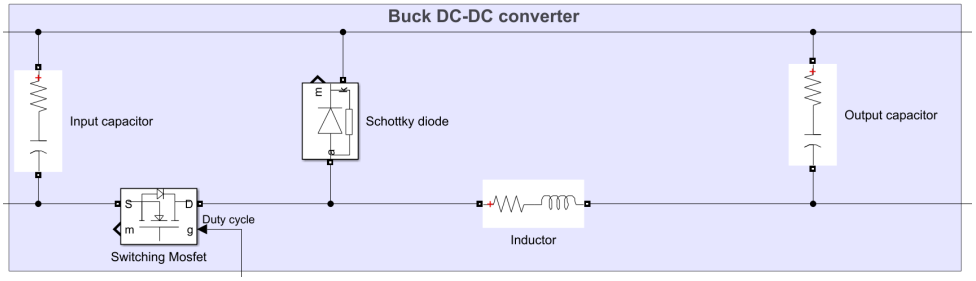

Figure 6.2: Buck DC-DC converter.

The modulation of output voltage is performed by imposing a specific duty cycle to the switching MOSFET placed at the input of the converter.
In fact, by switching on and off the MOSFET, the inductor is respectively charged and discharged. This permits to obtain a modulation on the output.
By observing Figure 6.3, it can be noticed that rising slope corresponds to the on time of the switch and negative slope corresponds to the off time of the switch. The following equations help to understand better the relationship between inductor current and output voltage.

$$\Delta I_L = \frac{(V_{in} - V_{out}) \cdot t_{on}}{L} = \frac{V_{out} \cdot t_{off}}{L} \tag{6.1}$$

By evaluating $V \cdot s$ balancing it is possible to derive the relationship between input and output voltage in continuous conduction mode (CCM), when inductor current does not reach 0A.

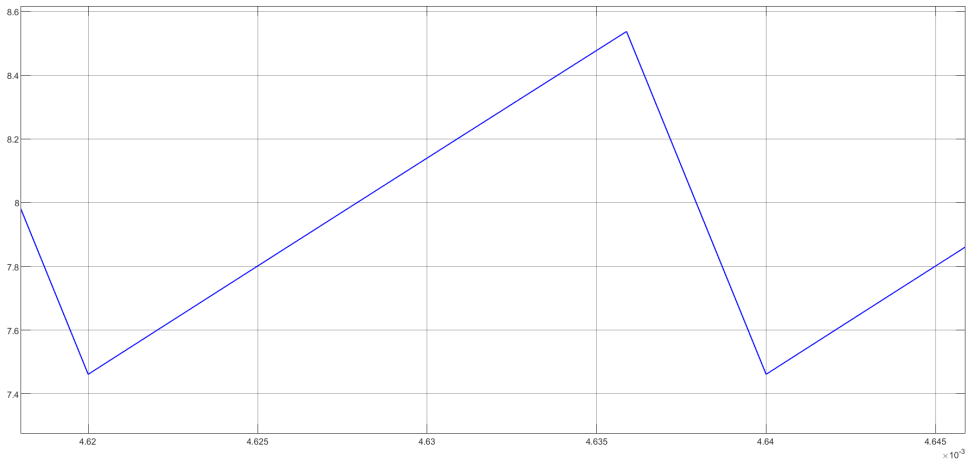

Figure 6.3: Inductor current during switching.

$$\begin{aligned} (V_{in} - V_{out}) \cdot t_{on} &= V_{out} \cdot t_{off} \\ V_{in} \cdot t_{on} &= V_{out} \cdot (t_{on} + t_{off}) \\ \frac{V_{out}}{V_{in}} &= \frac{t_{on}}{T_s} = \delta \end{aligned} \tag{6.2}$$

The study moves on to size the components of the buck converter.
Because of the fact that output voltage is imposed by the battery, duty cycle is straightforward and it changes during the charging phase.
Consequently, in order to choose the value of the inductor, it is necessary to impose the switching frequency and the wanted ΔI_L.
By design choices:

- $f_s = 50kHz$
- $\Delta I_L = 1A$

In order to obtain $\Delta I_L < 1A$ it is necessary to use δ_{min} for the derivation of L.

$$\begin{aligned} \delta_{min} &= \frac{V_{out\_min}}{V_{in}} = \frac{44.8V}{57.6V} = 0.78 \\ L &= \frac{V_{in} \cdot \delta_{min} \cdot (1 - \delta_{min})}{\Delta I_L \cdot f_s} = 200\mu H \end{aligned} \tag{6.3}$$

Due to supplier availability, purchased inductor for the prototype has been $L = 175\mu H$.
Design of output capacitor has been performed by imposing $\Delta V_{out} = 0.01V$.

$$C = \frac{\Delta I_L}{8 \cdot \Delta V_{out} \cdot f_s} = 250\mu F \tag{6.4}$$

Final capacitor purchased for the prototype has been $C = 220\mu F$.

6.1.2 Average current control

Modulation of duty cycle in order to obtain average current of 8A is performed by an average current control.

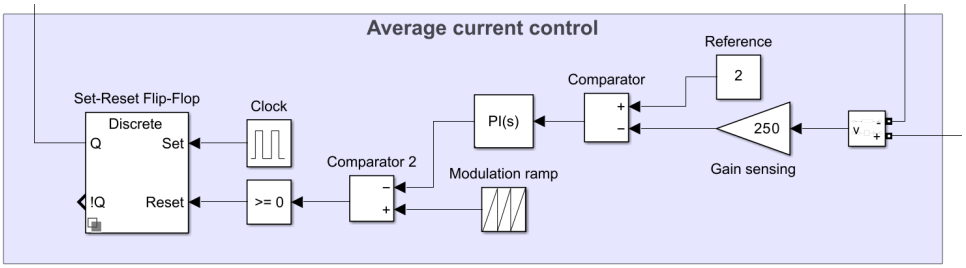

Figure 6.4: Average current control.

The controller, initially, has to amplify the value of voltage obtained by the current flowing through the sensing resistor. This resistor is chosen in a way that, with 8A flowing through it, voltage obtained after the amplification is equivalent to 2V. This is the reason why reference voltage for the comparison done before the PI controller is set to 2V.
The amplification performed before the comparison is sized in the following way, after having imposed the sensing resistor to $1m\Omega$.

$$\begin{aligned} \Delta V_{sense} &= R_{sense} \cdot I = 1m\Omega \cdot 8A = 8mV \\ Gain &= \frac{V_{ref}}{\Delta V_{sense}} = \frac{2V}{0.008V} = 250 \end{aligned} \tag{6.5}$$

The difference between V_{ref} and V_{gain} corresponds to the deviation between the reference value and the desired one (V_{error}).
This signal is then introduced into a PI controller that has the duty of providing a modulation signal (m) to the next comparator.
PI controller is composed by two fundamental parameters.

- Proportional K_P
- Integrative K_I

These parameters describe the behaviour of the controller and, consequently, of the system. The equation that describes how the PI controller works is the following.

$$m = K_P \cdot V_{error}(t) + K_I \cdot \int V_{error}(t)dt \tag{6.6}$$

Proportional parameter multiplies the instant error in order to have a fast response of the controller. The problem is that, whether it is used alone, it is not able to cancel the error, otherwise the output signal would start from zero again.
Therefore, it is necessary to introduce an integrative parameter.
Integrative parameter executes a integral of the instant error along time. This is very useful because it permits to cancel the error at regime and to maintain the output signal around the desired value.

A comparison between a modulation ramp and the output of the PI controller permits to reset a flip flop that drives the switching MOSFET. This means that when the value of the modulation ramp exceeds the average value of the PI controller, the switching MOSFET is turned off.

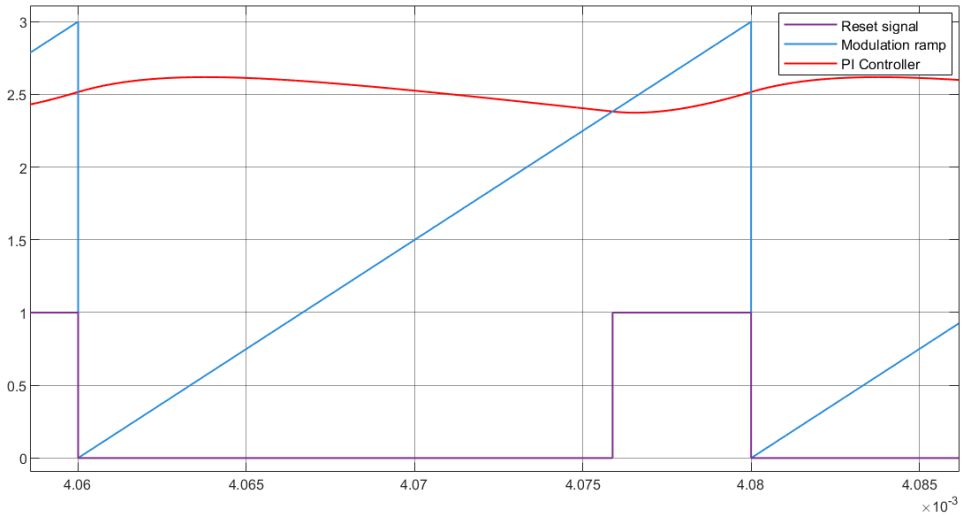

Figure 6.5: Modulation signal, modulation ramp and reset signal.

In order to turn on the MOSFET, a clock signal at a frequency of 50kHz is applied to the set input of the flip flop.
PI parameters have to be tuned in order to obtain the desired behaviour. A bode analysis has been performed by evaluating the transfer functions of the system blocks.

6.1.3 Bode analysis

By evaluating the block diagram of the system, it is possible to derive the equations that describe the behaviour of inductor current compared to the duty cycle.

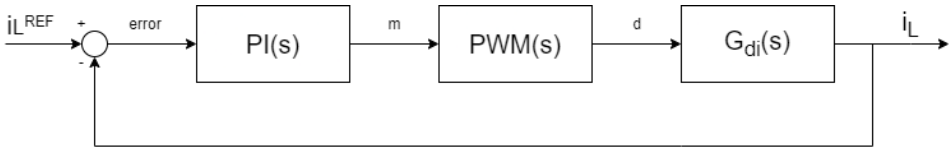

Figure 6.6: Current control loop.

From the block diagram in Figure 6.6, it is possible to notice that it is necessary to derive the equation of $G_{\delta i_L}(s)$ and $PI(s)$ in order to define the current control behaviour.
By analysing the buck converter, it is possible to obtain the variation of inductor current compared to the duty cycle's variation.

$$\begin{cases} L\frac{d\overline{I_L}}{dt} & = \overline{\delta} \cdot \overline{V_{in}} - \overline{V_o} \\ C\frac{d\overline{V_o}}{dt} & = \overline{I_L} - \overline{I_o} \end{cases} \tag{6.7}$$

By adopting small signal analysis ($\overline{X} = X + \hat{x}$). Where X represents the steady state variable and $\hat{x}$ refers to the small signal one.

$$\begin{cases} sL\widehat{i_L} &= \left(D + \hat{\delta}\right) \cdot (V_{in} + \widehat{v_{in}}) - (V_o + \widehat{v_o}) \\ sC\widehat{v_o} &= I_L + \widehat{i_L} - I_o - \widehat{i_o} \end{cases} \tag{6.8}$$

By considering $\widehat{v_{in}} = 0$, the equivalent circuit can be derived from the following equation.

$$\begin{cases} sL\widehat{i_L} &= \hat{\delta} V_{in} - \widehat{v_o} \\ sC\widehat{v_o} &= \widehat{i_L} - \widehat{i_o} \end{cases} \tag{6.9}$$

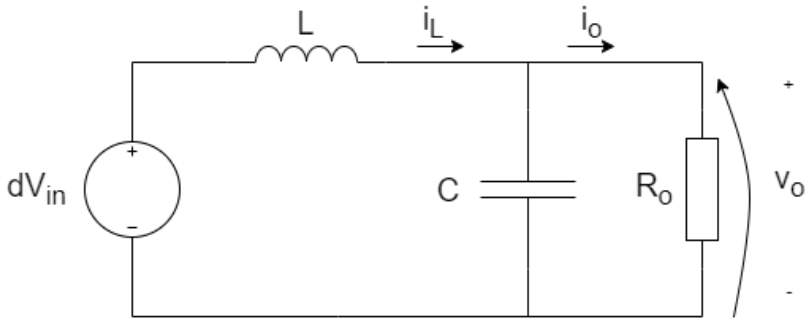

Figure 6.7: Equivalent scheme with small signal analysis.

It is then possible to derive the transfer function of $G_{\delta i_L}(s)$.

$$G_{\delta i_L}(s) = \frac{\widehat{i_L}}{\hat{\delta}} = \frac{V_{in}}{R_o} \cdot \frac{1 + sCR_o}{1 + s\frac{L}{R_o} + s^2 LC} \tag{6.10}$$

This means that the variation of inductor current compared to duty cycle presents a zero and a complex conjugate pole.

$$\begin{aligned} \omega_z &= \frac{1}{CR_o} = 378.8 krad/s \\ \omega_p &= \frac{1}{\sqrt{LC}} = 5 krad/s \end{aligned} \tag{6.11}$$

By analysing the bode diagram of the transfer function, reported in Figure 6.8, it is possible to notice that the amplification at ω_s (switching frequency) is almost equal to 0dB. This means that a signal at that frequency is not attenuated by the system. Consequently, the system is sensitive to noise.
For this reason, it is then necessary to analyse the behaviour of PI controller, which is described by the following equation.

$$PI(s) = K_P + \frac{K_I}{s} = \frac{K_I}{s} \cdot \left(1 + s\frac{K_P}{K_I}\right) \tag{6.12}$$

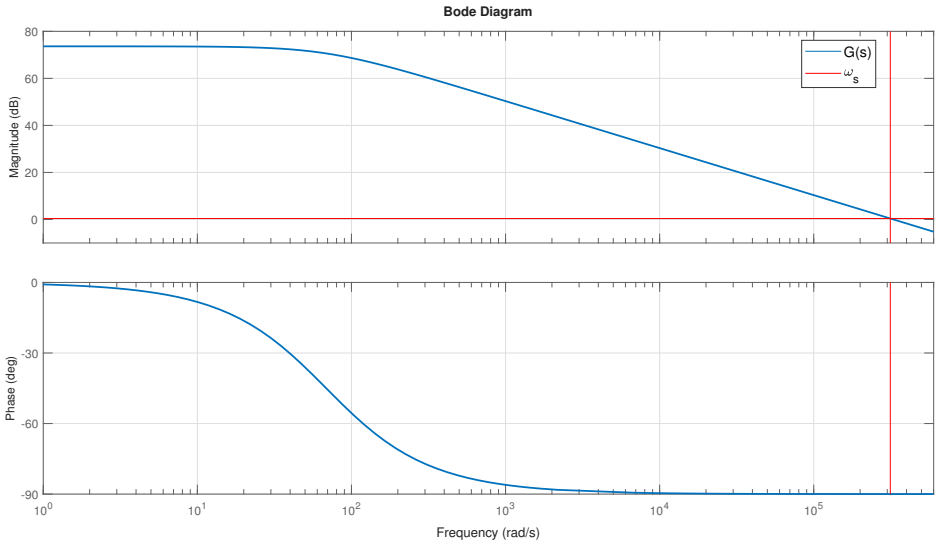

Figure 6.8: Bode diagram of $G_{\delta i_L}(s)$.

On the other hand, PI parameters have to be designed to attenuate noise signals, however it is also important that the regulator is able to let the system reach the desired output current in reasonable time.
Therefore, PI parameters are designed in a way that the gain of the system is 0dB at $\omega_c = 60krad/s$, which is almost $0.2 \cdot \omega_s$.
It is then possible to obtain the final transfer function of the open loop current control.

$$\begin{aligned} T(s) &= PI(s) \cdot PWM(s) \cdot G_{\delta i_L}(s) \\ &= \frac{K_I}{s} \cdot \left(1 + s\frac{K_P}{K_I}\right) \cdot \frac{1}{3} \cdot \frac{V_{in}}{R_o} \cdot \frac{1 + sCR_o}{1 + s\frac{L}{R_o} + s^2 LC} \end{aligned} \tag{6.13}$$

By imposing $K_P = 0.5$ and evaluating the module of the system at $\omega_c = 60krad/s$, it is possible to derive the value of K_I, starting from equation 6.13, that permits to reach the design choices.

$$K_I = \left[\left(\frac{3 \cdot R_o}{V_{in}} \cdot \frac{\left|1 + j\omega_c \frac{L}{R_o} + (j\omega_c)^2 LC\right|}{|1 + j\omega_c CR_o|}\right) - K_P\right] \cdot \omega_c = 16200 \tag{6.14}$$

Subsequently, it is possible to plot the bode diagram of the regulated system.
Figure 6.9 makes it clear that the system is stable and it is able to reach the desired current reference.
This can be achieved because ω_c (crossover frequency) is less than ω_s (switching frequency). Subsequently, all the harmonics are attenuated and the system can guarantee high gain at lower frequency in order to reach the reference current.
It is also important to take into account the phase of the system. In fact, at ω_c, phase margin is almost equal to 60° and this means that the system is stable.
After that, it is possible to evaluate the behaviour of the system by simulations performed on Simulink. In particular, the behaviour of inductor current is reported in order to verify the good functioning of limit charge.

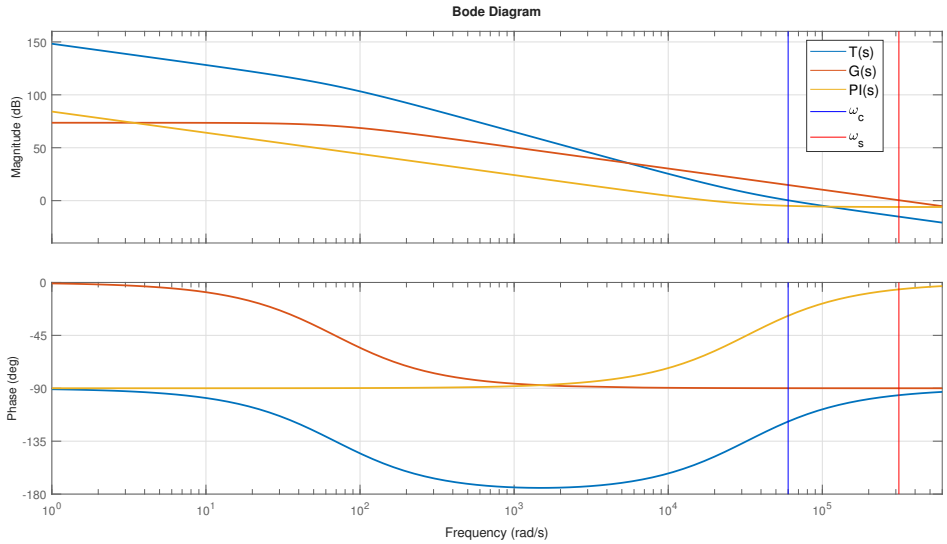

Figure 6.9: Open loop bode diagram of current loop control.

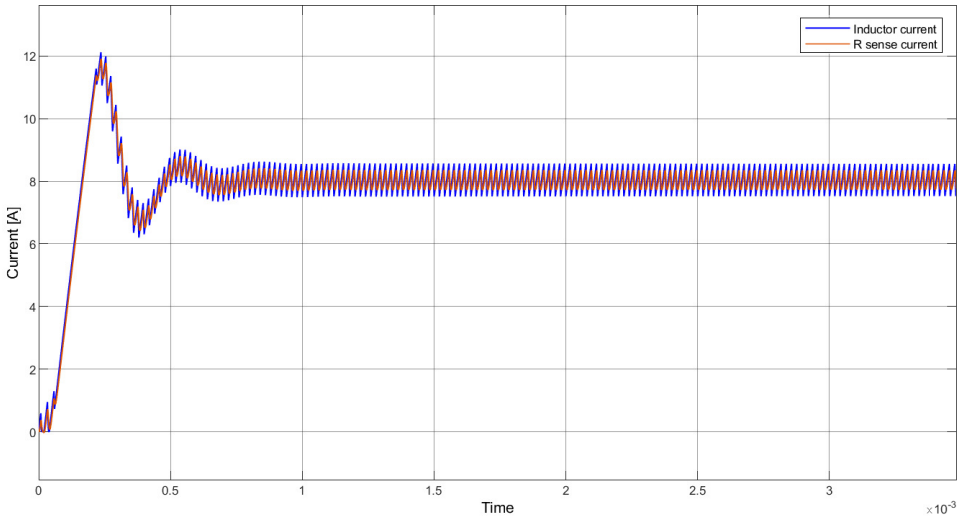

Figure 6.10: Inductor current with $K_P = 0.5$ and $K_I = 16200$.

What can be clearly seen in Figure 6.10 is the little overshoot and some oscillations which are present before the system is able to stabilize current to the desired one.
This is the reason why the trial and the error method is adopted for the evaluation of the best regulator parameters to obtain a better current behaviour.
Final values for PI regulator are $K_P = 0.6$ and $K_I = 3000$.
The behaviour of the inductor current is reported in Figure 6.13 and it is possible to notice that the current is able to reach the desired value without any overshoot or oscillations.
Final bode diagram of the system is then evaluated.
Figure 6.12 reports the characteristic of the closed loop current control which is described by the following equation.

$$G_{cl}(s) = \frac{T(s)}{1 + T(s)} \tag{6.15}$$

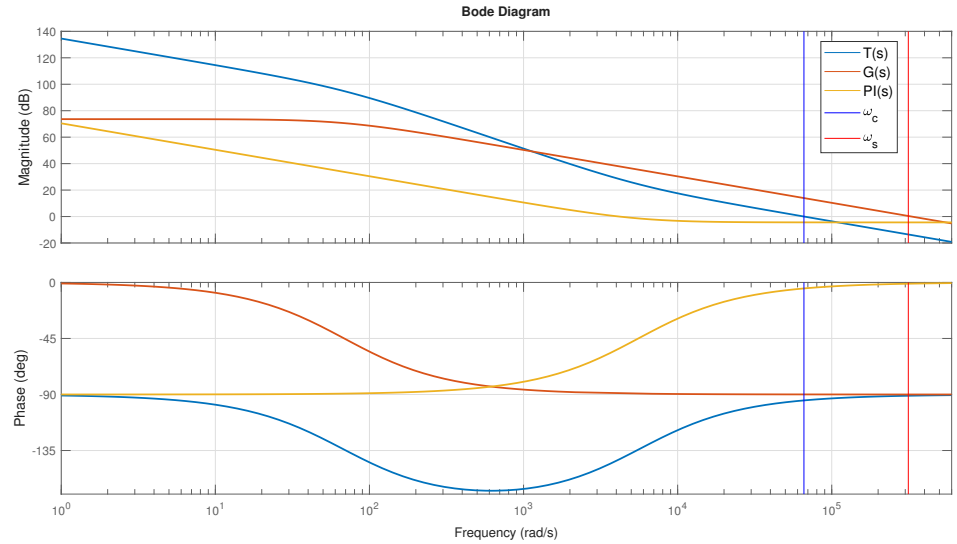

Figure 6.11: Final open loop bode diagram of current control.

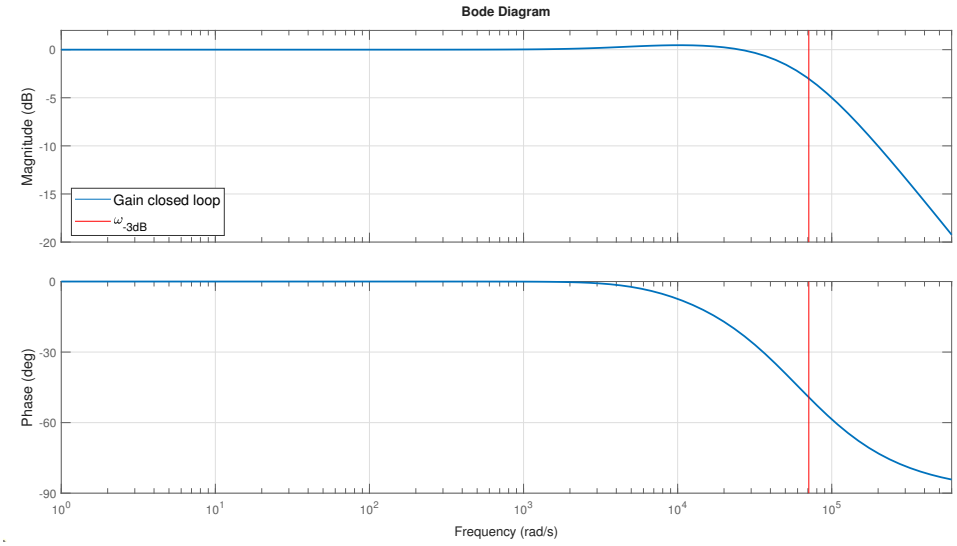

Figure 6.12: Closed loop bode diagram of current loop control.

As a consequence, it is possible to notice that the gain is almost 0dB for all the bandwidth, while the angular frequency at -3dB is almost equal to 70krad/s ($\approx 11kHz$) which is much less than the switching frequency.
Gain equal to 0dB means that the system is able to reach the reference current.

$$i_L = \frac{T(s)}{1+T(s)} \cdot i_L^{REF} = 1 \cdot i_L^{REF} \tag{6.16}$$

6.1.4 Results

Finally, after having dimensioned all the parts of the system, a simulation is performed in order to verify the good functioning of the circuit.

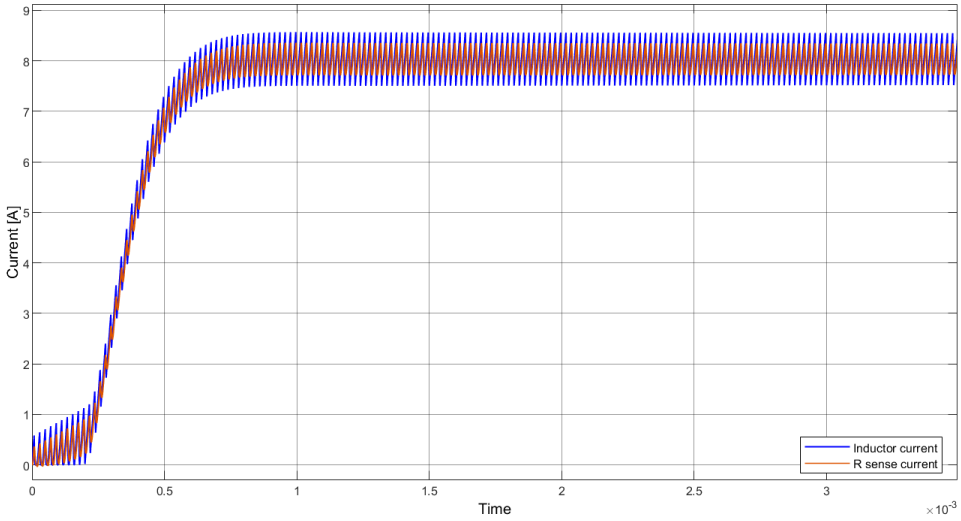

Figure 6.13: Inductor's and sense resistor's current on Simulink.

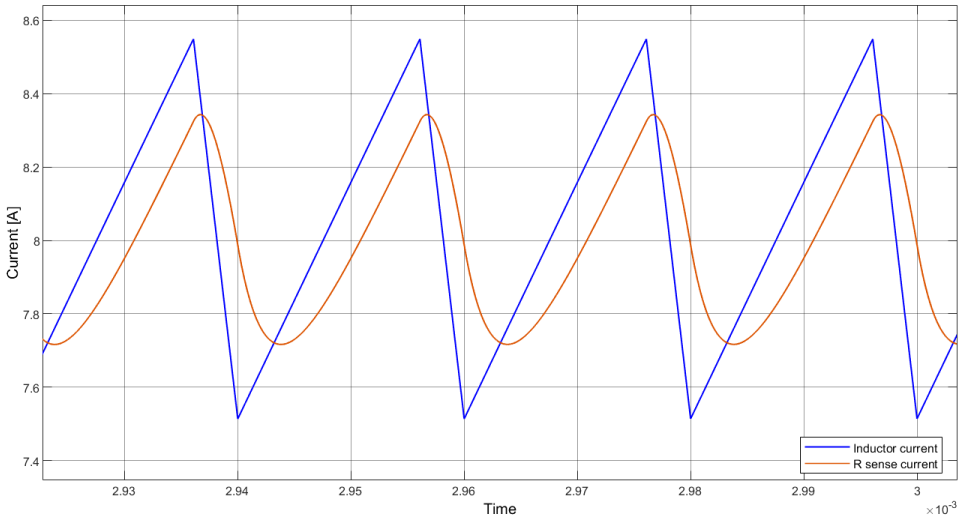

Figure 6.14: Zoom of inductor's and sense resistor's current on Simulink.

By evaluating Figure 6.13, it is possible to notice that inductor current reaches the desired value of 8A in almost 1ms. This is a good result because this application does not need fast rising time.
In addition, Figure 6.14 confirm the design expectations made in Section 6.1.1. In fact, ΔI_L is approximately equal to 1A as the specifications reported before.
The difference between inductor current and sense resistor current corresponds to the current flowing through the capacitor in order to maintain an almost constant output voltage.

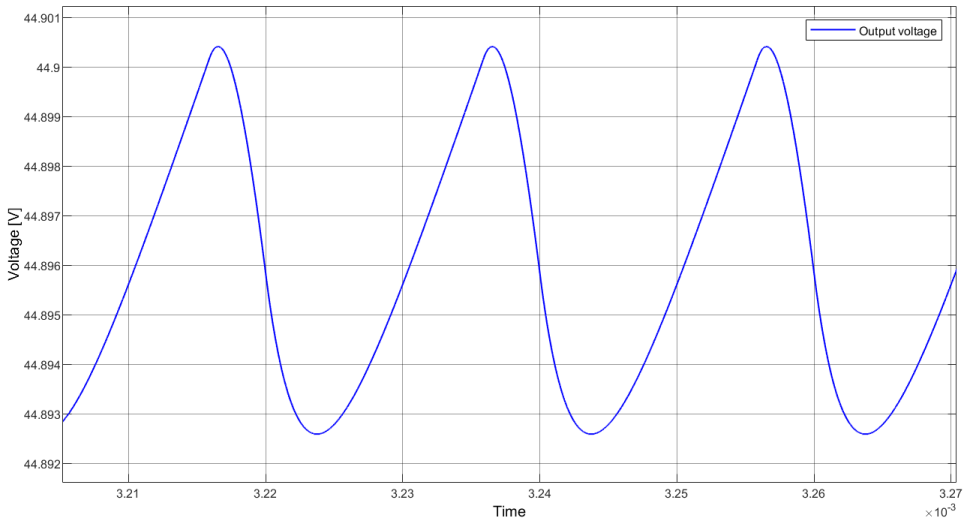

Figure 6.15: ΔV_{out} on battery with OCV equals to 44.8V on Simulink.

As in the case of inductor current, specifications are matched by evaluating ΔV_{out} reported in Figure 6.15. In fact, ΔV_{out} is approximately equal to 8mV.
For completeness, the behaviour of the system during a complete charge of a battery from 44.8V to 57.6V has been verified too.

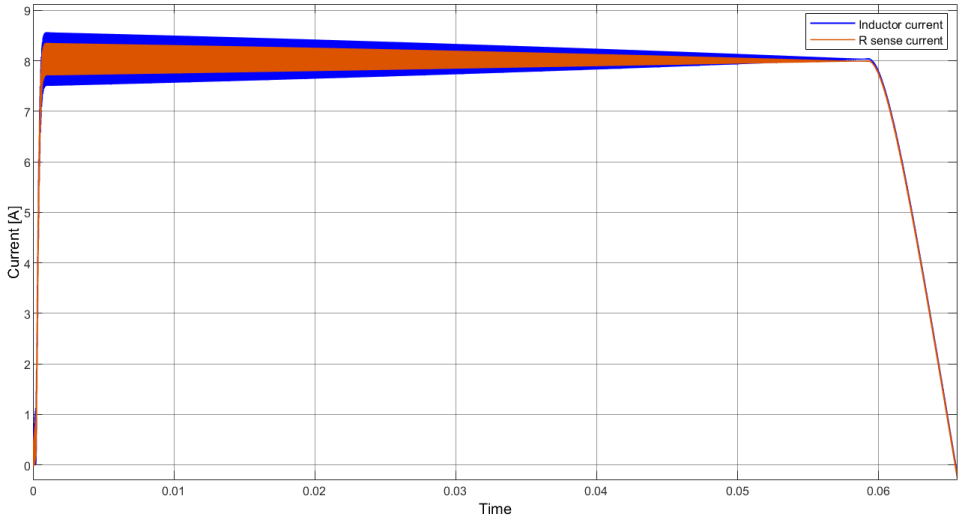

Figure 6.16: Inductor's and sense resistor's current during full battery charge on Simulink.

From Figure 6.16, it possible to notice that when output voltage increases, ΔI_L decreases. This can be verified by evaluating equation 6.1.
The graph also highlights that the drop of current is due to the fact that there are some impedance along the circuit. In fact, when output voltage reaches a value that permits to flow a current lower than 8A, the controller is not able to modulate the current any more until the battery is completely charged.

6.2 LTSpice

Having discussed how to develop the model of the circuit on Simulink, it is necessary to simulate the behaviour by using almost real components, in order to implement the previously tested limit charge feature in an effective way.

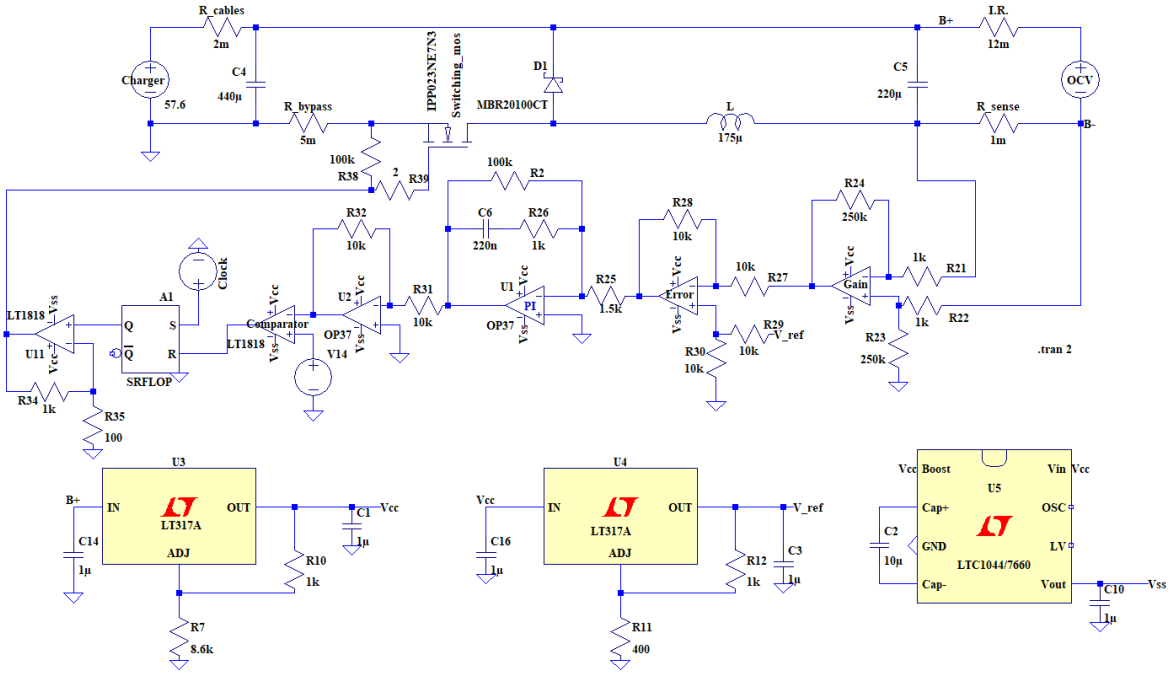

Figure 6.17: LTSpice schematic.

Figure 6.17 shows the schematic derived from the model implemented in Figure 6.1. The main parts have been converted into real components configuration, as reported below.

- Differential amplifier
- PI controller
- Inverting amplifier
- Comparator
- SR flip flop
- Voltage regulator
- Charge pump

As a matter of fact, a differential amplifier with gain derived from equation 6.5 is used, in order to measure the voltage provided by R_{sense}.

This amplification permits to obtain a voltage that is comparable with the reference voltage, which corresponds to the voltage needed on R_{sense} to reach 8A flowing on the circuit.
The difference $V_{error} = V_{ref} - V_{sense}$ is performed to obtain the error signal that corresponds to the deviation of the instant flowing current compared to the desired one. The circuit used to derive the error signal is again a differential amplifier with $Gain = 1$.
Subsequently, the error signal is introduced to the PI controller which generates the modulation signal as the output.
PI controller amplifier configuration is composed of two parts, the former performs the instant amplification of the error (K_P parameter) and the latter has the duty to perform the integration in time of the instant error (K_I parameter) to obtain the modulation signal without any deviation to the suitable one so as to generate the desired duty cycle. The equations that describe the behaviour of PI controller are reported as follows.

$$\begin{aligned} G_{PI}(s) &= -\frac{Z_2}{Z_1} = -\frac{R_2 + \frac{1}{sC}}{R_1} = -\frac{\frac{sCR_2+1}{sC}}{R_1} = -\frac{sCR_2+1}{sCR_1} \\ &= -\frac{R_2}{R_1}\left(\frac{sCR_2+1}{sCR_2}\right) = -K_P\left(\frac{sT_I+1}{sT_I}\right) \\ K_P &= -\frac{R_2}{R_1} = 0.6 \rightarrow R_1 = 1.5k\Omega;\ \ R_2 = 1k\Omega \\ K_I &= \frac{K_P}{T_I} = \frac{1}{CR_1} = 3000 \rightarrow C = 222nF \end{aligned} \tag{6.17}$$

From the fact that PI controller generates a negative signal, it is necessary to introduce an inverting amplifier with $Gain = 1$, in order to obtain the desired modulation signal.
This signal is then compared with a ramp signal and the comparison generates a signal which corresponds to the flip flop's reset. This process is the same reported in Figure 6.5.
Duty cycle can be derived by the ratio of the amplitude of modulation signal and the amplitude of ramp signal.

$$\delta = \frac{m}{V_{ramp}} \tag{6.18}$$

Duty cycle signal is then used to modulate the switching MOSFET with the aim of obtaining the desired current as final result.
Voltage regulators are also used because all the operational amplifiers need a supply voltage of 12V and this voltage is obtained from battery voltage as in real condition.
Voltage regulator is also used to generate the reference voltage used to control the current flowing through the system. This means that it is necessary to obtain a voltage as precise as possible and with very reduced oscillations.
The equation which permits to obtain the desired output voltage is the following one.

$$V_{out} = 1.25V\left(1 + \frac{R_2}{R_1}\right) \tag{6.19}$$

For the good functioning of the circuit it is necessary to provide also a negative voltage supply to the operational amplifiers. This is the reason why a charge pump component is used to generate -12V.

The functioning of the component is simple, it uses a *flying capacitor* that is alternatively charged by an input voltage at +12V and then discharged to the output capacitor in a way that it is flipped to obtain the inverting effect. The result is that a negative output voltage (-12V) is obtained starting from a positive one (+12V).

6.2.1 Results

The following paragraph of this paper moves on to report and analyse in greater detail the results of the simulation.

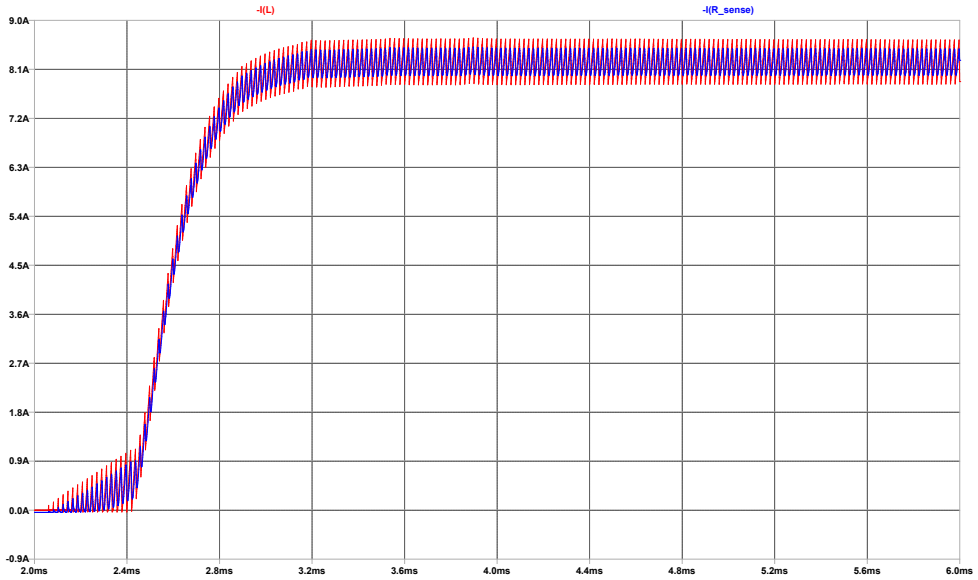

Figure 6.18: Inductor's and sense resistor's current on LTSpice.

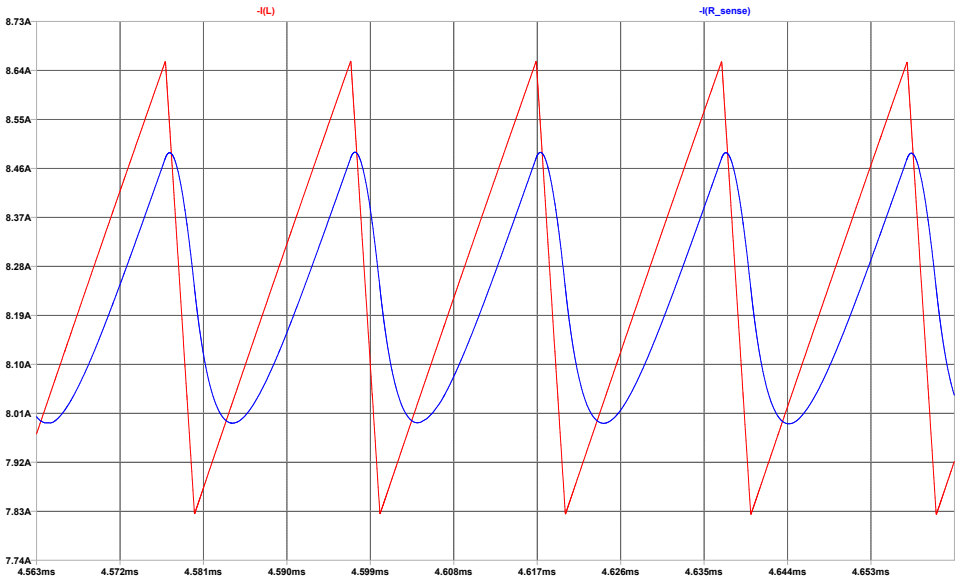

Figure 6.19: Zoom of inductor's and sense resistor's current on LTSpice.

Figure 6.18 confirm that the general behaviour of the system is almost the same as in Simulink model.
In fact, average inductor current is very close to 8A and, from Figure 6.19, ΔI_L is similar to the value calculated in equation 6.1.
As a confirmation of the system's good functioning, the plots obtained from Simulink and LTSpice simulations (Figures 6.13 and 6.18) are practically the same. The only differences are due to possible losses resulting from the real components' behavior used in the LTSpice model. For instance, initially, the inductor current does not start to grow rapidly as in the Simulink model, because the system starts from zero. Inductor and output capacitor need time to reach the desired operating point, such as the PI controller. In fact, due to the capacitor of PI regulator, duty cycle is a little bit lower and it causes the inductor to operate in discontinuous conduction mode (DCM) before capacitor (integrative part) takes action and PI is then able to supply the right duty cycle to the switching MOSFET.

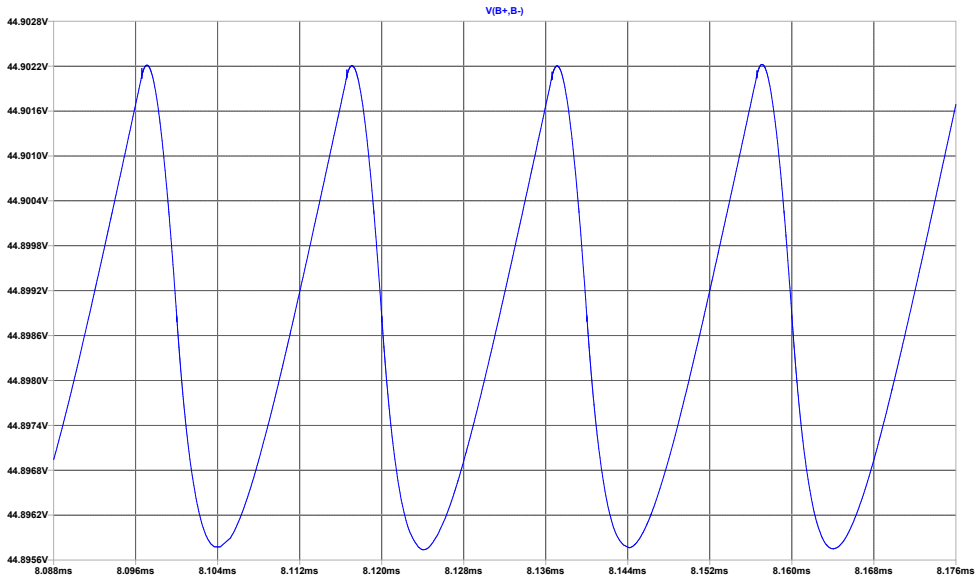

Figure 6.20: Output voltage on LTSpice simulation.

Figure 6.20 highlights that the output voltage is almost the same as in the Simulink model reported in Figure 6.15.
In fact, ΔV_{out} is similar to the one calculated from theoretical aspects.
It has to be taken into account even the fact that average voltage on the output of the battery is almost 44.9V because, as showed in Figure 4.4, there is a series resistor that corresponds to the internal resistance of the battery. This resistor has been imposed to $12m\Omega$ because it is a common value on that type of battery.
Consequently, the output voltage is increased by the voltage on that resistor caused by the flow of current.

$$\overline{V_{out}} = OCV + R \cdot \overline{I} = 44.8V + 12m\Omega \cdot 8A \approx 44.9V \tag{6.20}$$

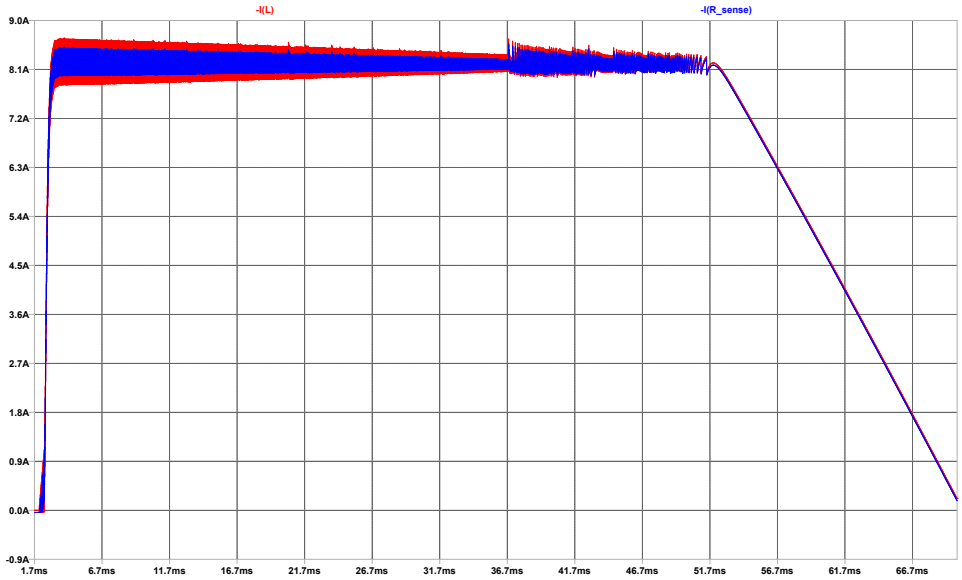

Figure 6.21: Inductor's and sense resistor's current during full battery charge on LTSpice.

As in Simulink model, a full battery charge simulation has been performed starting from LTSpice model.
What emerges from the results reported here is that current is constantly modulated at 8A until battery voltage reaches a value that does not permit charge limiter current to flow and it depends only on parasitic resistances present through the system. The current is constantly decreasing because of ΔV reduction between charger voltage and battery voltage.
What is interesting to notice in Figure 6.21 is that, at some point, the current is not precisely modulated any more. This is due to the fact that the system works at high duty cycle and this causes the modulation signal to exceed the maximum amplitude of ramp signal. As a result, switching MOSFET remains closed for another period. This effect does not create relevant problems because in this specific application the charge limiter does not require very precise current and very fast response. Nevertheless, the average current remains at 8A even though the current is not properly modulated. As a consequence, the only noticeable effect is related to the increase of ΔI_L.
From Figure 6.22, it is possible to observe the behaviour. In fact, when current decreases, both the error compared to the desired value and the modulation signal increase. The problem is that during the following period the modulation signal is always higher than the ramp one. This causes the switching MOSFET to remain closed. On the other hand, the current increases and the error signal decreases until modulation signal is lower than the ramp one and it causes the MOSFET to open.
In the figure, modulation has not been performed for two time periods, however it is verified that the system is able to auto-regulate itself to obtain an average current of 8A.

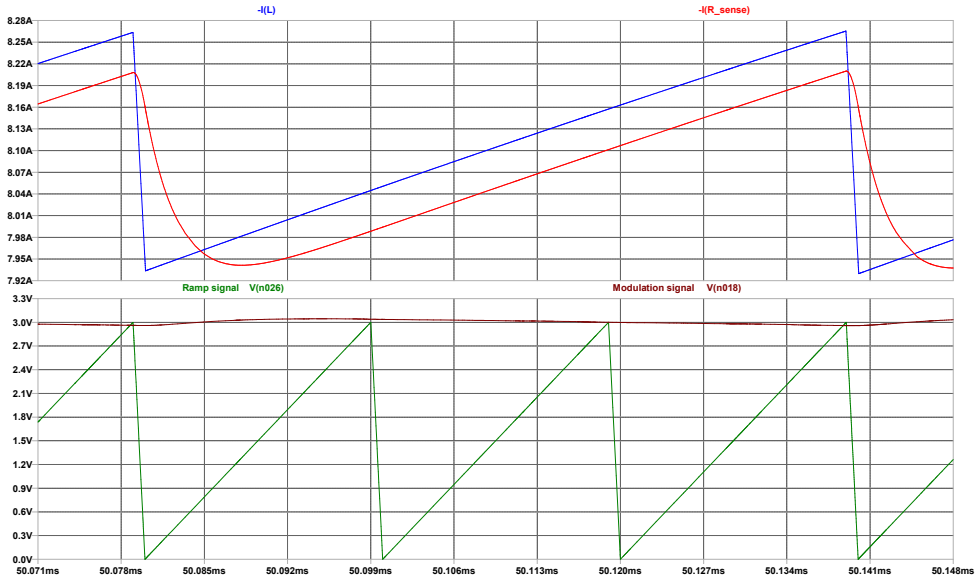

Figure 6.22: Not optimal modulation of current.

6.3 Final schematic

The working principles are the same as the ones reported in Figure 6.17. The only differences regard the generation of modulation signal which is managed by a TL494. This component is able to generate a sawtooth signal (carrier) by selecting a resistor and a capacitor to obtain the signal at the desired frequency.
This component is also internally composed by two operational amplifiers, whose outputs are then compared with the carrier signal in order to drive the output signal.
For clarifying the previous aspects, a functional block diagram of TL494 is reported below.

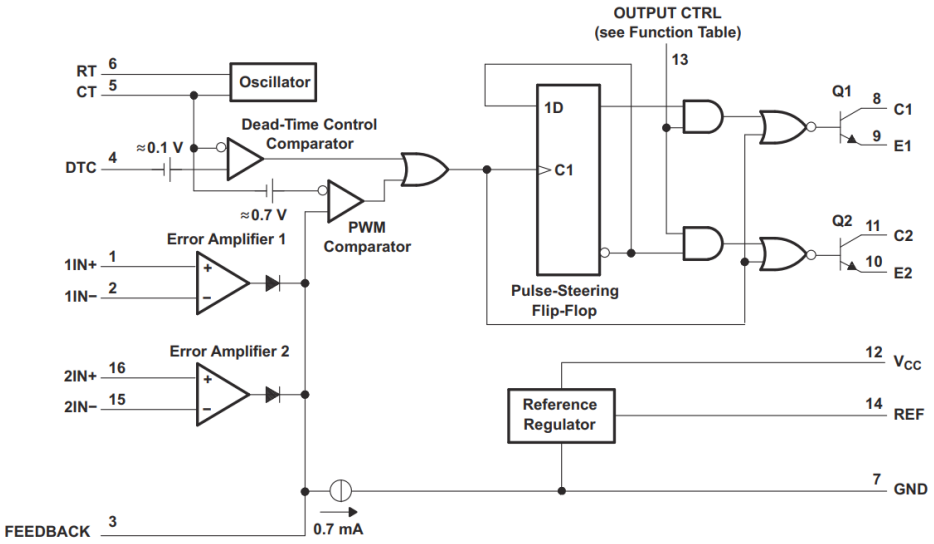

Figure 6.23: Functional block diagram of component TL494.
www.ti.com

Another difference to the LTSpice schematic is related to the presence of charge, discharge and pre-discharge MOSFETs. These MOSFETs are responsible for the normal charging and discharging operations.
In fact, when normal charge is working, the enable signal is off and the current is able to flow through the discharge and charge MOSFETs in order to bypass the buck converter. However, when the limit charge function is activated, charge MOSFET is switched off and the current is forced to flow through the buck converter and the system limits the charging current.
Two op-amp comparators are introduced to detect when the charging current exceeds some predefined thresholds before activating the limit charge function.
The driving signals for the MOSFETs are managed by a microcontroller (STM32 Nucleo-64) which detects when the current exceeds the thresholds and then it switches the status of the output pins. Those pins are then connected to the gate drivers because the Nucleo-64 is not able to provide enough power to the MOSFETs.
In the following chapter, the study analyses how the microcontroller manages all the possible charging situations.

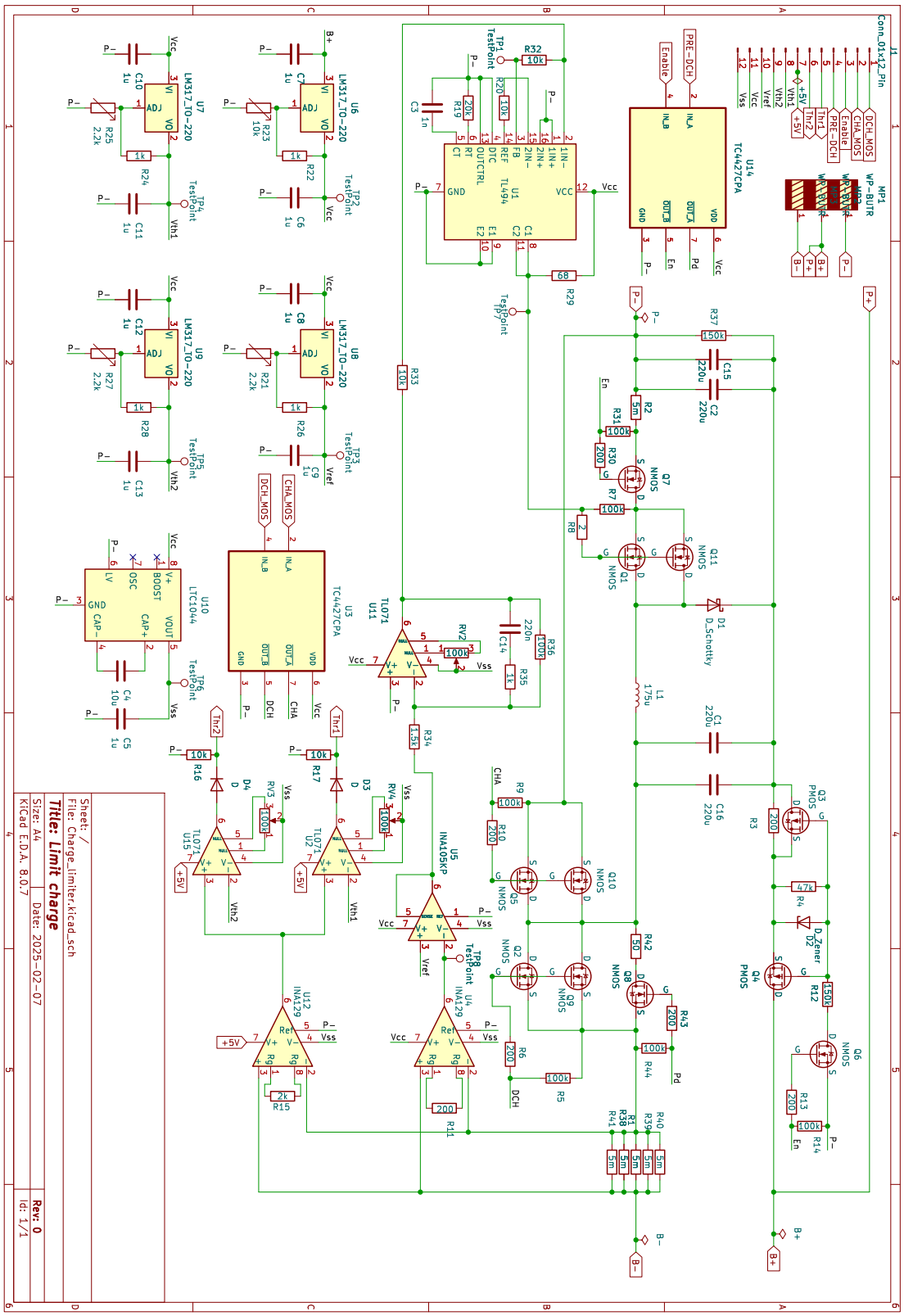

Figure 6.24: Complete schematic realized with KiCAD.

Chapter 7

Implementation

7.1 Real-Time Operating System (RTOS)

The following section moves on to describe in greater detail the implementation of a Real-Time Operating System (RTOS), which is essential for the overall system's control. This type of operating system permits to manage different *tasks*, and each task is executed in a way that apparently seems real-time. This effect is created by the fact that all the tasks are executed in parallel.
Practically, each task is a segment of code to which a priority is assigned. Priorities goes from *Low* to *High*. This means that when two tasks with same priority want to operate, one of them is executed for a fixed time and then, by context switching, it is suspended and preserved, then the other task can be executed. The process is repeated and permits to manage the execution of different tasks in an efficient way instead of waiting for the end of each task. The method which permits this operation is called *Round Robin*.

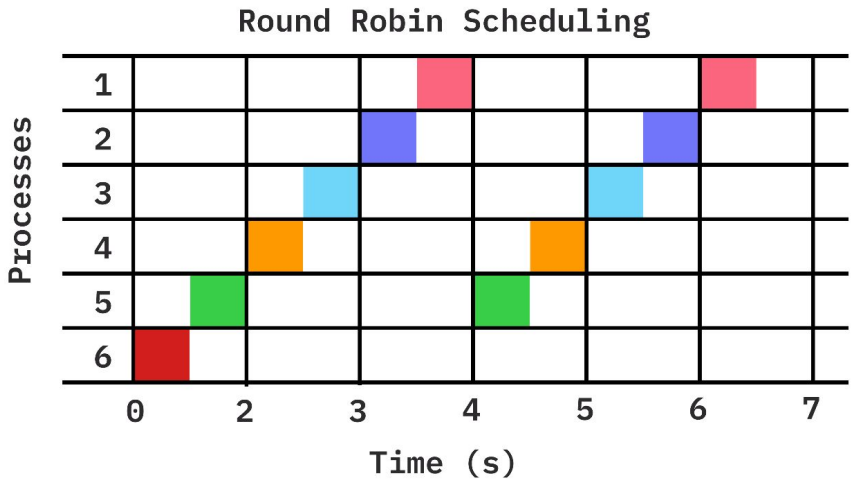

Figure 7.1: Round Robin scheduling with six equal priority tasks.
www.hackernoon.com

In the case where those two tasks have different priorities, if the one with lower priority (Task 1) is being executed and the one with higher priority (Task 2) wants to operate,

Task 1 has to be suspended in order to let Task 2 to be executed. As in the previous case, during context switching, Task 1 is saved and suspended, allowing Task 2 to operate until it completes its instructions, unless other tasks with the same or higher priorities need to take action. This process follows a *Priority preemptive* scheduling.

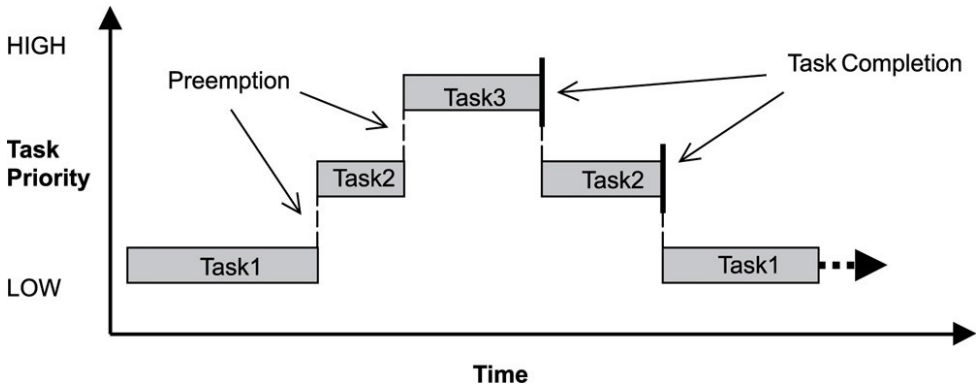

Figure 7.2: Priority preemptive scheduling with different priority tasks.
www.linkedin.com

Another useful function that RTOS implements, is the *Semaphore*.
Semaphores are used to synchronise tasks with other events. Practically, a task waits for a token before its execution. The token is released by a task when a specific condition is verified and the waiting task is ready to execute. Otherwise, the task remains in a blocked state.
There are two types of semaphores, which are mentioned and described below:

- **Binary:** simple on/off mechanism
- **Counting:** each time a token is released, the counter increments, and when a token is used that counter decreases

The instruction that releases the token allowing the task to be executed is *osSemaphoreRelease()*. While the instruction used to wait the releasing of a token is *osSemaphoreWait()*.

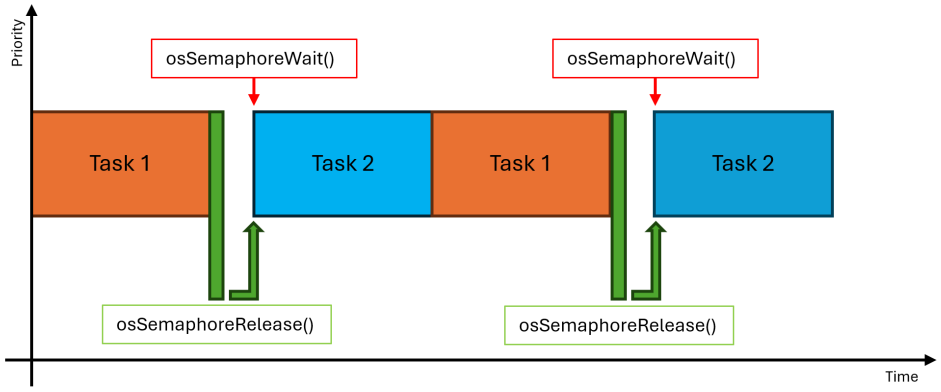

Figure 7.3: Example of Semaphore scheduling with two tasks.

7.1.1 STM32 Nucleo-64 board

The microcontroller used to implement the RTOS is a STM32 Nucleo-64 produced by STMicroelectronics.

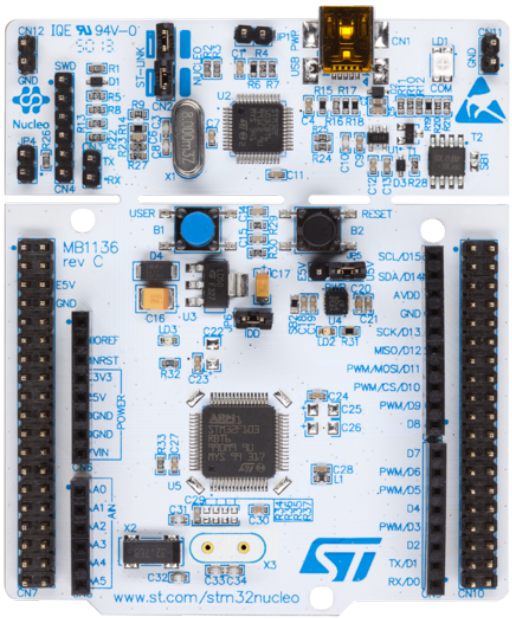

Figure 7.4: STM32 Nucleo-64 board.
www.st.com

This board is very powerful and it is part of STM32 family. STM32 indicates 32-bit microcontroller integrated circuits and they use ARM processor core, such as Cortex-M0, Cortex-M3, Cortex-M7, and so on.
They are internally composed of ARM processor core, flash memory, static RAM, debugging interface, and other peripherals.
Most of the boards are also Arduino pin-compatible which allows the user to use Arduino peripherals.
One of the most most commonly used boards for building prototypes is the Nucleo family board.
They can be found in different layouts and characteristics, for example Nucleo-32, Nucleo-64 and Nucleo-144. The number next to the name indicates the amount of pins that compose the board. Other differences can be found on clock frequency and memory size. However, this project will focus on the Nucleo-64 board.
This board is widely used because of its balance between performance and power consumption. In addition, it integrates the ST-LINK debugger/programmer which makes the programming and debugging phase simpler because it does not require other components. Programmers can also rely on a wide range of comprehensive, free software libraries and examples available in the STM32Cube environment.

The main features of Nucleo-64 are reported below:

- 32.768 kHz crystal oscillator
- 72 MHz Cortex-M4 core
- 3 LEDs: 1 user LED, 1 power LED and 1 communication LED
- 1 user and 1 reset push buttons
- Arduino Uno V3 expansion connector
- ST morpho extension pin headers
- ST-LINK USB or external sources power supply (3.3V, 5V, 7-12V)
- ST-LINK debugger and programmer
- 64 KB flash memory
- 16 KB SRAM

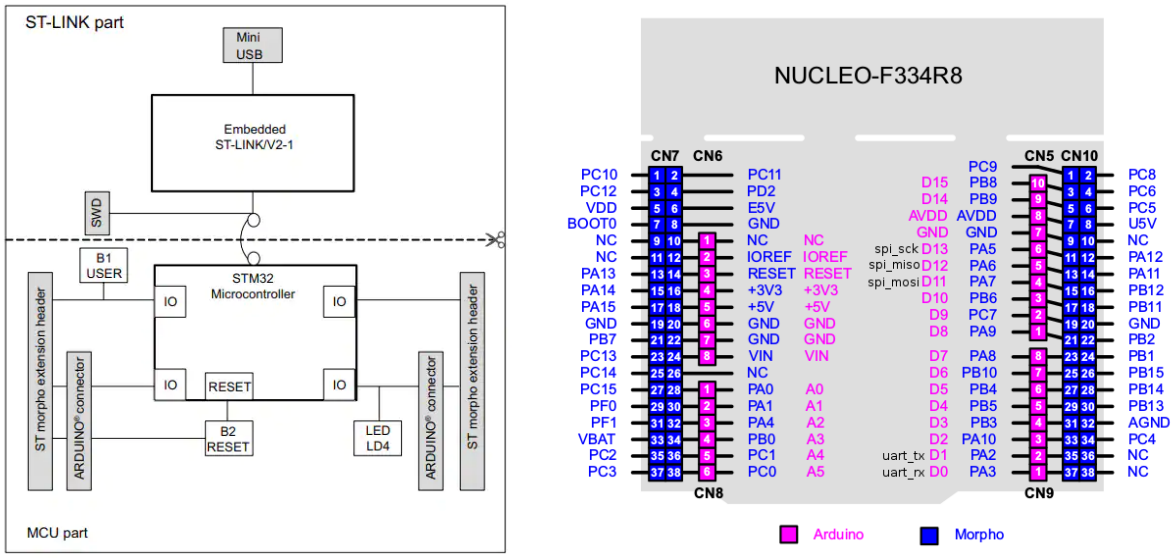

Figure 7.5: Nucleo-64 block diagram and pinout.
www.st.com

One of the main parts of the board is the set of I/O pins, which are essential for controlling and interacting with the external environment.
For this objective, Nucleo-64 uses general purpose input/output (GPIO) pins. Those pins do not have specific purposes and they are customizable by the programmer.
In fact, pin mode has to be configured, such as input or output, analog or alternate function (AF). They can also be configured with pull-up or pull-down resistors already integrated in the board.

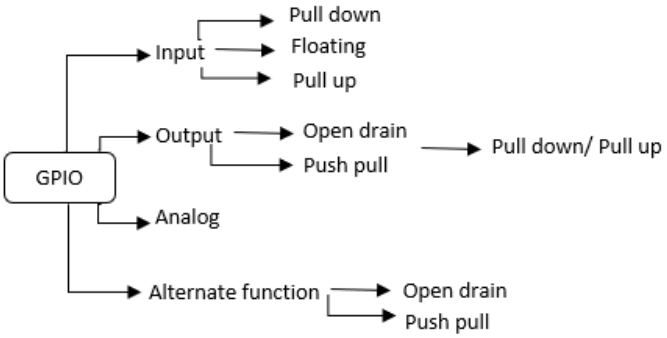

Figure 7.6: GPIO pin possible configurations.
www.wiki.st.com

7.1.2 STM32CubeIDE

With respect to the microcontroller, it also needs to be programmed. Therefore STMicroelectronics has developed a software ecosystem which allows users to configure all the board's peripherals and program the microcontroller's behaviour.
STM32CubeIDE is an advanced C/C++ development platform with peripheral configuration, code generation, code compilation, and debug features.
This platform permits to choose the type of Microcontroller Unit (MCU) that is going to be used and after that the user can configure whatever they want directly on the project environment.

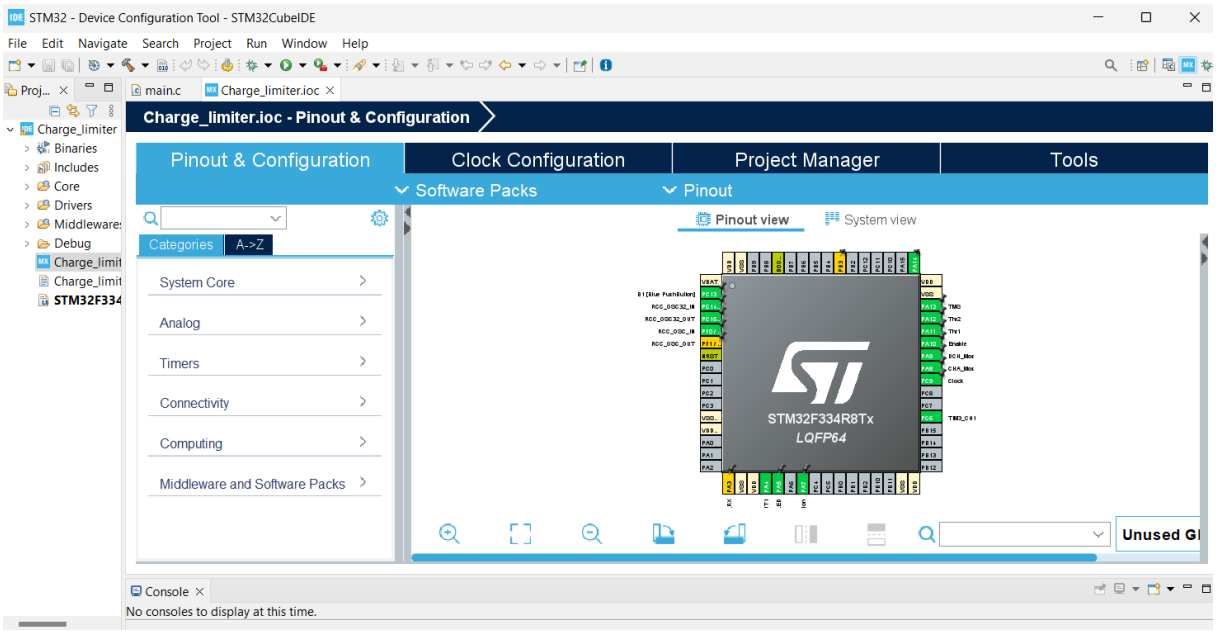

Figure 7.7: Device configuration tool on STM32CubeIDE.

7.1.3 Code

The code implemented to manage the correct functioning of the system by switching on and off the MOSFETs depending on the conditions encountered during a battery charging phase is divided into four tasks.

Task name	Priority
Normal charge	Normal
Threshold 1	Normal
Threshold 2	Normal
Limit charge	High

Table 7.1: Task's names and related priority.

Firstly, the normal charge is the task that permits the regular charge of the battery at a current imposed by the charger and its priority is normal. In practice, it maintains charging and discharging MOSFET closed, while the enable MOSFET remains open to let the current flow directly from charger to the battery.
The enable MOSFET is necessary to avoid any current to flow through the buck converter that could cause losses on charging power provided to the battery.
The normal charge has also the duty to verify if over-charge protection pin has been activated by threshold tasks. Then it opens charging MOSFET and, after some milliseconds, closes the enable MOSFET to allow the buck converter to limit the charging current to 8A by releasing the semaphore token which activates the limit charge task.

Secondly, the Threshold1 and Threshold2 tasks have the objective of verifying if certain thresholds are exceeded and have normal priority as well as in the normal charge task. This means that they are executed following the Round Robin schedule, explained in Section 7.1. They check if threshold input pins are activated, when it happens they count for a fixed amount of time. If threshold pin remains active, this means that current has continuously exceeded the threshold and the task has to activate the over-charge protection.
Two thresholds have been set, one activates limit charge function when current exceeds 102A for 20 seconds continuously; the other one activates the limiter function when current exceeds 122A for 5 seconds continuously.

The last task, which is the most important, is the limit charge function. It has high priority because, once activated, it should not be interrupted by other tasks. This task waits for the semaphore to be released before being activated. When it receives the token, the enable MOSFET is closed and the buck DC-DC converter starts to modulate the current autonomously. The duty of the limit charge task is to wait for 60 seconds before attempting to return to the normal charge task and charging the battery with a higher current. If thresholds are exceeded again, limit charge is activated again, it repeats the process and it increases the counter. When limit charge is activated five times, it remains active until the end of the charging phase.

The following code has been implemented to perform the tasks described above.

```
#include "main.h"
#include "cmsis_os.h"
#include <task.h>
#include <stdio.h>

osThreadId defaultTaskHandle;
osThreadId Normal_chargeHandle;
osThreadId Threshold1Handle;
osThreadId Threshold2Handle;
osThreadId Limit_chargeHandle;
osSemaphoreId myBinarySem01Handle;

uint16_t timer1=0;
uint16_t timer2=0;
uint16_t timer_limit=0;
uint16_t count=0;
uint16_t start=0;

void SystemClock_Config(void);
static void MX_GPIO_Init(void);
void StartDefaultTask(void const * argument);
void StartNormalCharge(void const * argument);
void StartThreshold1(void const * argument);
void StartThreshold2(void const * argument);
void StartLimitCharge(void const * argument);

int main(void)
{
  HAL_Init();
  SystemClock_Config();
  MX_GPIO_Init();

  osSemaphoreDef(myBinarySem01);
  myBinarySem01Handle = osSemaphoreCreate(osSemaphore(myBinarySem01), 1);

  /* definition and creation of defaultTask */
  osThreadDef(defaultTask, StartDefaultTask, osPriorityLow, 0, 128);
  defaultTaskHandle = osThreadCreate(osThread(defaultTask), NULL);

  /* definition and creation of Normal_charge */
  osThreadDef(Normal_charge, StartNormalCharge, osPriorityNormal, 0, 128);
  Normal_chargeHandle = osThreadCreate(osThread(Normal_charge), NULL);

  /* definition and creation of Threshold1 */
```

```
  osThreadDef(Threshold1, StartThreshold1, osPriorityNormal, 0, 128);
  Threshold1Handle = osThreadCreate(osThread(Threshold1), NULL);

  /* definition and creation of Threshold2 */
  osThreadDef(Threshold2, StartThreshold2, osPriorityNormal, 0, 128);
  Threshold2Handle = osThreadCreate(osThread(Threshold2), NULL);

  /* definition and creation of Limit_charge */
  osThreadDef(Limit_charge, StartLimitCharge, osPriorityHigh, 0, 128);
  Limit_chargeHandle = osThreadCreate(osThread(Limit_charge), NULL);

  osKernelStart();

  while (1)
  {

  }
}

void SystemClock_Config(void)
{
  RCC_OscInitTypeDef RCC_OscInitStruct = {0};
  RCC_ClkInitTypeDef RCC_ClkInitStruct = {0};

  RCC_OscInitStruct.OscillatorType = RCC_OSCILLATORTYPE_HSE;
  RCC_OscInitStruct.HSEState = RCC_HSE_BYPASS;
  RCC_OscInitStruct.HSEPredivValue = RCC_HSE_PREDIV_DIV1;
  RCC_OscInitStruct.HSIState = RCC_HSI_ON;
  RCC_OscInitStruct.PLL.PLLState = RCC_PLL_ON;
  RCC_OscInitStruct.PLL.PLLSource = RCC_PLLSOURCE_HSE;
  RCC_OscInitStruct.PLL.PLLMUL = RCC_PLL_MUL9;
  if (HAL_RCC_OscConfig(&RCC_OscInitStruct) != HAL_OK)
  {
    Error_Handler();
  }

  RCC_ClkInitStruct.ClockType = RCC_CLOCKTYPE_HCLK|RCC_CLOCKTYPE_SYSCLK
                              |RCC_CLOCKTYPE_PCLK1|RCC_CLOCKTYPE_PCLK2;
  RCC_ClkInitStruct.SYSCLKSource = RCC_SYSCLKSOURCE_PLLCLK;
  RCC_ClkInitStruct.AHBCLKDivider = RCC_SYSCLK_DIV1;
  RCC_ClkInitStruct.APB1CLKDivider = RCC_HCLK_DIV2;
  RCC_ClkInitStruct.APB2CLKDivider = RCC_HCLK_DIV1;

  if (HAL_RCC_ClockConfig(&RCC_ClkInitStruct, FLASH_LATENCY_2) != HAL_OK)
  {
    Error_Handler();
  }
```

```
}

static void MX_GPIO_Init(void)
{
  GPIO_InitTypeDef GPIO_InitStruct = {0};

  __HAL_RCC_GPIOC_CLK_ENABLE();
  __HAL_RCC_GPIOF_CLK_ENABLE();
  __HAL_RCC_GPIOA_CLK_ENABLE();
  __HAL_RCC_GPIOB_CLK_ENABLE();

  /*Configure GPIO pin Output Level */
  HAL_GPIO_WritePin(GPIOA, PD_Mos_Pin|LED_Pin|OverCHA_Protection_Pin
                    |CHA_Mos_Pin|DCH_Mos_Pin|Enable_Pin, GPIO_PIN_RESET);

  /*Configure GPIO pins : PD_Mos_Pin OverCHA_Protection_Pin CHA_Mos_Pin
                           DCH_Mos_Pin Enable_Pin */
  GPIO_InitStruct.Pin = PD_Mos_Pin|OverCHA_Protection_Pin|CHA_Mos_Pin
                        |DCH_Mos_Pin|Enable_Pin;
  GPIO_InitStruct.Mode = GPIO_MODE_OUTPUT_PP;
  GPIO_InitStruct.Pull = GPIO_NOPULL;
  GPIO_InitStruct.Speed = GPIO_SPEED_FREQ_LOW;
  HAL_GPIO_Init(GPIOA, &GPIO_InitStruct);

  /*Configure GPIO pins : Thr1_Pin Thr2_Pin */
  GPIO_InitStruct.Pin = Thr1_Pin|Thr2_Pin;
  GPIO_InitStruct.Mode = GPIO_MODE_INPUT;
  GPIO_InitStruct.Pull = GPIO_PULLDOWN;
  HAL_GPIO_Init(GPIOA, &GPIO_InitStruct);
}

/*NormalCharge task: sets CHA, DCH, PD, Enable MOSFETs signals to charge
the battery with maximum available current provided by the charger.
Checks for OverCHA_Protection_Pin to identify if limit charge needs to
be activated. If this condition occurs, it releases the token for limit
charge task activation.*/

void StartNormalCharge(void const * argument)
{
  for(;;)
  {
    HAL_GPIO_WritePin(GPIOA, CHA_Mos_Pin, GPIO_PIN_SET);
    HAL_GPIO_WritePin(GPIOA, DCH_Mos_Pin, GPIO_PIN_SET);
    HAL_GPIO_WritePin(GPIOA, PD_Mos_Pin, GPIO_PIN_SET);
    HAL_GPIO_WritePin(GPIOA, Enable_Pin, GPIO_PIN_RESET);
    if (HAL_GPIO_ReadPin(GPIOA, OverCHA_Protection_Pin))
    {
```

```
      HAL_GPIO_WritePin(GPIOA, CHA_Mos_Pin, GPIO_PIN_RESET);
      HAL_GPIO_WritePin(GPIOA, DCH_Mos_Pin, GPIO_PIN_SET);
      HAL_GPIO_WritePin(GPIOA, PD_Mos_Pin, GPIO_PIN_SET);
      HAL_Delay(10);
      HAL_GPIO_WritePin(GPIOA, Enable_Pin, GPIO_PIN_SET);
      osSemaphoreRelease(myBinarySem01Handle);
    }
  }
}

/*Threshold1 task: checks if limit charge circuit senses over-current
flowing through the battery. If it occurs, the task waits for 20
seconds and sets OverCHA_Protection_Pin high meaning that limit
charge activation is necessary. After that, timer is reset.*/

void StartThreshold1(void const * argument)
{
  for(;;)
  {
    if (HAL_GPIO_ReadPin(GPIOA, Thr1_Pin))
    {
      osDelay(1000);
      timer1++;
    }
    else
    {
      timer1 = 0;
    }
    if (timer1 == 20)
    {
      HAL_GPIO_WritePin(GPIOA, OverCHA_Protection_Pin, GPIO_PIN_SET);
      timer1 = 0;
      timer2 = 0;
    }
  }
}

/*Threshold2 task: checks if limit charge circuit senses over-current
flowing through the battery. If it occurs, the task waits for 5
seconds and sets OverCHA_Protection_Pin high meaning that limit
charge activation is necessary. After that, timer is reset.*/

void StartThreshold2(void const * argument)
{
  for(;;)
  {
    if (HAL_GPIO_ReadPin(GPIOA, Thr2_Pin))
```

```
    {
      osDelay(1000);
      timer2++;
    }
    else
    {
      timer2 = 0;
    }
    if (timer2 == 5)
    {
      HAL_GPIO_WritePin(GPIOA, OverCHA_Protection_Pin, GPIO_PIN_SET);
      timer1 = 0;
      timer2 = 0;
    }
  }
}

/*LimitCharge task: waits for the token to be released before being
executed. When it receives the token, the task sets CHA, DCH, PC and
Enable signals to let the buck converter modulating the current.
10ms of delay is introduced to avoid shortcircuit.
After limit charge activation, the task counts 60sec and after that
it resets OverCHA_Protection_Pin to return to NormalCharge task.
It also increases the count variable. After five activations,
LimitCharge task remains active until EoC.*/

void StartLimitCharge(void const * argument)
{
  for(;;)
  {
    osSemaphoreWait(myBinarySem01Handle, osWaitForever);
    if(start != 0)
    {
      count++;
      if(count < 5)
      {
        HAL_GPIO_WritePin(GPIOA, CHA_Mos_Pin, GPIO_PIN_RESET);
        HAL_GPIO_WritePin(GPIOA, DCH_Mos_Pin, GPIO_PIN_SET);
        HAL_GPIO_WritePin(GPIOA, PD_Mos_Pin, GPIO_PIN_SET);
        HAL_Delay(10);
        HAL_GPIO_WritePin(GPIOA, Enable_Pin, GPIO_PIN_SET);
        timer_limit = 0;
        while(timer_limit < 60)
        {
          HAL_Delay(1000);
          timer_limit++;
        }
```

```
        HAL_GPIO_WritePin(GPIOA, OverCHA_Protection_Pin, GPIO_PIN_RESET);
      }
      else
      {
        for(;;)
        {
          HAL_GPIO_WritePin(GPIOA, CHA_Mos_Pin, GPIO_PIN_RESET);
          HAL_GPIO_WritePin(GPIOA, DCH_Mos_Pin, GPIO_PIN_SET);
          HAL_GPIO_WritePin(GPIOA, PD_Mos_Pin, GPIO_PIN_SET);
          HAL_Delay(10);
          HAL_GPIO_WritePin(GPIOA, Enable_Pin, GPIO_PIN_SET);
          count = 0;
        }
      }
    }
    else
    {
      start = 1;
    }
  }
}

void HAL_TIM_PeriodElapsedCallback(TIM_HandleTypeDef *htim)
{
  if (htim->Instance == TIM6)
  {
    HAL_IncTick();
  }
}

void Error_Handler(void)
{
  __disable_irq();
  while (1)
  {
  }
}

#ifdef  USE_FULL_ASSERT
void assert_failed(uint8_t *file, uint32_t line)
{
}
#endif
```

In the following table, a summary of tasks' characteristics is reported.
The value of current at which the threshold tasks can react is settable by changing the reference voltage directly on the board.

Task	Current[A]	Reaction time [sec]	Duration time [sec]	Attempts
Normal charge	-	-	-	-
Threshold 1	102	20	-	-
Threshold 2	122	5	-	-
Limit charge	8	-	60	5

Table 7.2: Main tasks' parameters.

7.2 System connections

A simple representation of system connections and signal exchange is reported.

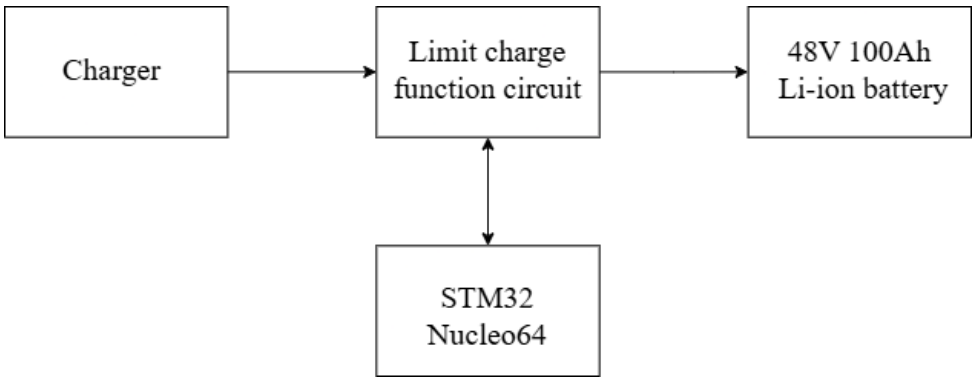

Figure 7.8: System connections.

Figure 7.2 illustrates the connections between each block. Specifically, the limit charge circuit is positioned between the charger and the battery to monitor the current flow and, in the event of limit charge activation, to regulate the current through a buck DC-DC converter.
The STM32 Nucleo64 is connected to the limit charge circuit to monitor the system's status. When the limit charge circuit sends a warning signal to the microcontroller, a threshold task identifies the warning. Subsequently, the limit charge task is activated, sending appropriate control signals to the MOSFETs on the limit charge board to regulate the charging current.

7.3 Board prototype

In order to evaluate whether the system is complete and works properly, the schematic reported in Figure 6.24 is implemented on a prototype board PCB.

7.3.1 Board

In Figures 7.9 and 7.10, it is reported respectively the top and the bottom of limit charge function circuit complete system.
For simplicity, the supply and the reference voltages are provided by an external voltage supplier instead of the voltage regulators.

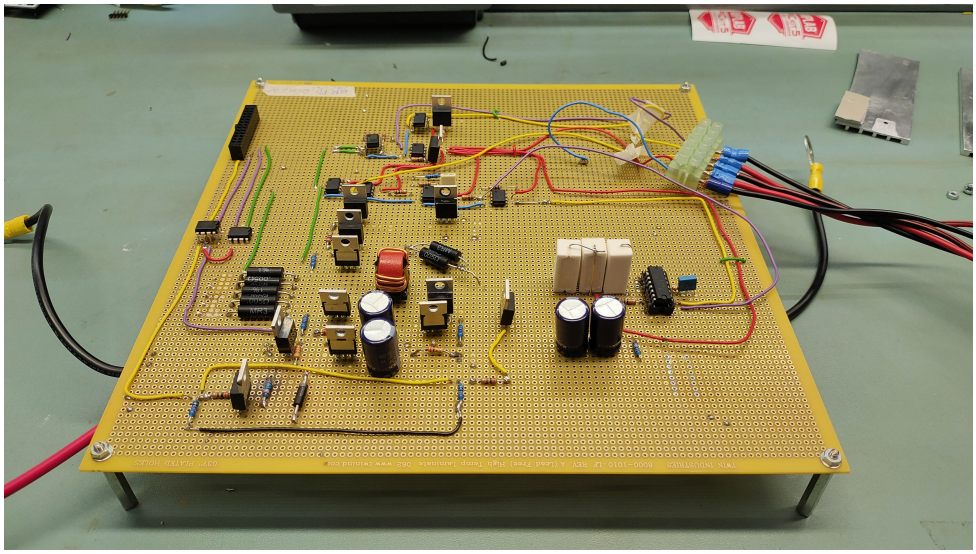

Figure 7.9: Top of board prototype.

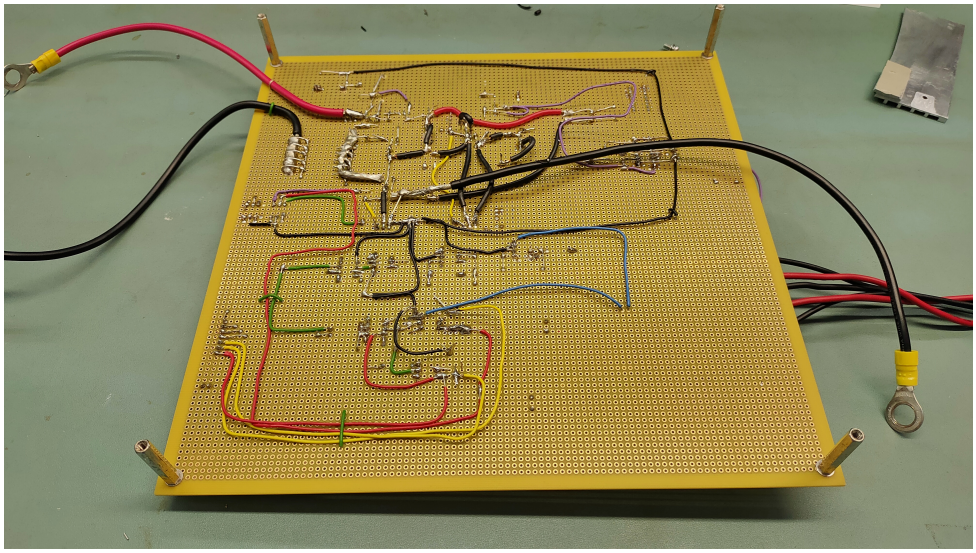

Figure 7.10: Bottom of board prototype.

7.3.2 Test results

In order to test the circuit, the necessary equipment is composed of:

- Board prototype
- 48V 100Ah TLC Li-ion battery
- Charger
- Voltage supplier
- STM32 Nucleo64

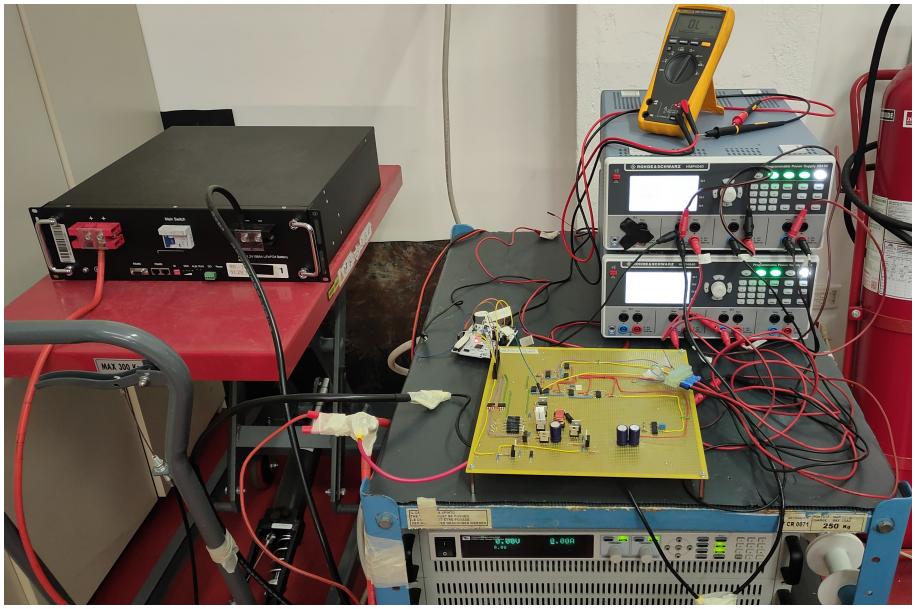

Figure 7.11: Board prototype testing setup.

In order to test the system, some heatsinks have been attached to the switching MOSFETs due to their increase in temperature. This fact is probably caused by the non-ideal turning on and off of the MOSFET. In fact, during the MOSFET's turning on phase, the voltage across the drain and the source does not fall immediately to zero. The same is related to the increase in the drain current. Both of these aspects cause some power to be dissipated by the MOSFET increasing the temperature.
The same behaviour can be related to the turning off of the MOSFET. In fact, the voltage across the drain and the source does not increase suddenly and the drain current does not fall instantly causing heat losses.
In Figure 7.12 is reported a graphical example of typical switching losses.

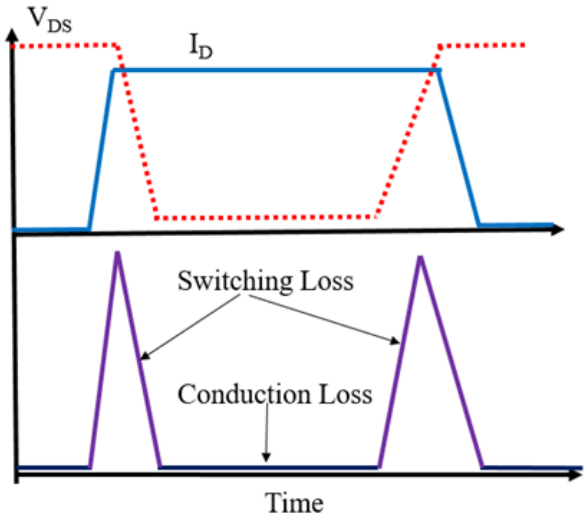

Figure 7.12: MOSFET switching losses example.
www.researchgate.net

Figures 7.13 and 7.14 report the charging current behaviour analysed by taking into account data of the battery BMS.

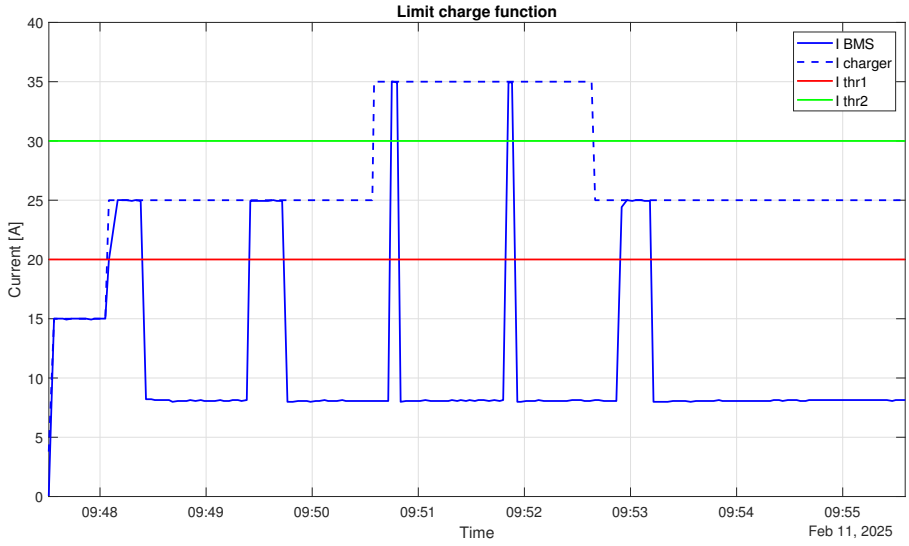

Figure 7.13: Charging current behaviour evaluating thresholds 1 and 2.

For the first test, threshold 1 and threshold 2 are respectively set to 20A and 30A. This means that when charging current exceeds 20A for 20 seconds, limit charge is then activated. Similarly, limit charge is also activated when current exceeds threshold 2 for 5 seconds.
In Figure 7.13, the current provided by the charger is initially set to 15A. Thereafter, it is possible to notice that the charging current is set to 25A, which is above threshold 1, and after 20 seconds the buck converter starts to limit the current to 8A for 60 seconds. When the predefined time for the limit charge to be active expires, the system turns off the buck converter, and the charging current returns to the maximum level provided by the charger. In this case, the current is again 25A and after 20 seconds limit charge is activated again.
When limit charge is deactivated for the third time, the current provided by the charger increases to 35A, which is above threshold 2, and limit charge is activated again after 5 seconds.
The process described above is repeated twice and it is important to notice that limit charge remains active when it is called for the fifth time for security reasons because some problems on the battery or on the system may be present and the charging phase is ended with limited current.
Figure 7.14 reports the behaviour of the system when threshold 1 is exceeded by the charging current five times.
In this case current is initially set to 15A as in the previous case and thresholds are the same as before too. When current increases to 25A, the system waits for 20 seconds before activating the limit charge function.
As in the previous case, limit charge is activated and deactivated five times, which means that there may be some problems and the battery is charged with limited current.

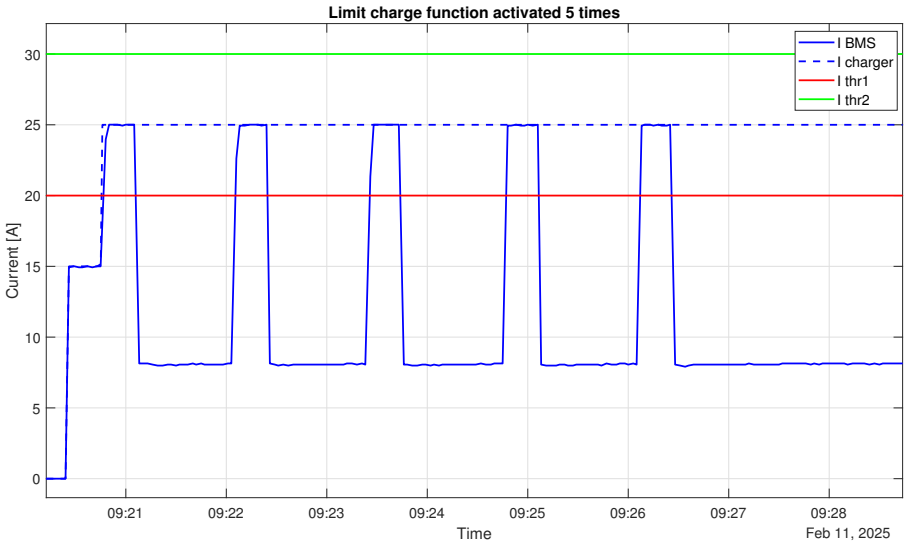

Figure 7.14: Charging current behaviour after 5 attempts.

7.4 PCB prototype

After having tested the system on a prototype board, a PCB prototype for the limit charge function circuit has been developed. The aim of the prototype is to test a semi-finished product and to put in evidence possible non ideal effects due to parasitic effects introduced by the manual soldering of wirings on the board prototype.

7.4.1 PCB design

The software used for developing the PCB is KiCAD. It is the same used for the schematic because it permits to design the PCB directly starting from it by setting each specific component footprint.
Figure 7.15 reports the final product design. During the design phase, it was important to evaluate the high charging current flow loop. This evaluation was necessary to minimize it and to separate it from the control circuit, so as to avoid any interference with small signal voltages and currents. Otherwise, the system may not be able to properly modulate the charging current due to the incorrect interpretation of control signals.
Figure 7.16 shows a photograph of the final PCB assembled, ready to be tested to verify the results obtained in Section 7.3.2.

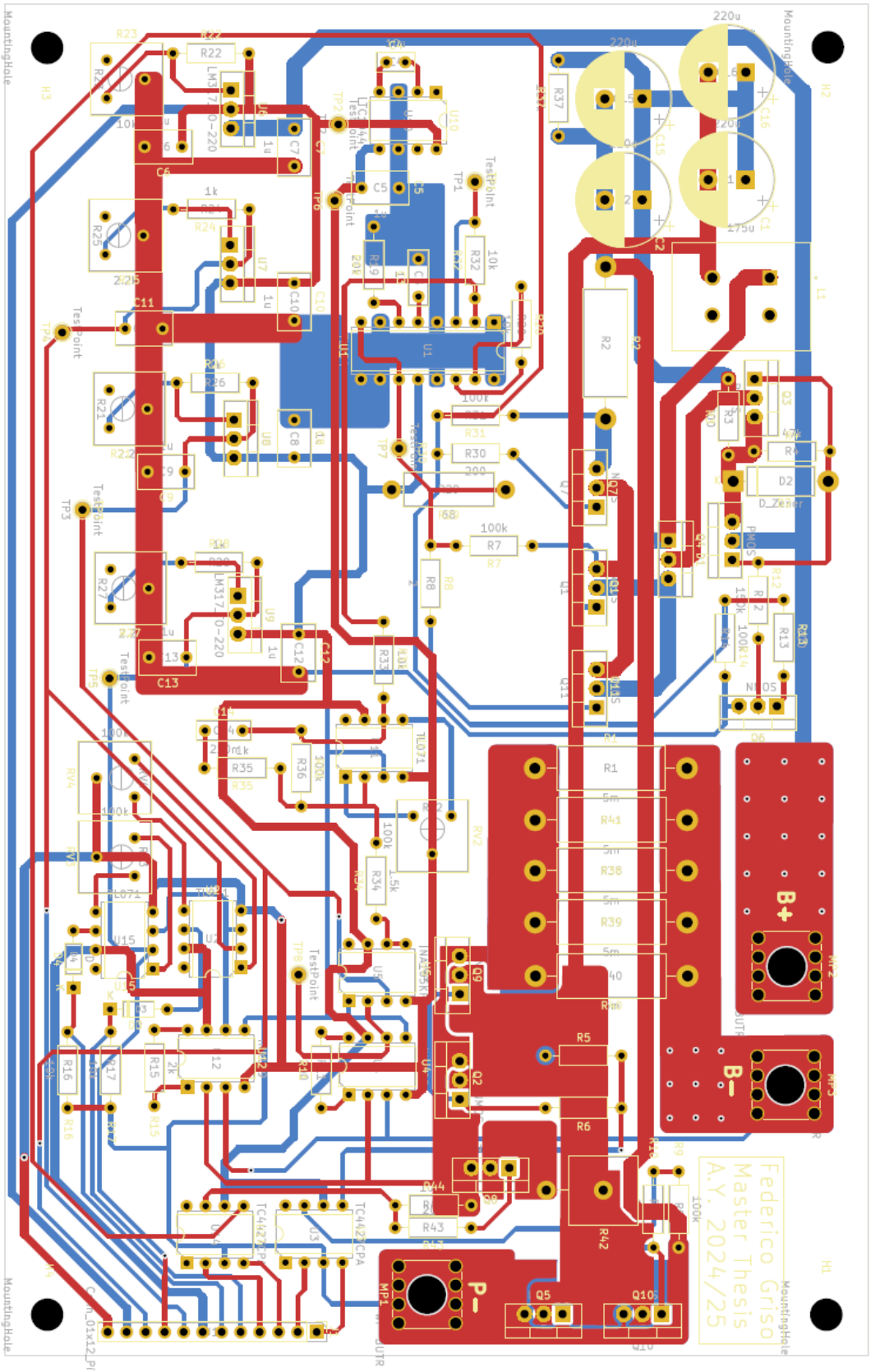

Figure 7.15: PCB design of the system with KiCAD.

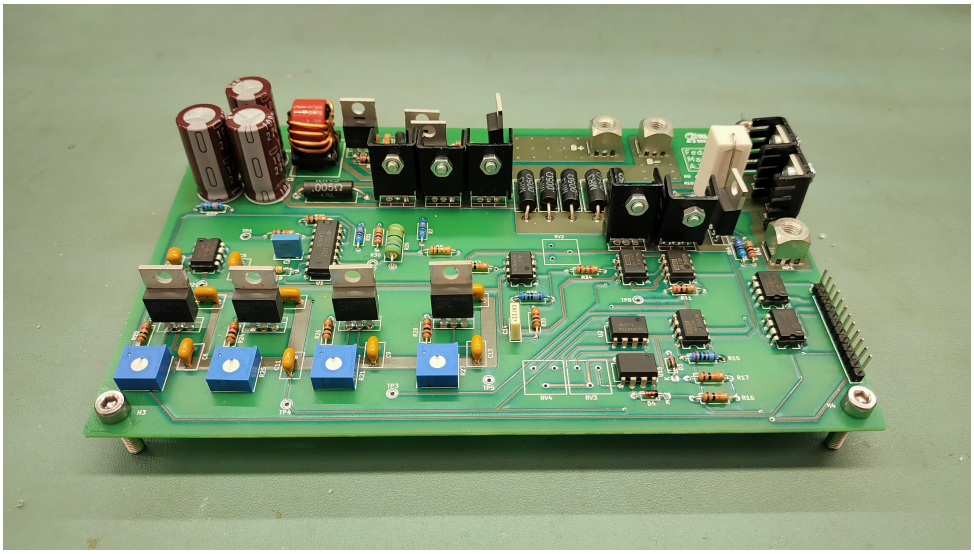

Figure 7.16: Top of PCB prototype.

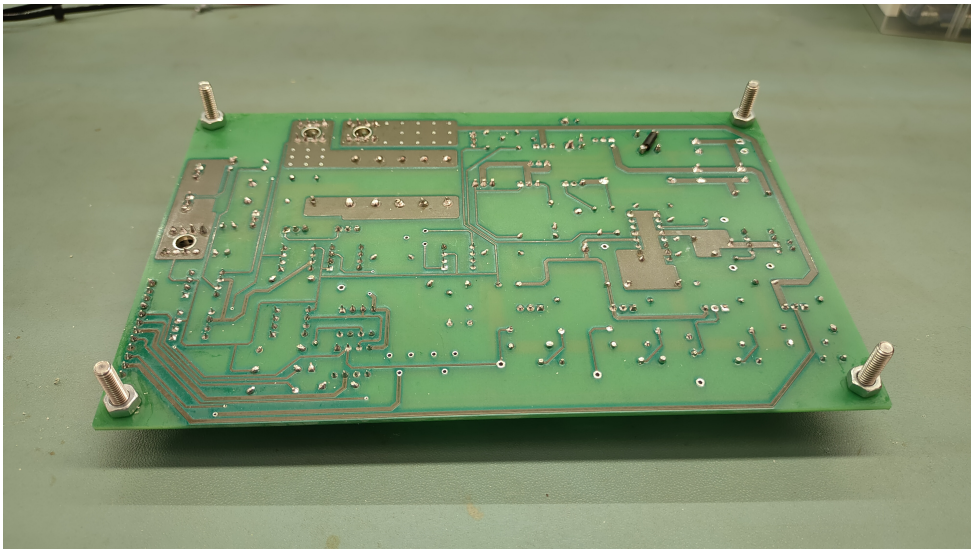

Figure 7.17: Bottom of PCB prototype.

7.4.2 Test results

The equipment necessary to test the PCB prototype is practically the same as the one used in Section 7.3.2, the only difference is the voltage supplier.
For what concerns the PCB, the reference voltages are derived directly from the battery voltage. To do so, some voltage regulators and a charge pump are introduced on the prototype. For this reason, the voltage supplier is not used any more.
The voltage regulators are implemented to derive V_{CC}, V_{ref}, V_{th1} and V_{th2}. Meanwhile, the charge pump is used to derive V_{SS} starting from V_{CC}.
In order to make the system as customizable as possible, each voltage regulator can be set to the desired voltage simply by individually adjusting the potentiometer resistance..

With respect to the voltage regulator that derive V_{CC} starting from the battery voltage, the use of a heatsink is necessary because of its high power dissipation. Otherwise, the consequence of not using a dissipation system could lead to thermal runaway of the component.
The equation that describes the power dissipated by the voltage regulator is the following one.

$$P_{diss} = (V_{in} - V_{CC}) \cdot I_{CC} = (57.6V - 12V) \cdot 0.2A = 9.12W \tag{7.1}$$

By examining the thermal resistance of the voltage regulator in the datasheet, the approximate temperature reached by the regulator in the absence of any dissipation system can be derived.

$$T = P_{diss} \cdot R_{\theta-ja} = 9.12W \cdot 21°\text{C}/W = 191.52°\text{C} \tag{7.2}$$

The introduction of a heatsink is necessary to reduce the thermal resistance of the voltage regulator junction to ambient, thereby lowering its operating temperature.
In Figure 7.18, the PCB prototype testing setup is shown.

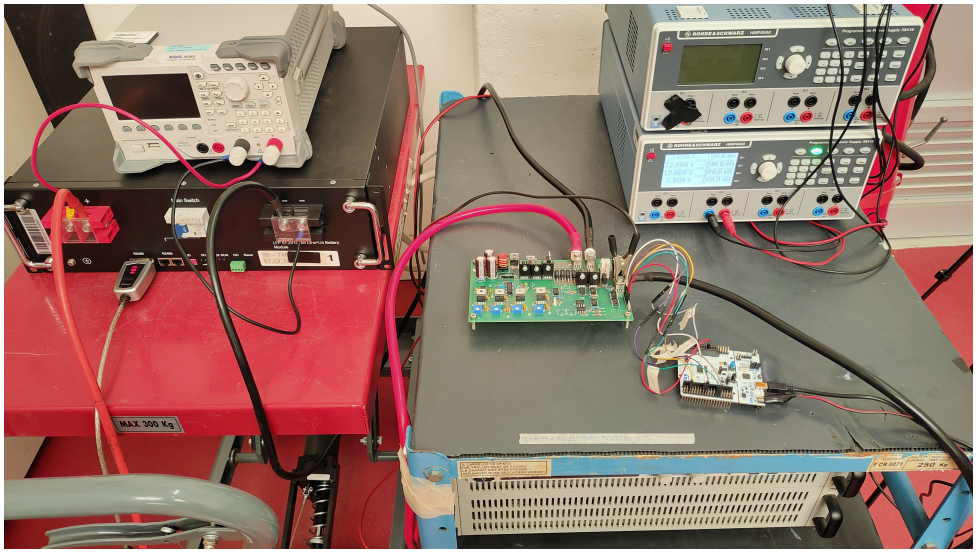

Figure 7.18: PCB prototype testing setup.

The system is then tested to verify if the behaviour highlighted in Section 7.3.2 is confirmed, even though the reference voltages are provided by the voltage regulators.
The threshold voltages are set to 0.75V and 0.925V in order to obtain 30A and 37A respectively for threshold 1 and threshold 2.
This means that when charging current exceeds threshold 1 for 20 seconds continuously, the limit charge current is activated. Similarly, when current exceeds threshold 2 for 5 seconds continuously the limit charge is activated.
Since the RTOS code is the same as in the previous test, the limit charge function attempts are set to five. When the fifth attempt is performed, the limit charge function remains active until the end of charge because some problems could be identified on the system and a safe charging current is necessary.
A more detailed account of the system behaviour is given in the following figures.

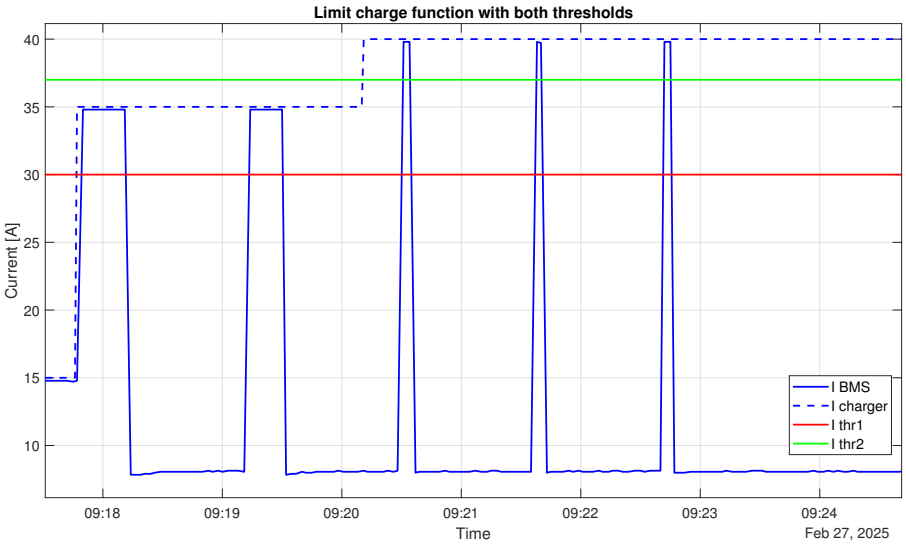

Figure 7.19: PCB limit charge behaviour exceeding both thresholds.

Initially, charger current has been set to 15A. When current is set to 35A, limit charge is activated after 20 seconds and it remains active for 60 seconds, limiting current to 8A. After 60 seconds, RTOS activates *normal charge* task, but current is again exceeding threshold 1 and after 20 seconds, limit charge is activated. After that, current is set to 40A, which is above threshold 2, and limit charge is activated after 5 seconds. The process is repeated 5 times and after the fifth attempt limit charge remains active until the end of charge because there may be some problems.

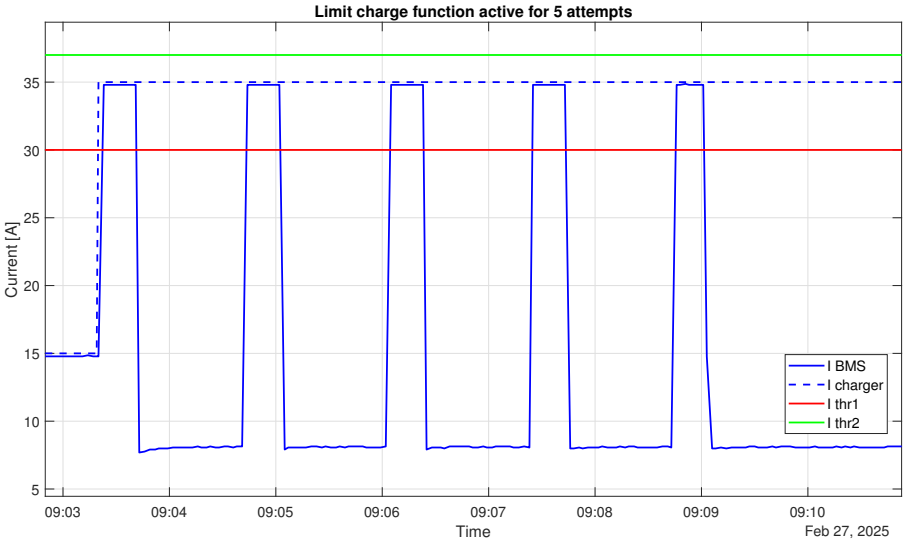

Figure 7.20: PCB limit charge behaviour after 5 activations.

Moving on now to consider Figure 7.20, the charger current has been set to 15A as in the previous test. When current is set to 35A, limit charge is activated after 20 seconds and it remains active for 60 seconds, limiting current to 8A. After 60 seconds, RTOS activates *normal charge* task, but current is again exceeding threshold 1 and limit charge

is activated after 20 seconds. Process is repeated 5 times and after that limit charge remains active until the end of the charging process because there may be some problems and it avoids possible over-current and over-temperature.
The results are practically the same as the ones obtained by testing the board prototype and the system is able to react in the cases where current exceeds both thresholds for the designed attempts.
The temperature behaviour of the buck converter has been analysed and the results are reported in Figure 7.21.

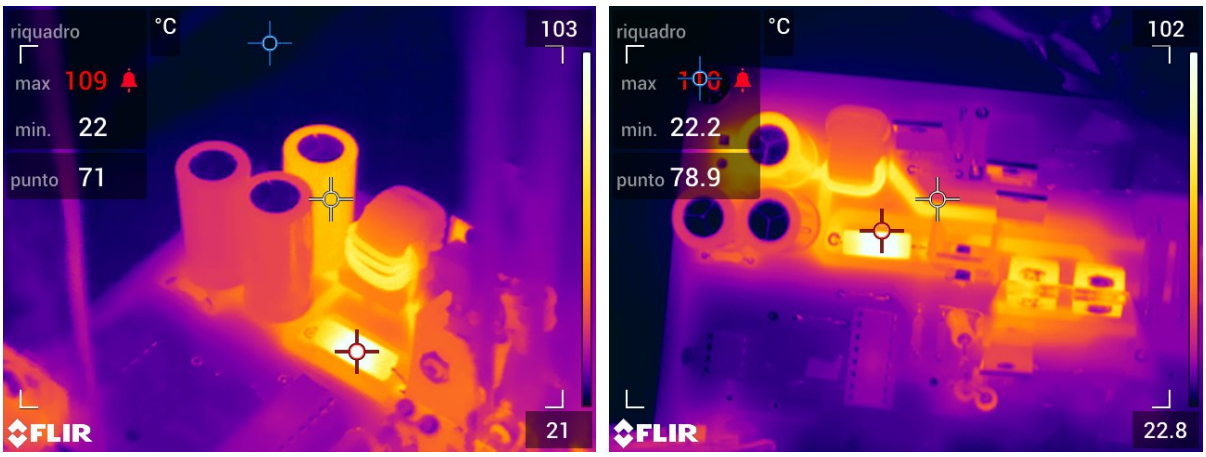

Figure 7.21: Buck DC-DC converter's temperature evaluation.

The photos were taken a few minutes after the activation of the limit charge function to evaluate the maximum temperature reached by the buck converter components after some operating time.
Some considerations can be derived by the evaluation of the photos. The system is able to operate without the risk of thermal runaway for the components. However, some improvements can be made to the PCB design, such as increasing the trace width. This helps to reduce the temperature rise of the trace itself and also lowers the ambient temperature for nearby components due to improved heat dissipation. The temperature reached by the trace is not worrisome but it can be improved.
The bypass resistor also presents high temperature ($\approx 100°C$) due to power dissipation but its maximum tolerable temperature reported on the datasheet is 275°C. However, by placing another resistance in parallel it is possible to halve the current flowing through each resistor and their operating temperature would significantly decrease.
Another possible critical component on the buck converter is the output capacitor. For this reason it is important to choose a capacitor which is able to tolerate the designed current ripple (1A). Thus, the output capacitor which has been chosen is capable of manage properly 2.25A at 100kHz with a maximum operating temperature of 125°C, which is much higher than the one needed for the limit charge function circuit.
In conclusion, the system is able to modulate the charging current at the desired value when it detects some potentially hazardous situations and it is able to operate without the need of auxiliary power supply because it can generate the reference voltages simply deriving them from the battery voltage.

The current thresholds have been set to lower values than the ideal ones (102A and 122A) due to safety reasons. The next step for the development of limit charge function circuit is the implementation of some design improvements previously identified with the objective of testing a new prototype with higher operating current.

Chapter 8

Conclusions

8.1 Comments on the project

To resume, this thesis has thoroughly analysed two different battery prototypes. The second prototype criticalities have led to the development of a limit charge function circuit based on a buck DC-DC converter and an average current control.
Initially, the buck DC-DC converter has been designed following some design choice constraints. Thereafter, the average current control loop has been designed by analysing the transfer functions of the block diagrams that compose the entire system.
After having evaluated the bode diagram of the transfer function, the PI regulator parameters have been derived.
Consequently, the simulation activity was conducted to refine the PI parameters obtained from the bode diagram.
Initially, the simulation was performed using Simulink, and through a process of trial and error, the PI parameters were improved.
After that, in order to have a better understanding of possible *real* system behaviour, the same test was performed on LTSpice which permits to use components with real simulated behaviour. The test performed on LTSpice confirmed the system behaviour observed on Simulink test.
In order to autonomously manage the BMS operations, a Real-Time Operating System (RTOS) has been programmed on a STM32 Nucleo-64 which is able to handle different tasks which appear simultaneously. The aim of the RTOS is to sense when charging current exceeds the predefined thresholds and then activate the buck converter which limits the charging current.
Therefore, the limit charge function circuit has been tested on a board prototype PCB with discrete components with the aim of testing the real system behaviour in order to subsequently design a PCB prototype.
After having verified the good functioning of the board prototype, a PCB design has been conducted on KiCAD software. Particular attention has been paid to separating the power current loop from the control signal circuit in order to avoid any interference with control signals caused by high current flow.
In conclusion, the PCB prototype has been tested with good results. The system is able to modulate the charging current to the designed one when some possible unsafe situations occur.

The system is programmed to attempt the normal charge five times after the first activation of the limit charge function. This choice was made to ensure the system can verify if any potential hazardous situations are still present. However, after five attempts, it is likely that some problems are present, and the battery is charged with a safe current value.
This thesis outlined that the limit charge function circuit is an essential part of the battery BMS because it can guarantee the continuity of charging process, even if some unusual situations occur. In particular, when multiple strings of batteries are connected together, the limit charge function avoids any power losses because all batteries are able to reach 100% SoC during a charging phase, even if some of them are imbalanced. This prevents any of them from opening the charging MOSFETs and interrupting the charging process.

8.2 Future developments

The first PCB prototype for implementing a limit charge function circuit on a battery BMS is complied with the initial objectives of the project. However, some improvements can be brought to the design.
During the testing process of the PCB, some heat dissipation from MOSFETs and buck DC-DC converter had to be handled.
In particular, the switching MOSFETs began warming up during the limit charge activation. The phenomenon is explained in Figure 7.12 and was resolved by mounting some heatsinks on them.
Possible improvements can be made by investigating in more detail the rising and falling time during switching phase.
Moreover, adding more parallel MOSFETs to the charging and discharging ones can bring multiple benefits. For example, the equivalent resistance R_{dc-on} decreases significantly and a subsequent reduction in parasitic resistance can be evaluated. Furthermore, by adding parallel MOSFETs, the current flowing through each MOSFET decreases which reduces their power dissipation.
The output capacitor of the buck converter reported a slight increase in temperature. Although this did not indicate significant warnings, potential design improvements can be made by reducing current ripple during its operation. The V_{CC} voltage regulator also exhibited some heat dissipation, as shown in equation 7.2. This can be solved by adopting pre-constructed buck converter which is able to reduce the input voltage (battery voltage) to V_{CC} with better efficiency compared to a simple voltage regulator.
Figure 7.21 highlights that some buck converter traces reported heat dissipation as well. This is likely due to non-ideal design trace width, which can be easily solved by modifying the PCB design to increase their width.
In conclusion, this thesis has outlined several future project developments. As a result, the company is now well-positioned to develop a more comprehensive and optimized limit charge function circuit.
The RTOS can be enriched with additional tasks to handle the battery discharging process. This enhancement would enable the creation of a board that can serve as a foundational starting point for designing a comprehensive BMS architecture around it.

Appendix A

Matlab scripts

A.1 Battery characterization

This appendix includes the codes used to extrapolate graphs presented in this thesis from Excel files produced by Digatron and the BMS of batteries.
The script used to extract data from files and to plot the desired graphs based on the log data from Digatron and the BMS are reported below:

```
close all
clc

%%%%%%%%%%%%%%%%%%%%% Data extraction from file %%%%%%%%%%%%%%%%%%%%%

Dig=readtable("Name_of_Digatron_file.xlsx");
BMS=readtable("Name_of_BMS_file.xls");

%%%%%%%%%%%%%%%%%%%%%%%%%%%% x-axis limit %%%%%%%%%%%%%%%%%%%%%%%%%%%%

xl=datetime('Initial_date');
xh=datetime('Final_date');

%%%%%%%%%%%%%%%%%%%%% Voltage and current graph %%%%%%%%%%%%%%%%%%%%%

figure
yyaxis left
plot(Dig.TimeStamp, Dig.Voltage, 'LineWidth', 1.5)
hold on
plot(BMS.Date_Time, BMS.Total_Voltage, 'LineWidth', 1.5)
ylabel("Voltage")
hold on
yyaxis right
plot(Dig.TimeStamp, Dig.Current, 'LineWidth', 1.5)
hold on
plot(BMS.Date_Time, BMS.Current_I, 'LineWidth', 1.5)
grid on
```

```
set(gca, 'Position', [0.05,0.089,0.885,0.87])
set(gca, 'FontSize', 12)
set(gcf, 'Position', [400,232,1080,607])
xlabel("Time")
ylabel("Current")
title("Cycles of CH/DCH Btr #1 - Supplier A")
legend("V Digatron", "V BMS", "I Digatron", "I BMS")
xlim([xl xh])

%%%%%%%%%%%%%%%%%%%%%%%%%%%%%% Cell voltage %%%%%%%%%%%%%%%%%%%%%%%%%%%%%%

figure
plot(BMS.Date_Time, BMS.Vol_Cell01, BMS.Date_Time, BMS.Vol_Cell02,
     BMS.Date_Time, BMS.Vol_Cell03, BMS.Date_Time, BMS.Vol_Cell04,
     BMS.Date_Time, BMS.Vol_Cell05, BMS.Date_Time, BMS.Vol_Cell06,
     BMS.Date_Time, BMS.Vol_Cell07, 'LineWidth', 1.5)
grid on
hold on
plot(BMS.Date_Time, BMS.Vol_Cell08, BMS.Date_Time, BMS.Vol_Cell09,
     BMS.Date_Time, BMS.Vol_Cell10, BMS.Date_Time, BMS.Vol_Cell11,
     BMS.Date_Time, BMS.Vol_Cell12, BMS.Date_Time, BMS.Vol_Cell13,
     BMS.Date_Time, BMS.Vol_Cell14, 'LineWidth', 1.5, 'LineStyle', '--')
hold on
plot(BMS.Date_Time, BMS.Vol_Cell15, BMS.Date_Time, BMS.Vol_Cell16,
    'LineWidth', 1.5, 'LineStyle', '-.')
set(gca, 'Position', [0.05,0.089,0.885,0.87])
set(gca, 'FontSize', 12)
set(gcf, 'Position', [400,232,1080,607])
xlim([xl xh])
ylabel("Voltage")
xlabel("Time")
title("Cell voltage on Btr #1 - Supplier A")
legend("Voltage cell01", "Voltage cell02", "Voltage cell03",
       "Voltage cell04", "Voltage cell05", "Voltage cell06",
       "Voltage cell07", "Voltage cell08", "Voltage cell09",
       "Voltage cell10", "Voltage cell11", "Voltage cell12",
       "Voltage cell13", "Voltage cell14", "Voltage cell15",
       "Voltage cell16")

%%%%%%%%%%%%%%%%%%%%%%%%%% SOC and current %%%%%%%%%%%%%%%%%%%%%%%%%%%%%%

figure
yyaxis left
plot(BMS.Date_Time, BMS.SOC, 'LineWidth', 1.5)
ylim([-10 110])
ylabel("SOC")
hold on
```

```
set(gca, 'Position', [0.05,0.089,0.885,0.87])
set(gca, 'FontSize', 12)
set(gcf, 'Position', [400,232,1080,607])
xlim([xl xh])
yyaxis right
plot(BMS.Date_Time, BMS.Current_I, 'LineWidth', 1.5)
ylabel("Current")
xlabel("Time")
title("SOC and Current on Btr #1 - Supplier A")
grid on
legend("SOC", "Current")

%%%%%%%%%%%%%%%%%%%%%%%%%%%% Temperature %%%%%%%%%%%%%%%%%%%%%%%%%%%%

figure
plot(BMS.Date_Time, BMS.Temp_PCB, BMS.Date_Time, BMS.Temp_internal,
     BMS.Date_Time, BMS.Temp01, BMS.Date_Time, BMS.Temp02,
     BMS.Date_Time, BMS.Temp03, BMS.Date_Time, BMS.Temp04,
    'LineWidth', 1.5)
grid on
set(gca, 'Position', [0.05,0.089,0.885,0.87])
set(gca, 'FontSize', 12)
set(gcf, 'Position', [400,232,1080,607])
xlim([xl xh])
ylabel("Temperature")
xlabel("Time")
title("Temperature on Btr #1 - Supplier A")
legend("T_{PCB}", "T_{internal}", "T01", "T02", "T03", "T04")

%%%%%%%%%%%%%%%%%%%%%%%%%%%% Ah per step %%%%%%%%%%%%%%%%%%%%%%%%%%%%

figure
plot(Dig.TimeStamp, Dig.AhStep, 'LineWidth', 1.5)
grid on
set(gca, 'Position', [0.05,0.089,0.885,0.87])
set(gca, 'FontSize', 12)
set(gcf, 'Position', [400,232,1080,607])
xlim([xl xh])
ylabel("Ah per step")
xlabel("Time")
title("Ah Btr #1 - Supplier A")
ylim([-2 110])
```

The script enables the plotting of all the main waveforms used to analyse battery behaviour, allowing for a comprehensive evaluation of all related aspects.
The plotted graphs are as follows:

- Voltage and current vs time
- Cell voltages vs time
- State of charge vs time
- Temperature of BMS and cells vs time
- Ampere per hour charged/discharged vs time

Some examples are reported below.

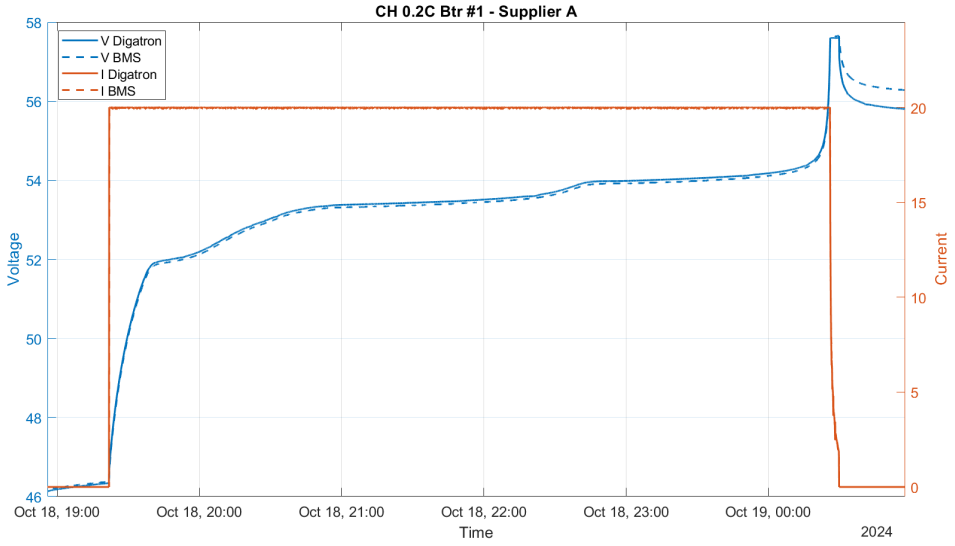

Figure A.1: Charge at 0.2C.

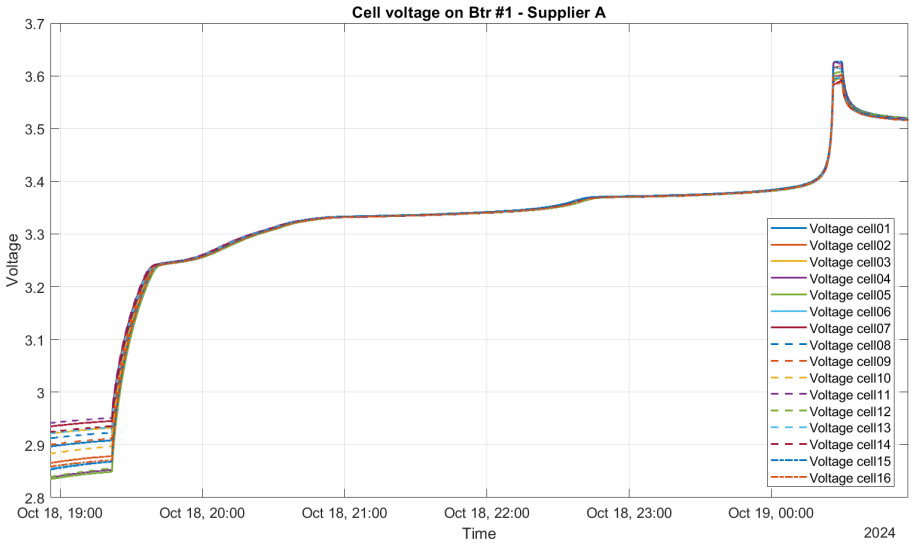

Figure A.2: Cell voltages at charge 0.2C.

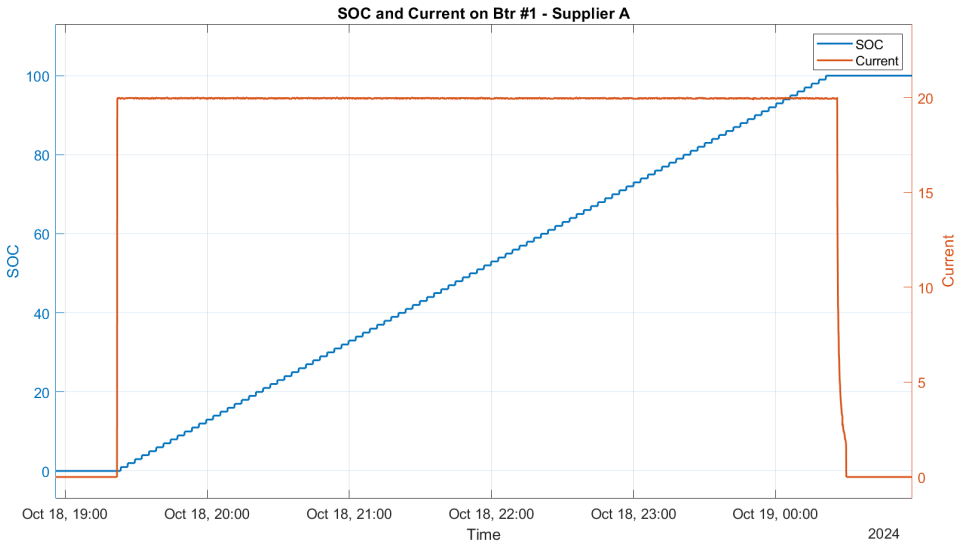

Figure A.3: State of charge at charge 0.2C.

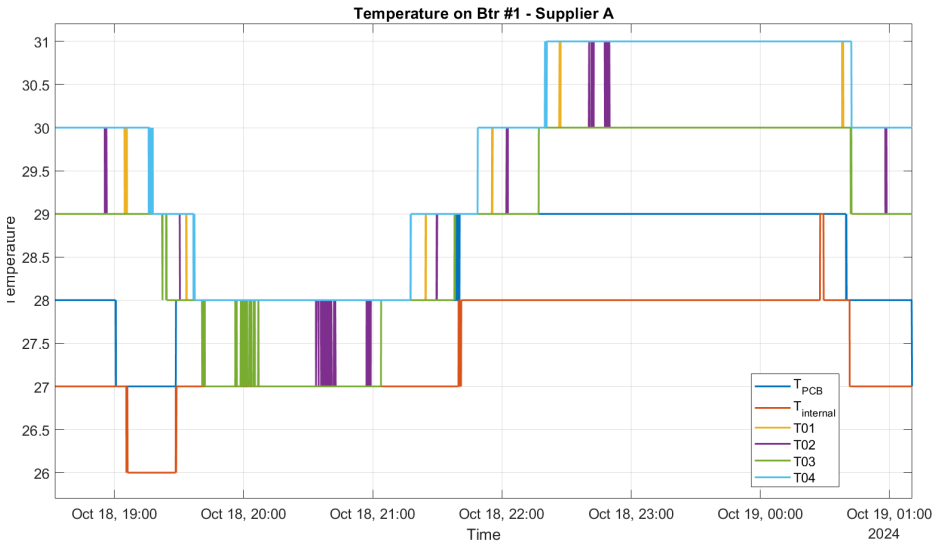

Figure A.4: Temperature of BMS and cells at charge 0.2C.

A.2 Bode plot

The following code is the one used on Section 6.1.3 to derive the frequency behaviour of the open loop and closed loop current control.

```
close all
clc

V=57.6;
C=220*10^-6;
L=175*10^-6;
Ki=3000;
```

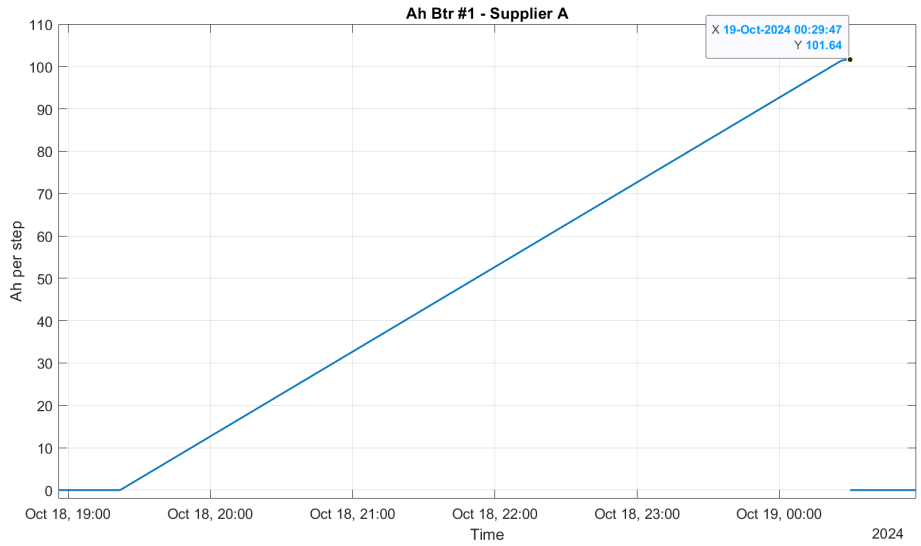

Figure A.5: Ampere per hour at charge 0.2C.

```
Kp=0.6;
Ro=0.012;
Gi=tf([C*Ro 1], [L*C L/Ro 1]);
PI=tf([Kp/Ki 1], [1 0]);
bode(V/Ro*Gi*Ki*PI/3, V/Ro*Gi, Ki*PI, {1, 600000})
xlim([1 600000])
hline = findall(gcf, 'type', 'line');
set(hline, 'LineWidth', 1.5);
ax=findobj(gcf,'type','axes');
mag_ax=ax(1);
phase_ax=ax(2);
ax_xlim=phase_ax.XLim;
phase_ylim=phase_ax.YLim;
mag_ylim=mag_ax.YLim;

hold(phase_ax, 'on')
plot(phase_ax,[66000 66000],[phase_ylim(1) phase_ylim(2)], 'b')
plot(phase_ax,[314000 314000],[phase_ylim(1) phase_ylim(2)], 'r')

hold(mag_ax,'on')
plot(mag_ax,[66000 66000],[mag_ylim(1) mag_ylim(2)], 'b')
plot(mag_ax,[314000 314000],[mag_ylim(1) mag_ylim(2)], 'r')

grid on
legend("T(s)", "G(s)", "PI(s)", "\omega_c", "$\omega_s$")
set(gca, 'Position', [0.06,0.09,0.92,0.85])
set(gcf, 'Position', [400,232,1080,607])

figure
```

```
bode((V/Ro*Gi*Ki/3*PI)/(1+V/Ro*Gi*Ki/3*PI, {1 600000})
xlim([1 600000])
hline = findall(gcf, 'type', 'line');
set(hline, 'LineWidth', 1.5);
ax1=findobj(gcf, 'type', line');
mag_ax1=ax1(1);
phase_ax1=ax1(2);
ax1_xlim=phase_ax1.XLim;
phase_ylim1=phase_ax1.YLim;
mag_ylim1=mag_ax1.YLim;

hold(phase_ax1, 'on')
plot(phase_ax1, [71000 71000], [phase_ylim1(1) phase_ylim1(2)], 'r')

hold(mag_ax1, 'on')
plot(mag_ax1, [71000 71000], [mag_ylim1(1) mag_ylim1(2)], 'r')

grid on
legend("Gain closed loop", "\omega_{-3dB}")
set(gca, 'Position', [0.06,0.09,0.92,0.85])
set(gcf, 'Position', [400,232,1080,607])
```

Bibliography

[1] Sabri Baazouzi et al. "Design, Properties, and Manufacturing of Cylindrical Li-Ion Battery Cells—A Generic Overview". In: *Batteries* 9.6 (2023). ISSN: 2313-0105. URL: https://www.mdpi.com/2313-0105/9/6/309.

[2] Yevgen Barsukov and Texas Instruments. "Battery Cell Balancing: What to Balance and How". In: ().

[3] Joel Brunarie et al. "Lithium-ion (Li-ion) battery technology evolves to serve an extended range of telecom applications". In: *2011 IEEE 33rd International Telecommunications Energy Conference (INTELEC)*. 2011, pp. 1–9. DOI: 10.1109/INTLEC.2011.6099890.

[4] Hossam A Gabbar, Ahmed M Othman, and Muhammad R Abdussami. "Review of battery management systems (BMS) development and industrial standards". In: *Technologies* 9.2 (2021), p. 28.

[5] Diego Nieto Hummes et al. "A comparative study of different battery geometries used in electric vehicles". In: *Latin American Journal of Energy Research* 10.2 (Nov. 2023), pp. 94–114. DOI: 10.21712/lajer.2023.v10.n2.p94-114. URL: https://periodicos.ufes.br/lajer/article/view/42550.

[6] IEC. *Secondary cells and batteries containing alkaline or other non-acid electrolytes - Secondary lithium cells and batteries for use in industrial applications*. Standard IEC 62620. Vernier, Geneva, Switzerland: International Electrotechnical Commission, 2014.

[7] Reiner Korthauer. *Lithium-ion batteries: basics and applications*. Springer, 2018.

[8] S Megahed and W Ebner. "Lithium-ion battery for electronic applications". In: *Journal of Power Sources* 54.1 (1995), pp. 155–162.

[9] Muhammad Nizam et al. "Battery management system design (BMS) for lithium ion batteries". In: *AIP Conference Proceedings*. Vol. 2217. 1. AIP Publishing. 2020.

[10] Robert Schröder, Muhammed Aydemir, and Günther Seliger. "Comparatively Assessing different Shapes of Lithium-ion Battery Cells". In: *Procedia Manufacturing* 8 (2017). 14th Global Conference on Sustainable Manufacturing, GCSM 3-5 October 2016, Stellenbosch, South Africa, pp. 104–111. ISSN: 2351-9789. DOI: https://doi.org/10.1016/j.promfg.2017.02.013. URL: https://www.sciencedirect.com/science/article/pii/S2351978917300173.

[11] Weixiang Shen, Thanh Tu Vo, and Ajay Kapoor. "Charging algorithms of lithium-ion batteries: An overview". In: *2012 7th IEEE Conference on Industrial Electronics and Applications (ICIEA)*. 2012, pp. 1567–1572. DOI: 10.1109/ICIEA.2012.6360973.

[12] John T Warner. *Lithium-ion battery chemistries: a primer*. Elsevier, 2019.